Spring 5-17-2010

Deconvoluting the Engineering and Assembly Instructions for Complex Iii Activity

Sarah C. Hokanson
University of Pennsylvania, Sechobot@gmail.com

Deconvoluting the Engineering and Assembly Instructions for Complex Iii Activity

Abstract
In respiratory systems, membrane-bound Complex III catalyzes the oxidation of ubiquinone and the reduction of a soluble cytochrome with the bioenergetic formation of a transmembrane proton gradient ($\Delta\mu H+$). Complex III turnover is initiated by a unique two electron oxidation of ubiquinone at the Qo site; one electron is delivered to a high potential chain containing an iron-sulfur cluster, cytochrome c1 and cytochrome c2, and a second electron is transferred to a low potential chain that terminates at the Qi site. All Complex III electron tunneling reactions are reversible, and a critical part of Complex III maintaining productive turnover is its suppression of energy-wasting reverse electron transfer reactions. The key to uncovering the controversial mechanism of Qo oxidation is determining how Complex III is regulated such that productive electron-transfer steps overwhelm unproductive steps.

This thesis focuses on understanding the structural and biochemical tolerances of the redox cofactors in Complex III and applying that knowledge towards the design of a simple, but robust, amphiphilic maquette that is capable of transmembrane proton and electron transfer. In chapter two, kinetic studies of heme c1 mutants reveal that R. sphaeroides Complex III is engineered to withstand large changes in heme c1 active site residues while still preserving heme c1 midpoint potential and enzyme turnover. In chapter three, the maquette approach was applied toward developing a simple model protein (AP6) that retained the minimum engineering requirements for Complex III electron and proton transfer reactions but lacked the complexity found in the natural system. The AP6 peptide assembles as a four-α-helix bundle protein and can potentially bind up to six hemes tightly across a membrane interface. Chapter four demonstrates that AP6 successfully performs quinol-cytochrome c oxidoreductase activity in hundreds of milliseconds. AP6 is the first example of a synthetic enzyme capable of near-natural turnover rates. Chapter five focuses on defining the thermodynamic limit for maquette activity. This work supports the further development of simple model proteins to study aspects of Complex III mechanism.

Degree Type
Dissertation

Degree Name
Doctor of Philosophy (PhD)

Graduate Group
Biochemistry & Molecular Biophysics

First Advisor
P. Leslie Dutton

Keywords
Complex III, maquette, electron transfer, protein design

DECONVOLUTING THE ENGINEERING AND ASSEMBLY INSTRUCTIONS FOR COMPLEX III ACTIVITY

Sarah Chobot Hokanson

A DISSERTATION

in

Biochemistry and Molecular Biophysics

Presented to the Faculties of the University of Pennsylvania

in

Partial Fulfillment of the Requirements for the

Degree of Doctor of Philosophy

2010

Supervisor of Dissertation:	Graduate Group Chair:
_____	_____
P.Leslie Dutton, Ph.D., FRS Eldridge Reeves Johnson Professor of Biochemistry and Biophysics and Director of the Johnson Foundation for Molecular Biophysics	Kathryn Ferguson, Ph.D. Associate Professor of Physiology and Chair, Biochemistry and Molecular Biophysics Graduate Group

Dissertation committee:

Jane M. Vanderkooi, Ph.D., Professor of Biochemistry and Biophysics

Feng Gai, Ph.D., Associate Professor of Chemistry

S. Walter Englander Ph.D., Jacob Gershon-Cohen Professor of Medical Science and Professor of Biochemistry and Biophysics

Cecilia Tommos, Ph.D., Research Assistant Professor of Biochemistry and Biophysics

Tomoko Ohnishi, Ph.D., Professor of Biochemistry and Biophysics

Marilyn Gunner, Ph.D., Professor of Physics (City College of New York)

Deconvoluting the engineering and assembly requirements
for Complex III assembly

To Les, for believing in second chances and in me

and
To Chris, the patron saint of patience

Acknowledgements:

I came to Penn from the very supportive research environment of the Elliott laboratory at Boston University, and I must thank Sean (HP) for believing in my abilities as a science major when countless others (including me) had their doubts. Sean, I would not be writing this thesis without your influence and support. But most importantly, I must thank you for making me apply to Penn, and more importantly, for not letting me apply to Clemson. I will finally admit that perhaps you knew what you were doing all along when you pushed me to believe in my own potential, and I certainly appreciate the impact your mentoring has had on my development as a scientist.

I applied to Penn to work for Dr. P. Leslie Dutton, and I am so pleased that I joined his laboratory to complete this thesis work. Les, you are a fabulous force of nature far beyond anything I could have ever expected. It has been my pleasure to learn from you over the last five years, and I continue to be in awe of you and all that you have accomplished with your life in and outside of the laboratory. Though you are undoubtedly a brilliant scientist that will be remembered for your contributions to the fields of electron transfer and protein design, your legacy for me will always be your charm and vibrant personality that truly inspires people to be excited about science. It is also worth noting that your attention to every detail is spectacular, and I can only hope to develop this skill as I move on to do future experiments as a post-doc. Your laboratory has given me every opportunity to succeed, and has shaped my career as a scientist. Thank you not just teaching me scientific concepts and techniques, but how to approach questions with unwavering enthusiasm and creativity.

I have always said that alongside every successful Les Dutton, there must be a Chris Moser. I am so glad this principle continues to be true. Chris, without your patience and willingness to share your (seemingly unlimited) breadth of knowledge, this thesis would just be a string of "Friday afternoon experiments" that seemed interesting to me rather than the complete story that it has become. I have enjoyed our time together, and I will sincerely miss working and talking with you on a daily basis.

The Dutton laboratory is a very collaborative place, and I am so glad to have worked alongside such talented scientists on many different projects. Bohdana - I appreciate all of the time you spent teaching me laboratory techniques, particularly during my time as a rotation student. Your mentorship on the AP6 project pushed me to be a better scientist, and so much of my success with those experiments was due to your encouragement and guidance. Greg and Paul - you are two of the most capable students I have worked with, and I know great things lie ahead for you as you move forward to graduate programs. Thank you for your help with AP6. Ross, Lee, Tammer, and Bruce – thank you for sharing your protein, quinone, and heme stocks for my quinol-cyt.*c* oxidoreductase assay, and for helpful discussions as my experiments using soluble maquettes took shape. Molly – best of luck to you as you complete your thesis. I know you'll continue to be a rock star. And finally, to Doug and Haibo – I will always be a member of "team bc_1" first and foremost, and both of you were sources of support and encouragement that I could not have lived without during my bumpy set of bc_1 experiments. Our discussions (and time spent at conferences) kept me sane when it seemed like nothing would ever work.

I also had the pleasure of working with collaborators at universities near and far, and those discussions were crucial to the development of my thesis project, as well as my personal development as a scientist. Much of my electron transfer calculations were done in conjunction with ongoing experiments in the Weiner and Cecchini laboratories, and their perspective as EPR spectroscopists taught me a whole new way of thinking about electron transfer reactions in proteins. I also had several wonderful discussions with Artur Osyczka, Fevzi Daldal, and Colin Wraight as I developed my Complex III projects, and their input really helped me appreciate many aspects of the large field of Complex III bioenergetics how my work contributed to it.

I really appreciate the support and guidance of my thesis committee members: Dr. Jane Vanderkooi, Dr. S. Walter Englander, Dr. Feng Gai, Dr. Cecilia Tommos, Dr. Tomoko Ohnishi, and Dr. Marilyn Gunner. My committee members have always provided excellent feedback during our sessions together, and I consistently looked forward to meeting with them. I would also like to thank Dr. Gunner for serving as my external reviewer during the final stages of my dissertation. It has been a pleasure to interact with you thus far and I am so grateful that you took time out of your busy schedule to be a part of my thesis defense.

It is a shame that there isn't a section in our manuscripts or talks for those people in our lives that co-author the moral support portion of our work. I am pleased to finally have an appropriate space to talk about the people outside of the laboratory who bring out the very best qualities in me simply by offering me their unconditional love and support. My family is comprised of my biggest fans, and they have always believed in me (even if they didn't always understand when I explained what I was working on). The support of

my parents, my sister, and my extended family means so much to me, and I am so lucky that they are such a big part of my life. I love all of you very much. My three best friends, Kristen, Elliot, and Victoria, are the glue that holds me together in both good times and in stressful times. I always feel close to all of you, even though we are cities apart. And finally, I must thank the love of my life, my husband David. I never expected that the best thing to come out of graduate school would be our marriage, but then again, before I met you, I also wasn't fully aware that life existed outside of the laboratory doors. Though you are a fantastic scientist yourself, your contribution to this thesis work is ironically that you were able to tear me away from it every now and again. (Though maybe when I am a post-doc, I will let you teach me more about molecular biology.) You continually make me a better and more complete person, and I am so happy that we found one another.

ABSTRACT

DECONVOLUTING THE ENGINEERING AND ASSEMBLY INSTRUCTIONS FOR COMPLEX III ACTIVITY

Sarah Chobot Hokanson

P. Leslie Dutton, Ph.D., FRS

In respiratory systems, membrane-bound Complex III catalyzes the oxidation of ubiquinone and the reduction of a soluble cytochrome with the bioenergetic formation of a transmembrane proton gradient ($\Delta\mu_H+$). Complex III turnover is initiated by a unique two electron oxidation of ubiquinone at the Qo site; one electron is delivered to a high potential chain containing an iron-sulfur cluster, cytochrome c_1 and cytochrome c_2, and a second electron is transferred to a low potential chain that terminates at the Qi site. All Complex III electron tunneling reactions are reversible, and a critical part of Complex III maintaining productive turnover is its suppression of energy-wasting reverse electron transfer reactions. The key to uncovering the controversial mechanism of Qo oxidation is determining how Complex III is regulated such that productive electron-transfer steps overwhelm unproductive steps.

This thesis focuses on understanding the structural and biochemical tolerances of the redox cofactors in Complex III and applying that knowledge towards the design of a simple, but robust, amphiphilic maquette that is capable of transmembrane proton and electron transfer. In chapter two, kinetic studies of heme c_1 mutants reveal that *R. sphaeroides* Complex III is engineered to withstand large changes in heme c_1 active site residues while still preserving heme c_1 midpoint potential and enzyme turnover. In

chapter three, the maquette approach was applied toward developing a simple model protein (AP6) that retained the minimum engineering requirements for Complex III electron and proton transfer reactions but lacked the complexity found in the natural system. The AP6 peptide assembles as a four-α-helix bundle protein and can potentially bind up to six hemes tightly across a membrane interface. Chapter four demonstrates that AP6 successfully performs quinol-cytochrome *c* oxidoreductase activity in hundreds of milliseconds. AP6 is the first example of a synthetic enzyme capable of near-natural turnover rates. Chapter five focuses on defining the thermodynamic limit for maquette activity. This work supports the further development of simple model proteins to study aspects of Complex III mechanism.

Table of Contents

List of Illustrations

Chapter 1

Chapter 2

Chapter 3

Chapter 4

Chapter 5

Chapter 6

Figures

List of Tables

Chapter 2

Chapter 3

Chapter 4

Chapter 5

Chapter 1: Introduction

Thirty years ago, Peter Mitchell won the Nobel Prize for the development of the Q-cycle model that advanced our understanding of Complex III. While the principle tenets of his Q-cycle still hold true today, Mitchell did not explain the specific mechanism that allows the Qo site to perform this Q-cycle efficiently without undue energy loss. Though much speculation on Qo site mode of molecular action and regulation has been introduced over the thirty years after Mitchell collected his Prize, no single mechanism has been universally accepted. In this introductory chapter, the history behind the search for the true Qo mechanism is discussed, and the current models for the mechanism of Complex III electron tunneling reactions are examined. Portions of this chapter have been included in the following references [1, 3, 4] and are reprinted with permission from SpringerLink, the *Journal of Bioenergetics and Biomembranes* [3, 4], and *Biochimica et Biophysica Acta – Bioenergetics* [1].

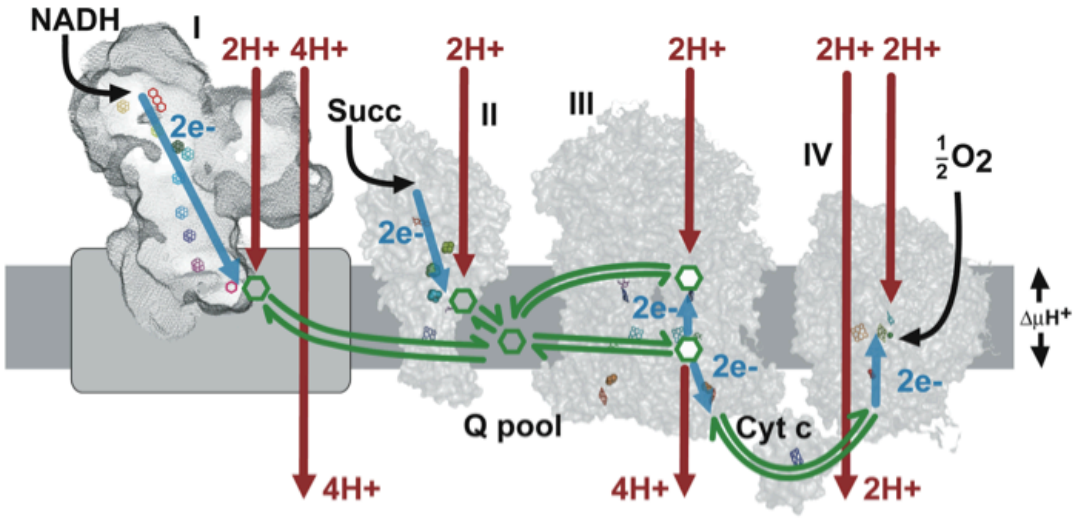

Figure 1.1: A contemporary view of the mitochondrial respiratory chain, which contains (left to right) Complex I, Complex II, Complex III, cytochrome *c*, and Complex IV. Blue arrows indicate electron tunneling pathways, red arrows indicate the direction of proton translocation, black arrows indicate the arrival/placement of substrate molecules, and green arrows indicate the position and movement of quinone molecules. This figure was modified from a figure presented in *Biochimica et Biophysica Acta – Bioenergetics* [1].

1.1 A summary of mitochondrial respiration

We now mostly understand the basic electron tunneling reactions (Figure 1.1 blue arrows) that connect the complexes within the mitochondrial respiratory chain together. In Complexes I and II, flavin-containing nicotinamide adenine dinucleotide (NADH) and succinate dehydrogenase sites are connected via ubiquinone sites in the membrane domain. These sites collect single electrons of the tunneling chains into pairs for two electron and two proton quinone oxidation-reduction before exchanging with a membranous quinone pool. Complex III interacts with the quinone pool via two ubiquinone oxidation-reduction sites, Qo and Qi, Once reduced Qo is bound to Complex

III, one electron reduces cytochrome c_1 while the other electron equivalent passes through two *b*-type hemes and reduces a quinone molecule at the Qi site. In the terminal Complex IV, cytochrome *c* electron transfer leads to dioxygen reduction.

Although the overall stoichiometries of redox-linked proton exchange (red arrows, Figure 1.1) are known, the basics these are coupled to the electron tunneling reactions of ubiquinone (Complexes I, II and III) or dioxygen (Complex IV) that generate the transmembrane electrochemical proton gradient ($\Delta\mu_H+$) remain undefined and controversial. The most information is known about Complex IV, as the key intermediate redox states of the stepwise four-electron reduction of dioxygen have been resolved structurally [7, 8] and spectroscopically [9-11]. However, the molecular mechanism of its driven proton pump remains to be determined. Information about the operation of the Qs site in Complex II is limited [12]; most experiments have been focused on the redox chemistry of its FeS clusters [13, 14] and heme *b* [15-17] instead. Incomplete structural information available for Complex I has limited the resolution of its proton pumping mechanism, though several hypotheses exist in the literature at present [18-23]. One of the most controversial questions left unanswered about the operation of the mitochondrial respiratory chain is the molecular mechanism of ubiquinone oxidation-reduction, proton exchange and energy coupling at the Qo site in Complex III. In sharp contrast to Complex IV, the redox intermediate states of Qo have proven difficult to access, lack clear spectroscopic signatures, and remain highly uncertain.

1.2 Redox cofactors in the mitochondrial respiratory chain

Energy obtained by electron transfer through the mitochondrial respiratory chain is also used to pump protons from the mitochondrial matrix into the intermembrane

space, creating an electrochemical proton gradient across the mitochondrial inner membrane ($\Delta\mu_H+$). This electrochemical proton gradient allows adenosine triphosphate (ATP) synthase to use the flow of protons to generate ATP from adenosine diphosphate (ADP) and inorganic phosphate. In the absence of ADP, protons cannot flow back to the matrix, and the pH and electrical gradients are at maximum. As respiration with outward proton pumping proceeds, the free energy change for proton expulsion increases and approaches the magnitude of that for electron transfer. When the coupled reaction becomes non-spontaneous, respiration stops, and this state is called a static head. The formation of reactive oxygen species is supported by static head conditions in the mitochondrial respiratory chain [24].

There are many different types of redox-active cofactors responsible for proton-coupled electron transfer reactions within the mitochondrial respiratory chain. These cofactors span a wide range of midpoint potentials, and are linked together in long chains that extend over long distances within these proteins to link together remote catalytic sites.

1.2.1 Quinones. There are two main types of quinones found in biological systems – benzoquinones and naphthoquinones. Ubiquinone is a lipid-soluble benzoquinone with a long isoprenoid side chain. Plastoquinone and menaquinone are ubiquinone analogs found in plant chloroplasts and bacteria respectively. Quinones can participate in one or two electron transfer processes coupled to the transport of one or two protons. Therefore, there are three different redox states that exist for quinone cofactors – quinone (oxidized), semiquinone (half reduced), quinol (fully reduced) – and three corresponding protonation states for each redox state. All nine quinone states are

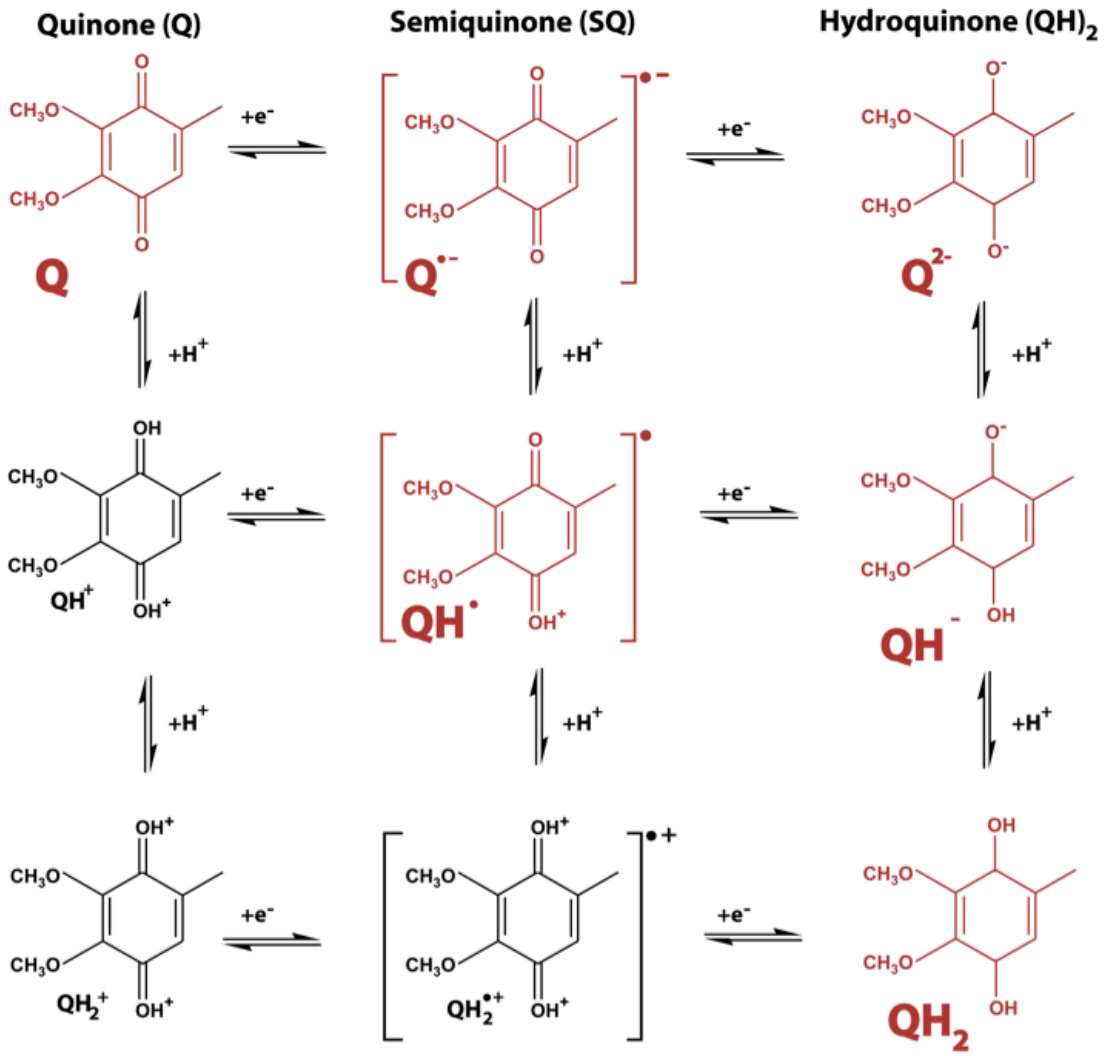

Figure 1.2: Thermodynamic box of nine possible ubiquinone redox/protonation states (ubiquinone is drawn here without its isoprenoid side chain). Shown in red are the quinone states that have been observed in biological systems, while shown in black are thermodynamically unfavored states. This figure was modified from a similar figure shown in the thesis of Bruce Lichtenstein [2].

depicted in Figure 1.2, though only the states depicted in red have been observed in biology.

Quinones are regulated in membrane complexes through the stability of their semiquinone redox state, which is related to the redox potential difference between their

QH_2/SQ and SQ/Q couples. The stable equilibrium constant for the intermediate semiquinone state at complete redox equilibrium is referred to as a semiquinone stability constant, or K_{stab}:

$$K_{stab} = \frac{[SQ]^2}{[Q][QH_2]} = 10^{(E_mSQ/QH_2 - EmQ/SQ) / 0.06}$$

Equation 1.1

Log Kstab values greater than one mean that the semiquinone is a dominant species during a redox titration, while log $K_{stab} < -4$ means that the semiquinone will be barely observable spectroscopically, if at all.

1.2.2 Hemes. Hemes consist of an iron ion coordinated to a large heterocyclic organic ring called a porphyrin. The most common porphyrin scaffold in biology is protoporphyrin IX (PPIX), otherwise known as heme *b*. The heme *b* biosynthesis pathway is highly conserved across biological organisms, and is initiated in the mitochondrion by the synthesis of D-aminolevulinic acid (dALA) from glycine and succinyl-CoA.

In addition to heme *b*, there are two other main forms of hemes found in the mitochondrial respiratory chain. *c*-type hemes contain a modified FePPIX where the two vinyl side chains are uniquely covalently attached to cysteine thiol residues within the protein. In the mitochrondrial respiratory chain, heme *c* is most notably found in the cytochrome c_1 subunit of Complex III and its redox partner, cytochrome c_2. Heme *a* is found in Complex IV, and is also synthesized through modification of FePPIX. The C-8 methyl group of FePPIX is oxidized into a formyl group and the vinyl group on C-2 is converted into a hydroxyethylfarnesyl side chain.

1.2.3 NAD^+ / $NADP^+$. Nicotinamide adenine dinucleotide (NAD^+) and its close analog nicotinamide adenine dinucleotide phosphate ($NADP^+$) consist of two nucleotides joined by a pair of bridging phosphate groups. The plus sign in the abbreviations for these cofactors does not indicate their net charge, but rather that the nicotinamide ring is in its oxidized form with a positive charge on the nitrogen atom. Both cofactors undergo reversible reduction of the nicotinamide ring. As a substrate molecule undergoes oxidation, the oxidized form of the nucleotide accepts a hydride ion (or the equivalent of a proton and two electrons) and is transformed into the reduced form (NADH or NADPH). More than 200 enzymes are known to catalyze reactions in which NAD^+ (or $NADP^+$) accepts a hydride ion from a reduced substrate, or NADH (or NADPH) donates a hydride ion to an oxidized substrate. In Complex I, hydride transfer from NADH to a bound quinone cofactor initiates the proton pumping mechanism of the mitochondrial respiratory chain.

1.2.4 FAD / $FADH^{\bullet}$ / $FADH_2$. Flavin adenine dinucleotide (FAD) consists of a riboflavin moiety that is bound to the phosphate group of an ADP molecule. The fused ring structure of the flavin also undergoes reversible reduction, accepting either one or two electrons in the form of one or two hydrogen atoms (each atom is the equivalent of one electron and one proton) from a reduced substrate. After one electron transfer reaction, like quinones, FAD can form a semiquinone state. This semiquinone state also has an equilibrium-based stability constant related to the two redox couples of the flavin moiety. FAD is covalently bound to Complex II, and is responsible for initiating Complex II electron transfer via the oxidation of succinate to fumarate.

1.2.5 FeS cluster. In FeS clusters, iron molecules are present in association with inorganic sulfur atoms or with the sulfur atoms of cysteine residues, or both. There are three main structural motifs of biological FeS clusters, though exceptions do exist in hydrogenase enzyme families. The simplest FeS cluster is the [2Fe-2S] cluster, which is comprised of two iron ions bridged by two sulfide ions and coordinated by four cysteine-based thiol ligands. [4Fe-4S] clusters feature four iron ions and four sulfide ions placed at the vertices of a cubane-like structure. In these FeS clusters, the iron ions are typically coordinated by cysteine thiol ligands. Finally, proteins also coordinate 3Fe-4S centers, which feature one less iron ion than the more common [4Fe-4S] form. Three sulfide ions bridge two iron ions each, while the fourth sulfide bridges three iron ions. Complexes I and II each contain combinations of these different types of FeS clusters. Complex III contains a variation of a [2Fe-2S] cluster, where two histidine residues, rather than two cysteine thiol groups, coordinate one of the two iron atoms. This type of [2Fe-2S] cluster is named for John Rieske, after the Complex III iron-sulfur protein (ISP) domain was isolated in 1964 [25, 26].

1.3 Complex III – what we know

In 1976, Peter Mitchell developed the Q-cycle theory, which explained how the proton coupled electron transfer of Complex III was driven by its ubiquinone cofactors [27, 28]. According to Mitchell's proposal, which also incorporated the previous observation of "oxidant-induced reduction of cytochrome *b*" by Chance [29] and a suggested role for semiquinone by Wikstrom and Berden [30], a reduced quinone molecule at the interface between the high and low potential chains of Complex III (bound at the Qo site) initiates a bifurcated electron transfer reaction upon its oxidation.

One electron is accepted by the iron-sulfur cluster (FeS), and follows the *c*-chain via cytochrome c_1 to external *c*-type cytochromes (Figure 1.3). The other electron passes through two *b*-type hemes and reduces a quinone molecule at the Qi site. This unique

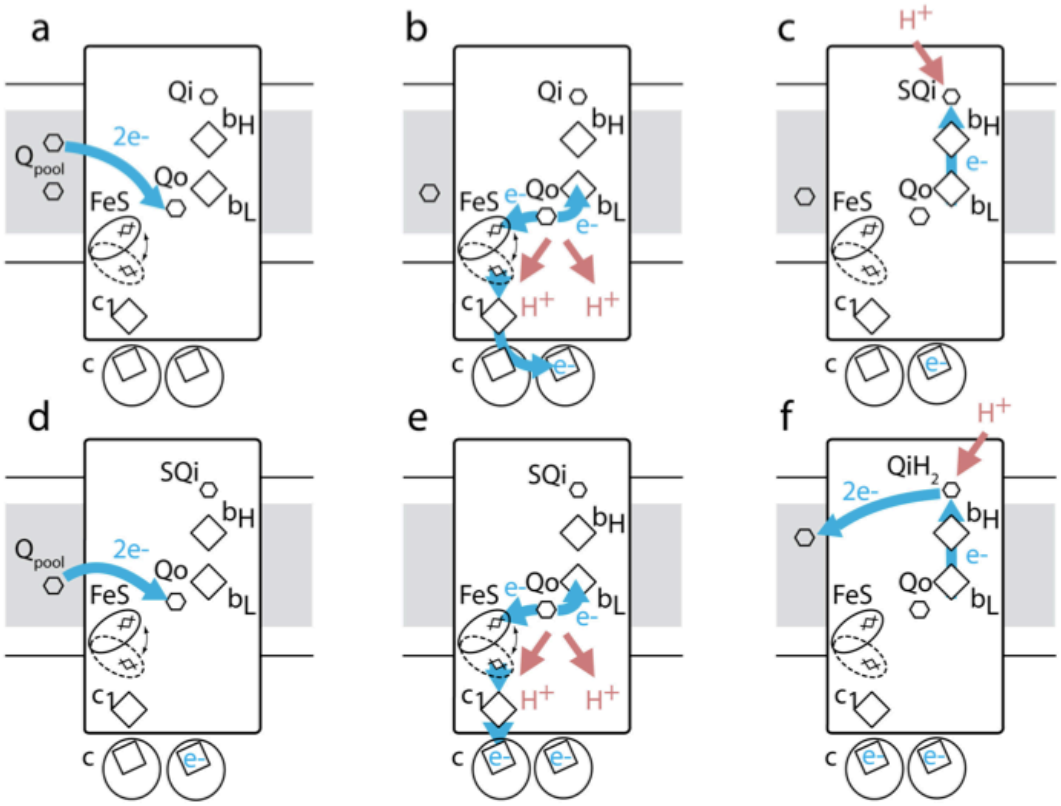

Figure 1.3: Each panel represents a step in the electron and/or proton transfer process of one complete Q-cycle (Complex III is represented here as a monomer for simplicity). a) One reduced quinol molecule is delivered to the Qo site from the Q-pool. b) The Qo site becomes oxidized, transferring two protons across the membrane and distributing two electrons to the high and low potential chains of bc_1. c) A proton and electron are delivered to the Qi site, forming a stable semiquinone intermediate. d) The Q-pool delivers another reduced quinol molecule to the Qo site to restart Complex III turnover. e) The Qo site turns over again, delivering a second set of electrons to the high potential *c*-chain and the low potential *b*-chain, as well as two more protons across the membrane. f) Upon receiving an additional proton and an electron from heme b_H, the Qi semiquinone becomes fully reduced, and delivers a reduced quinol back to the Qpool. The net result of this cycle is oxidation of one quinol, reduction of two cytochromes *c*, two electrogenic transmembrane electron transfers, uptake of two protons from one membrane face and delivery of 4 protons to the other. Reprinted with permission from SpringerLink and the *Journal of Bioenergetics and Biomembranes* [3].

electron split sets into motion a quasi-equilibrium state of Complex III that balances the redox potentials of the high potential c-chain and low potential *b*-chain evenly on either side of the redox potential of the quinone pool. This quasi-equilibrium behavior shows that Complex III catalysis is rapidly and readily reversible [6]. Collapse of this quasi-equilibrium into complete equilibrium, in which all chains and pools reach the same redox potential, takes place on a tens of seconds timescale and can be assisted by the short-circuiting action of redox mediator dyes.

Under normal forward electron transfer conditions**,** the efficiency of Complex III turnover is high, and deleterious short circuit or bypass reactions involving either Qo or heme b_L are minimal [31]. Short circuit reactions are defined as any electron transfer reaction between two Complex III cofactors that results in an unproductive loss of energy [6]. Alternatively, bypass reactions result when the electron transfer processes at the Qo site are intercepted by an extraneous reagent, such as oxygen, which steals the electron from Complex III and initiates harmful side reactions that produce reactive oxygen species [32, 33]. In order for the Qo site to be efficient, these reactions must be suppressed, even though the driving forces for these reactions are highly favorable. Understanding Qo site engineering means understanding how electron transfer is regulated such that productive electron-transfer steps overwhelm unproductive steps.

1.3.1 Considering Qo movement in its active site. Crystal structures have failed to convincingly resolve oxidized or reduced quinone in the Qo site [34-36]; in fact, the Qo site appears to be large enough to potentially accommodate two sequential positions for a moving ubiquinone headgroup [24, 37], or conceivably bind multiple ubiquinones at the same time [38-40]. However, we do know that whatever the specific

electron tunneling distances between Qo-FeS and Qo-b_L are, the distances in Complex III in general are engineered to allow for millisecond Qo oxidation and avoid short-circuit reactions that would be a danger even to a concerted mechanistic model, such as direct electron transfer between FeS and b_L.

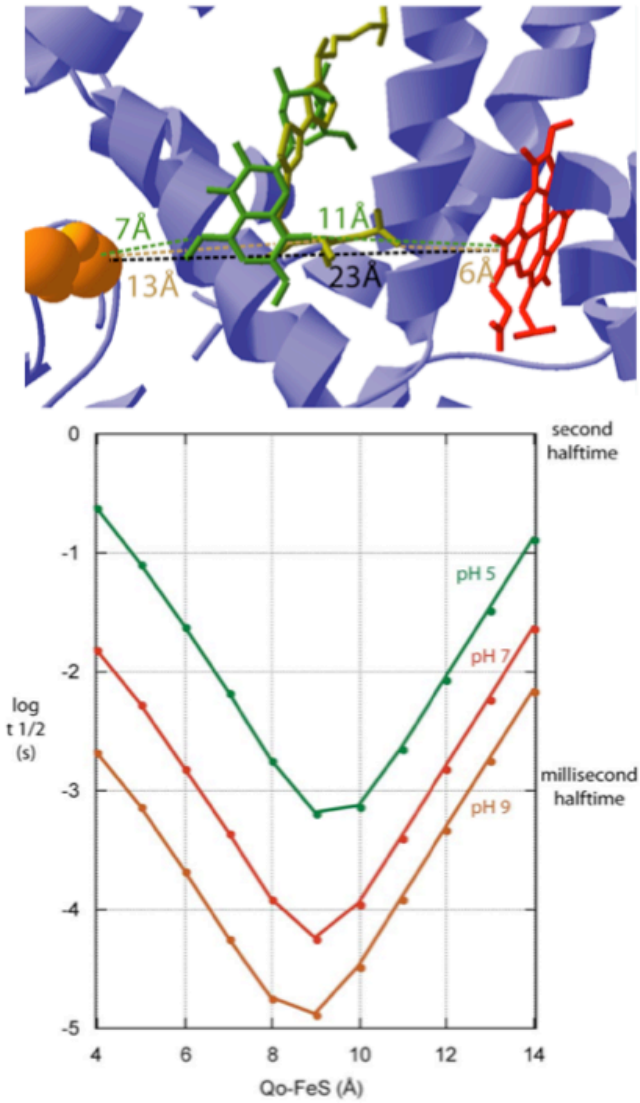

Figure 1.4 (top panel): Crystal structure of FeS-Qo-b_L active sites, drawn from PDB file 1PPJ [5]. Heme b_L is depicted in red, the FeS cluster is drawn in orange, and two Qo site inhibitors myxothiazol (yellow) and stigmatellin (green) are shown bound in the Qo site. Distances between the cofactors were calculated using Pymol, where 23 Å represents the distance between the FeS cluster and b_L , 7 and 11 Å represent stigmatellin distances from the FeS cluster and b_L respectively, and 13 and 6 Å represent myxothaizol distances from the FeS cluster and b_L respectively. (bottom panel) The halftime of b_L reduction (s^{-1}) vs. Qo-FeS distance.

Shown in Figure 1.4 are two Qo inhibitor molecules, myxothiazol (yellow) and stigmatellin (green), bound at the Qo site, with their respective distances to the other cofactors measured using Pymol software [41]. Myxothiazol binds closer to b_L in the Qo niche than stigmatellin does, and could still allow some quinone to approach the Qo pocket distally. This could explain the observations in the literature that myxothiazol has no effect on the semiquinone signal attributed to Qo [42], and permits considerably more superoxide production by Complex III than stigmatellin [43, 44].

As described in the Appendix, the Dutton laboratory has developed an electron transfer rate expression that offers a simple way to examine parameters that directly relate to the oxidoreductase activity of a particular mitochondrial enzyme [1, 45, 46]. The Moser-Dutton equation defines the rate of electron transfer as a function of distance (R), midpoint potential (included in ΔG°), reorganization energy (λ), and protein packing density (ρ). Using this equation, a range of Qo-FeS distances can be considered to determine the effect changing the location of Qo in its active site has on the rate of b_L reduction. Figure 1.4 depicts the halftime of heme b_L reduction vs. Qo-FeS cluster distance and demonstrates that millisecond b_L reduction rates are maintained as long as the Qo-FeS distance falls between 6 and 11 Å at pH 7. Though it is well-established that the uphill electron tunneling step between reduced Qo and the FeS cluster is rate-limiting as long as Qo falls within this 6-11 Å range [47], should Qo favor binding more closely (within 4 Å) to the FeS cluster, Qo to b_L electron tunneling becomes rate limiting and slows b_L reduction by two orders of magnitude. Likewise, should Qo bind closely to the b_L heme, Qo oxidation rates are limited by Qo-FeS cluster electron tunneling. This general trend is upheld using equilibrium midpoint potentials at several different pH

values, though the reaction rates for Qo oxidation increase as the pH becomes more alkaline, increasing the range of FeS-Qo distances that will maintain millisecond catalysis.

1.3.2 Previous models for Qo site mechanism. Without the direction of structural information on Qo binding, a range of mechanistic models has emerged with no real consensus as to which one is the most successful. The work of Osyczka *et al*. prompted revision of all contemporary Q-cycle models in order to accommodate suppression of unwanted short-circuits in a reversible, energy-coupling mechanism evident in Complex III [6, 48]. However, it was made clear that models that are truly concerted two-electron transfer reactions [6], with no detectable semiquinone intermediate state on more than a femtoseconds timescale, were not prone to the same kind of short circuit possibilities as sequential models that included a semiquinone intermediate state [47, 49]. Therefore, all sequential mechanisms that exploit the properties of a semiquinone intermediate [24, 48, 50-52], must be modified to include effective gating mechanisms, sensitive to different combinations of redox states of the FeS, Qo and heme b_L redox partners, to promote productive catalysis and prevent unproductive short-circuits.

While there are numerous ways that reversible Q-cycle models can be modified to impede short circuits, Osyczka *et. al*. made it clear that a minimum of two gates or barriers are mandatory to regulate Qo redox states. This model has been amplified by Peter Rich, who introduced a double, "logic gated" electron transfer model for Qo site electron transfer [52]. In short, this model suggests that reduced quinone is forbidden from binding in the Qo site if FeS and heme b_L are not both oxidized, and oxidized

quinone is forbidden from binding if both of its redox partners are not reduced. This can, in principle, be achieved by regulation of oxidized and reduced quinone binding by manipulation of the conformations of Qo hydrogen bonding partners by the redox and protonation states of heme b_L and FeS (see also [6, 48].

Crofts *et al*. modified their sequential mechanism [53] to introduce more redox-state sensitive gating to avoid short circuits [24, 50]. They propose that when a semiquinone intermediate is formed, it can move closer to oxidized heme b_L and participate in productive electron transfer. However, when heme b_L is reduced, there is a Coulombic repulsion which keeps the semiquinone away from reduced heme b_L, towards the FeS end of the site, and inhibits the unproductive, and energetically favorable, short-circuit reduction of semiquinone by heme b_L. While in principle Coulombic interactions could provide a redox-state sensitive gate to inhibit a short-circuit reaction, more than one gate is needed. The Coloumbic push of semiquinone from reduced heme b_L moves it closer to FeS, which when oxidized, can accept an electron from the semiquinone in another type of short circuit. A second gate for this type of model requires the FeS and semiquinone to overcome their coulombic *attraction* and enter some sort of conformation to prevent energetically favorable, but wasteful electron transfer. In addition, the site must be designed to overcome a coulombic *repulsion* between semiquinone and reduced FeS. This would allow a favorable interaction between semiquinone and reduced FeS, fostering productive and rapid reverse reactions in which oxidized quinone is doubly reduced by FeS and heme b_L

1.3.3 Possibilities for Qo site thermodynamics. The thermodynamics of concerted and sequential mechanisms are distinctly different even in wild-type Complex

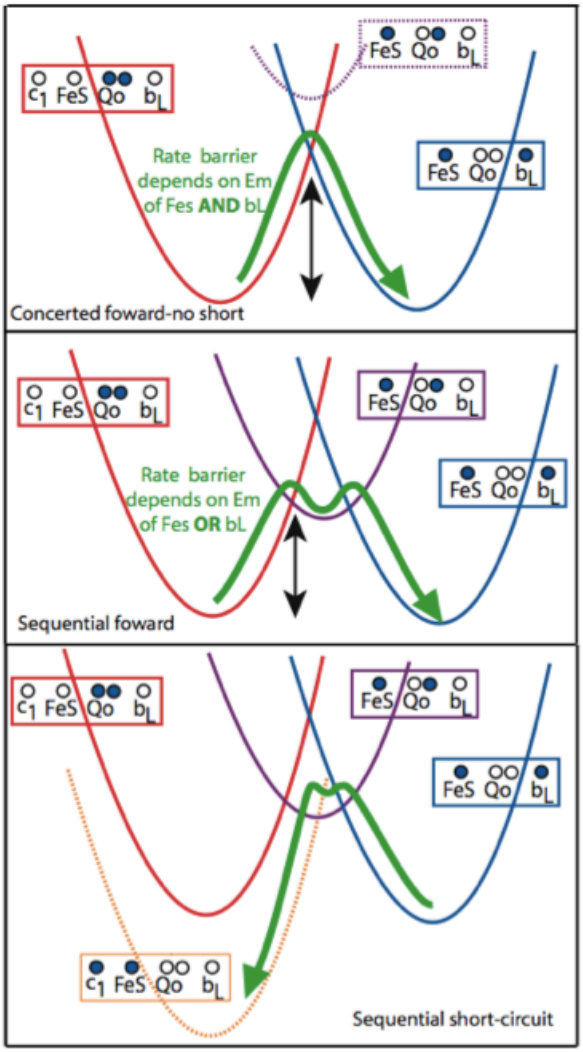

Figure 1.5: Electron transfer reaction energy surfaces for Qo site operation by concerted and sequential mechanisms. Marcus-like parabolic potential surfaces are shown for each redox state. In a concerted reaction (top), electron transfer to form a semiquinone state (purple) takes more thermal energy than forming the two-electron transition state. In a sequential mechanism (middle), electron transfer to form a semiquinone intermediate state takes less energy than the simultaneous two electron transfers, but leaves Complex III potentially exposed to highly exergonic short-circuit reactions such as the one illustrated in the bottom panel. Reprinted with permission from SpringerLink and the *Journal of Bioenergetics and Biomembranes* [3].

III. Figure 1.5 illustrates that the energetic landscape for a concerted mechanism at Qo has an activation barrier that depends on both FeS *and* heme b_L redox midpoint potentials[3]. In this mechanism, the activation barrier for forming the semiquinone

intermediate (purple curve) is significantly higher; normally semiquinone formation would be minimal, but not impossible. In contrast, the sequential mechanism will have a reduced quinone oxidation rate that depends on *either* the midpoint potential of the FeS *or* the heme b_L. Experimentally, changing the midpoint potential of the FeS often changes the rate; however, changing the heme b_L midpoint potential has proven more difficult and the changes that have been made are modest. Thus, how or if the heme b_L midpoint potential affects the rate is still unclear.

The bottom panel of Figure 1.5 illustrates the energetic picture of one of the short-circuit reactions [3]. The rapid reversibility of the reactions at the Qo site means reverse electron transfer is on roughly the same timescale as the forward reaction, and will reform the same amount of semiquinone that is formed by the initial electron transfer between Qo and the FeS cluster. However, the short-circuit reduction of reoxidized FeS is highly favorable and energetically disastrous; if Complex III is operating by a sequential mechanism, redox-state activated gates must be present to avoid unproductive short-circuit reactions.

1.3.4 Previous attempts to isolate SQo. Direct observation of a Qo semiquinone state has proven to be extremely controversial due to the limitations in measuring such an unstable state. In 1979, Takamiya and Dutton redox-poised *R. sphaeroides* membranes and extracted the quinone cofactors to determine the amount of quinone oxidized and the amount reduced as a function of poised redox potential [54]. From these experiments, they defined the size and redox potential of the quinone pool: 19 out of 25 quinones per reaction center had a midpoint potential at pH 7 of 90 mV. They

also examined the redox-poised membranes for evidence of a Qo semiquinone by EPR spectroscopy, but did not detect a clear signal.

de Vries *et al*. announced the trapping of a Qo semiquinone in mitochondrial Complex III as a 2,3-dimercaptopropanol (BAL)-sensitive signal uncovered under non-equilibrium conditions [55]. BAL chelates heavy metals and is suggested to destroy the Rieske FeS center, allowing for a direct probe of the Qo site. Compared with the antimycin-sensitive semiquinone signal discovered at Qi (g = 2.005, 10 G wide) [56], the signal attributed to Qo in these experiments was narrower (8.8 G), had a slightly different g value (2.006), and required less power to saturate. Since this signal was obtained using non-equilibrium methods, the redox midpoint potential of the semiquinone couples could not be determined. However, Junemann *et al*. revisited these experiments and revealed that de Vries's semiquinone signal was insensitive to a more modern collection of Qo site inhibitor compounds, such as myxothiazol, MOA-stilbene, and stigmatellin [57]. Therefore, based upon this evidence, it remains unlikely the data published by de Vries *et al*. was indicative of a Qo semiquinone state.

In recent years, two new EPR-based approaches emerged and revealed semiquinone signals that were sensitive to stigmatellin, a tight binding Qo site inhibitor. The first approach was explored by Cape *et al*. using anaerobic freeze-quenching techniques after rapid mixing of antimycin-inhibited Complex III isolated from *R. capsulatus* with decylubiquinone in the Qo active site [32]. This stigmatellin-sensitive signal had a g-value of 2.0054 with a 11.9 G line width. Although this signal does appear at or near the Qo site, it does not appear to have a clear magnetic interaction with the

Rieske FeS cluster, raising questions about whether or not it is representative of a true Qo semiquinone intermediate.

The Dutton laboratory explored the second approach; their experiments used light-activated photosynthetic membranes with heme(s) b_L and/or heme c_1 knocked out, deliberately driving the thermodynamics of Qo to maximize semiquinone production [42]. After a series of light flashes, the high potential *c*-chain became highly oxidized in this system, stimulating the oxidation of Qo by the quinone pool and loading the low potential *b*-chain with reducing equivalents. This experimental setup, where the high potential chain is very oxidized, proved to be very favorable for stripping an electron from a second quinol at Qo to form a semiquinone. The g-value of the signal observed under these conditions was determined to be 2.0040 and the line width was 11.7 G. Because the stoichiometry of the redox components involved in the pseudo-equilibrium between the *b*- and *c*-chains and the quinone pool was known, the split between the redox couples for this quinone species was estimated to be approximately 880 mV, with the QH_2/SQ couple ~410 mV at pH 9. Therefore, from this data the effective stability constant for Qo was estimated to be 10^{-15}. However, this data was obtained using chromatophore membranes with massive mutational changes (cofactor knockouts), causing many in the field to argue that this signal, even if it was attributable to a Qo semiquinone, was not indicative of a mechanistic state that could be observed in wild-type chromatophores.

Even though an EPR signature attributed to a Qo semiquinone has been experimentally isolated and characterized, it is not yet clear if this is a legitimate, transient mechanistic intermediate, or a side reaction forced into existence by

experimental design. Therefore, it is still too soon to reject the possibility that the normal Qo site mechanism is concerted, with the transfer of both electrons occurring in a very short interval, leaving no time for an oxidized quinone to relax into any intermediate state.

1.3.5 Complex III activity is unaffected by Qo binding site mutations. The Qo site mechanism is also surprisingly resilient to mutational modifications at the Qo site. Though the mostly conserved glutamate (E) of the Qo active site PEWY sequence is often given a carefully orchestrated role controlling the proton transfer reactions of QH_2 oxidation at the Qo site [24, 50], replacement of the glutamate group with non-polar or even basic groups had almost no effect on any of the equilibrium properties of the Qo site or its redox partners [51]. As the Qo site appears to have residue redundancy that compensates for mutagenic changes easily, a specific network of protons within the active site may not be necessary for preserving productive Qo site electron tunneling. Instead, the tunneling network itself must be designed to raise barriers that suppress unwanted short circuit reactions.

1.3.6 Redox properties of the quinone sites in Complex III. The bifurcated electron transfer that occurs within Complex III is completely dependent upon its ability to modify the redox environment of the ubiquinone pool at each of its quinone binding sites, Qo and Qi. The environment of the Qi binding site forces the quinone redox couples to be very similar. The redox couples and stability constant for Qi have been measured (log K_{stab} is -2.3 at neutral pH) using EPR spectroscopy, and under mildly alkaline conditions, the redox midpoint potentials of the oxidized quinone, semiquinone, and fully reduced quinol can reach equilibrium at equal one third concentrations. At Qo,

the first electron is removed from the reduced quinol at a relatively oxidizing midpoint potential to head down the high potential *c*-chain, while the second electron is removed at a relatively reducing midpoint potential and is transferred to the low potential *b*-chain. Therefore, unlike Qi, the redox couples at Qo have a very large difference in midpoint potential, and a very low K_{stab} value.

As shown in figure 1.6, there are eight possible combinations of redox states for Qo and its redox partners, heme b_L and FeS. Half of these states are equilibrium states readily achieved by simple redox poising (shown in black), and half are non-equilibrium states have yet to be experimentally characterized (shown in red and green). The green states are particularly important since they are the enzyme-substrate and enzyme-product

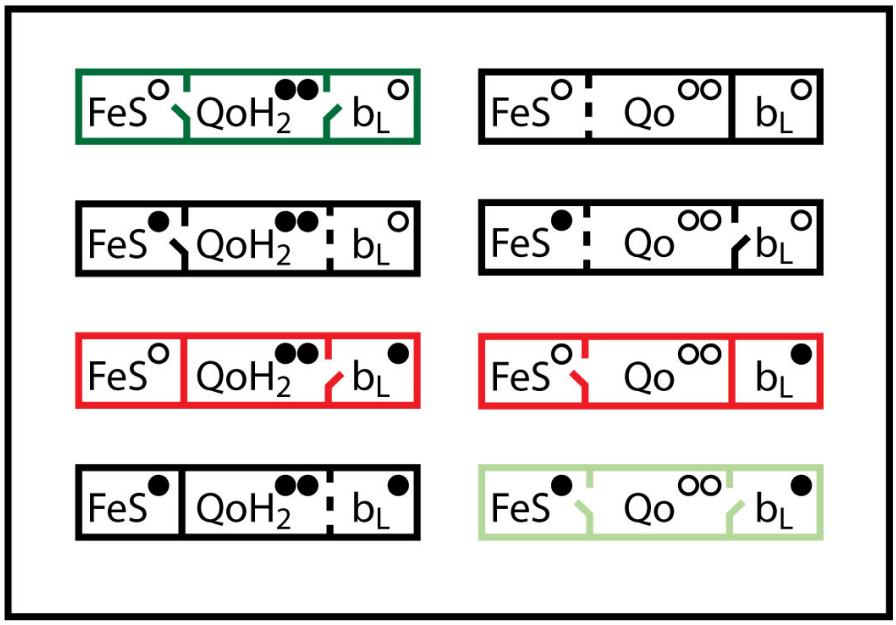

Figure 1.6: Eight possible redox state combinations for the Qo site and its electron transfer partners, FeS and heme b_L. Equilibrium states are shown in black, productive transient intermediates are shown in green, and non-physiological quasi-equilibrium states are shown in red. Solid lines indicate closed gates, and solid lines with a break in the middle indicate open gates for electron transfer. Dashed lines indicate that a gating mechanism is optional for this electron transfer. Reprinted with permission from SpringerLink and the *Journal of Bioenergetics and Biomembranes* [3].

states immediate to physiologically productive quinone oxidation- and reduction-coupled energy transduction at the Qo site, while the states shown in red are subject to short-circuit reactions that are high in driving force and physiologically unproductive. Assuming a sequential-gated Qo site mechanism in this model, the gates controlling semiquinone activity must be open so that catalysis can occur in the green states, while the gates are closed in the red states in order to protect Complex III from short circuiting.

1.3.7 Redox properties of other Complex III cofactors. Understanding the engineering design of Complex III and the operating limits of failure of the Q-cycle requires an understanding of the redox properties of each redox-active component. The redox properties of the cofactors in Complex III are well-described by redox titrations performed across a wide range of pH values, as shown in Figure 1.7 [4]. The FeS cluster has a pKox near neutral pH in both *R. capsulatus* and *R.sphaeroides*. Cytochrome c_1 has pKox and pKred values close to one another near neutral pH, and a weak pH dependency (much less than 1 H^+ / 1 e^-). Previous measurements of the Qpool size and redox properties are included on the left graph as a green dashed line [54], and Qi redox properties were also previously measured under conditions where its semiquinone species is readily accessible by EPR measurements [58].

The Dutton [4] and Crofts [50] laboratories have measured redox prorperties of the *b*-hemes in recent years. Original redox titrations of the *b*-hemes revealed three redox active species [59], which are now resolved in Figure 1.7 as b_L and two different forms of b_H - b_H^{high} and b_H^{low}. Heme b_L displays a strong coupling to protons at acidic pH values, and is pH independent at pH values more alkaline than its pKred (pH ~ 8.5). These redox properties are unchanged in the presence of the Qi inhibitor antimycin. The

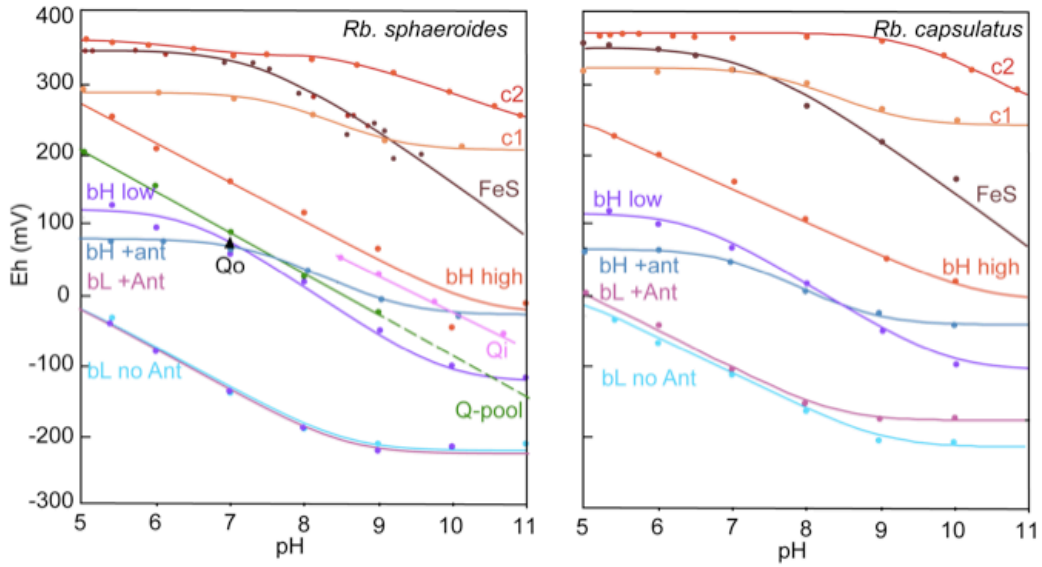

Figure 1.7: Redox midpoint potentials of the components of Complex III in two different species of photosynthetic bacteria as a function of pH, as determined experimentally by Haibo Zhang. Reprinted with permission from SpringerLink and the *Journal of Bioenergetics and Biomembranes* [4].

redox behavior of b_H is directly coupled to the redox state of Qi, and is also altered when antimycin is bound to the Qi site. 80% of heme b_H centers are in the low potential form at acidic pH values, though this number is reduced to 55% at alkaline pH values [4].

1.4 Developing a simple tunneling view of Complex III activity

The redox midpoint potentials and electron tunneling distances of the cofactors in Complex III were inputted into the Moser-Dutton equation to calculate k_{et}. These rates are used to present an an elementary view of Complex III electron tunneling that is expanded upon experimentally in chapter two.

1.4.1 A single turnover view of Complex III electron tunneling. Figure 1.8 shows a single, two electron turnover of Complex III when all of its redox components are oxidized except for the Qo site, with its measured 10^{-15} K_{stab} constant [42] providing

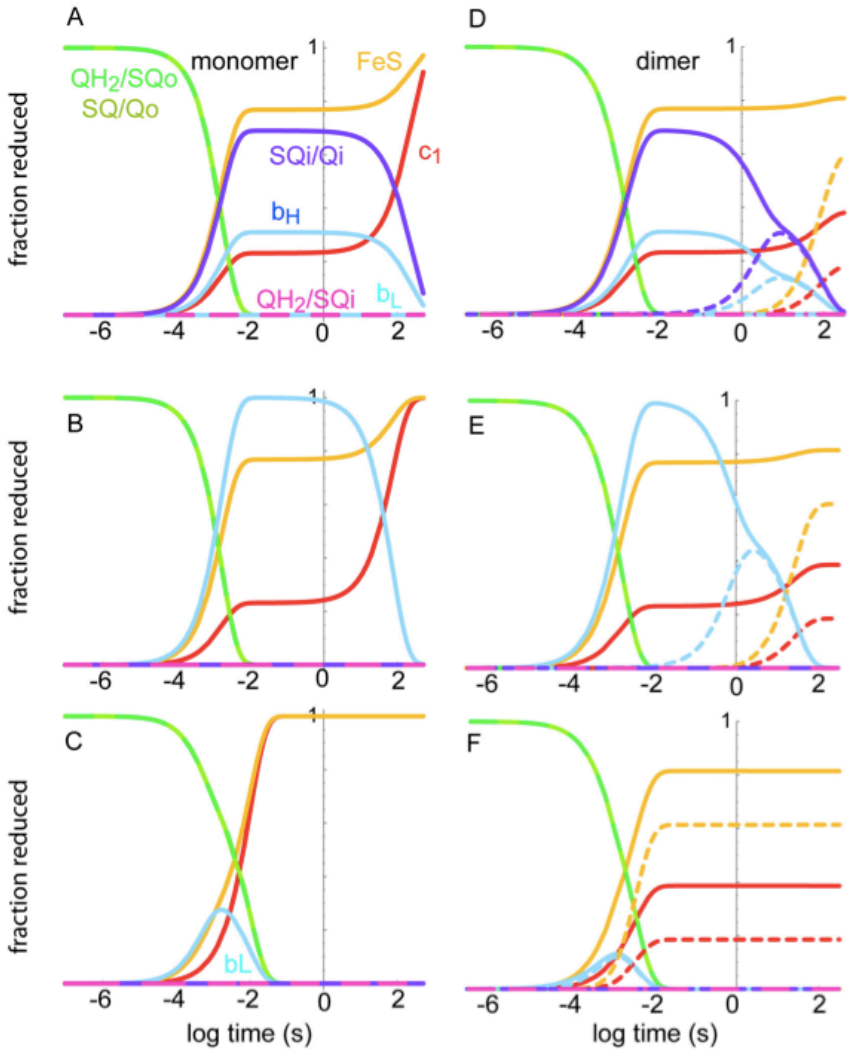

Figure 1.8: Electron tunneling calculations for Complex III. Shown on the left (A, C, E) are rate calculations that assume that Complex III is functional as a monomer, and shown on the right (B, D, F) are those for a functional dimer. Dashed lines in the right-hand side graphs represent the redox centers in the second half of the dimer introduced into the calculations. (A and D) All redox centers considered. (B and E) Calculating all centers except Qi, which has been effectively "inhibited" by extending the electron transfer distance to 50 Å. C and F) Considering site directed mutants where heme b_H is not incorporated [6]. Figure modified from data presented in *Biochimica et Biophysica Acta – Bioenergetics* [1].

for millisecond catalysis of quinone oxidation. FeS is modeled as moving between two sites, distal and proximal to the Qo site with a rate of about 10^5 s^{-1} [60]. Heme b_L is only transiently reduced as the electron comes to reside on heme b_H and Qi. Also, when the

electron can get as far as Qi, short-circuit reactions through reverse reactions and a Qo semiquinone are slowed to a minutes timescale.

These calculations can be modified to include inhibitors or mutations that limit Complex III turnover. For example, the addition of antimycin at the Qi site or b_H knockout mutations can be considered in our system of rate equations. Heme b_H reduction is dominant in the presence of antimycin, with short-circuits still taking place relatively slowly on a tens of seconds timescale (under non-membrane energized conditions), representing what is observed under single turnover flash experiments. However, when heme b_H is knocked out, the electron cannot escape from b_L and is prone to millisecond short-circuit reactions that are comparable to the rate of catalysis. Because rapid short-circuit reactions are not observed experimentally in these knockouts, the redox couples of Qo (and therefore, its stability constant), must be modulated in some way to allow catalysis in certain redox states while making the semiquinone (and therefore, short-circuit reactions) inaccessible in others.

Structurally, Complex III is a dimer, but whether or not it acts as a functional dimer remains controversial. We can compare Complex III as a functional monomer or dimer using the Moser-Dutton equation. With an edge-to-edge spacing of 14.7 Å between the two heme b_L cofactors, functionally significant electron tunneling between the two halves of the dimer could take place on a reasonable timescale. This is shown in the right panels of Figure 1.8, mirroring the conditions described above. Redox equilibration of the low potential chains is shown to take place on a seconds timescale, depending upon the presence of Qi. Short-circuit reactions occur in both halves of the dimer, even though reduced quinone has only been introduced at one of the Qo sites.

However, with the same fixed stability constant, of 10^{-15}, the heme *b* knockout allows the electron to linger on b_L, with cross-dimer redox equilibration occurring on a millisecond timescale. Therefore, the electron tunneling contact between both halves of the dimer is occurs on the same timescale as catalysis, indicating that Complex III has effectively increased the concentration of active Qo sites available when the complex is partially reduced.

1.5 Finding new ways to study an old problem

It has been decades since Peter Mitchell developed the Q-cycle mechanism with little resolved about the mechanism of Qo turnover in Complex III. In order to address these unanswered questions, the field of bioenergetics must develop a fresh perspective and new experimental techniques. In chapter two, *R. sphaeroides* Complex III proteins with modifications to their heme c_1 are studied to understand how Complex III redox reactions within the high and low potential chains are interconnected.

This thesis also applies the principles of *de novo* protein design towards developing a new model system to study Complex III turnover. In chapter three, the development and characterization of the first functional amphiphilic maquette, AP6, is presented. AP6 extracts the basic engineering requirements from the *b*-subunit of Complex III to perform proton-coupled electron transfer across a membrane interface. In chapter four, AP6 enzymatic function is quantified using standard Complex III activity assays, and AP6 is revealed as the first maquette to achieve activity within two orders of magnitude of a natural protein system. Manipulating the thermodynamics of the rate-limiting quinol to heme electron transfer step in this maquette system is explored in chapter five. Finally, chapter six will conclude with the development of a simple model

for Complex III that can be applied by the field of bioenergetics to study specific Qo redox states.

1.6 References

1. Moser, C.C., et al., *Electron tunneling chains of mitochondria.* Biochimica Et Biophysica Acta-Bioenergetics, 2006. **1757**(9-10): p. 1096-1109.
2. Lichtenstein, B.R., *Graduate Thesis.* 2010.
3. Chobot, S.E., et al., *Breaking the Q-cycle: finding new ways to study Qo through thermodynamic manipulations.* Journal of Bioenergetics and Biomembranes, 2008. **40**(5): p. 501-507.
4. Zhang, H.B., et al., *Quinone and non-quinone redox couples in Complex III.* Journal of Bioenergetics and Biomembranes, 2008. **40**(5): p. 493-499.
5. Berry, E.A. and L.S. Huang, *Observations concerning the quinol oxidation site of the cytochrome bc1 complex.* FEBS Lett, 2003. **555**(1): p. 13-20.
6. Osyczka, A., et al., *Reversible redox energy coupling in electron transfer chains.* Nature, 2004. **427**(6975): p. 607-12.
7. Tsukihara, T., et al., *The whole structure of the 13-subunit oxidized cytochrome c oxidase at 2.8 A.* Science, 1996. **272**(5265): p. 1136-44.
8. Yoshikawa, S., et al., *Redox-coupled crystal structural changes in bovine heart cytochrome c oxidase.* Science, 1998. **280**(5370): p. 1723-9.
9. Adelroth, P., P. Brzezinski, and B.G. Malmstrom, *Internal electron transfer in cytochrome c oxidase from Rhodobacter sphaeroides.* Biochemistry, 1995. **34**(9): p. 2844-9.
10. Karpefors, M., et al., *Formation of the "peroxy" intermediate in cytochrome c oxidase is associated with internal proton/hydrogen transfer.* Biochemistry, 2000. **39**(47): p. 14664-9.
11. Wikstrom, M., M.I. Verkhovsky, and G. Hummer, *Water-gated mechanism of proton translocation by cytochrome c oxidase.* Biochim Biophys Acta, 2003. **1604**(2): p. 61-5.
12. Cheng, V.W., et al., *Alternative sites for proton entry from the cytoplasm to the quinone binding site in Escherichia coli succinate dehydrogenase.* Biochemistry, 2008. **47**(35): p. 9107-16.
13. Cheng, V.W., et al., *The iron-sulfur clusters in Escherichia coli succinate dehydrogenase direct electron flow.* J Biol Chem, 2006. **281**(37): p. 27662-8.
14. Hagerhall, C., et al., *The trinuclear iron-sulfur cluster S3 in Bacillus subtilis succinate:menaquinone reductase; effects of a mutation in the putative cluster ligation motif on enzyme activity and EPR properties.* Biochim Biophys Acta, 1995. **1229**(3): p. 356-62.
15. Tran, Q.M., et al., *Escherichia coli succinate dehydrogenase variant lacking the heme b.* Proc Natl Acad Sci U S A, 2007. **104**(46): p. 18007-12.

16. Tran, Q.M., et al., *The quinone binding site in Escherichia coli succinate dehydrogenase is required for electron transfer to the heme b.* J Biol Chem, 2006. **281**(43): p. 32310-7.
17. Maklashina, E., et al., *Retention of heme in axial ligand mutants of succinate-ubiquinone xxidoreductase (complex II) from Escherichia coli.* J Biol Chem, 2001. **276**(22): p. 18968-76.
18. Ohnishi, T. and J.C. Salerno, *Conformation-driven and semiquinone-gated proton-pump mechanism in the NADH-ubiquinone oxidoreductase (complex I).* FEBS Lett, 2005. **579**(21): p. 4555-61.
19. Yano, T., W.R. Dunham, and T. Ohnishi, *Characterization of the delta muH+-sensitive ubisemiquinone species (SQ(Nf)) and the interaction with cluster N2: new insight into the energy-coupled electron transfer in complex I.* Biochemistry, 2005. **44**(5): p. 1744-54.
20. Ohnishi, T., et al., *Thermodynamic and EPR studies of slowly relaxing ubisemiquinone species in the isolated bovine heart complex I.* FEBS Lett, 2005. **579**(2): p. 500-6.
21. Hirst, J., *Energy transduction by respiratory complex I--an evaluation of current knowledge.* Biochem Soc Trans, 2005. **33**(Pt 3): p. 525-9.
22. Hirst, J., *Towards the molecular mechanism of respiratory complex I.* Biochem J, 2010. **425**(2): p. 327-39.
23. Fato, R., et al., *Differential effects of mitochondrial Complex I inhibitors on production of reactive oxygen species.* Biochim Biophys Acta, 2009. **1787**(5): p. 384-92.
24. Crofts, A.R., et al., *Proton pumping in the bc1 complex: a new gating mechanism that prevents short circuits.* Biochim Biophys Acta, 2006. **1757**(8): p. 1019-34.
25. Rieske, J.S., W.S. Zaugg, and R.E. Hansen, *Studies on the Electron Transfer System. Lix. Distribution of Iron and of the Component Giving an Electron Paramagnetic Resonance Signal at G = 1.90 in Subfractions of Complex 3.* J Biol Chem, 1964. **239**: p. 3023-30.
26. Rieske, J.S., R.E. Hansen, and W.S. Zaugg, *Studies on the Electron Transfer System. 58. Properties of a New Oxidation-Reduction Component of the Respiratory Chain as Studied by Electron Paramagnetic Resonance Spectroscopy.* J Biol Chem, 1964. **239**: p. 3017-22.
27. Mitchell, P., *Possible molecular mechanisms of the protonmotive function of cytochrome systems.* J Theor Biol, 1976. **62**(2): p. 327-67.
28. Mitchell, P., *The protonmotive Q cycle: a general formulation.* FEBS Lett, 1975. **59**(2): p. 137-9.
29. Chance, B., et al., *Energy-coupling mechanisms in mitochondria: kinetic, spectroscopic, and thermodynamic properties of an energy-transducing form of cytochrome b.* Proc Natl Acad Sci U S A, 1970. **66**(4): p. 1175-82.
30. Wikstrom, M.K. and J.A. Berden, *Oxidoreduction of cytochrome b in the presence of antimycin.* Biochim Biophys Acta, 1972. **283**(3): p. 403-20.
31. Boveris, A., *Determination of the production of superoxide radicals and hydrogen peroxide in mitochondria.* Methods Enzymol, 1984. **105**: p. 429-35.

32. Cape, J.L., M.K. Bowman, and D.M. Kramer, *A semiquinone intermediate generated at the Qo site of the cytochrome bc1 complex: importance for the Q-cycle and superoxide production.* Proc Natl Acad Sci U S A, 2007. **104**(19): p. 7887-92.
33. Sun, J. and B.L. Trumpower, *Superoxide anion generation by the cytochrome bc1 complex.* Arch Biochem Biophys, 2003. **419**(2): p. 198-206.
34. Iwata, S., et al., *Complete structure of the 11-subunit bovine mitochondrial cytochrome bc1 complex.* Science, 1998. **281**(5373): p. 64-71.
35. Lange, C. and C. Hunte, *Crystal structure of the yeast cytochrome bc1 complex with its bound substrate cytochrome c.* Proc Natl Acad Sci U S A, 2002. **99**(5): p. 2800-5.
36. Gao, X., et al., *Structural basis for the quinone reduction in the bc1 complex: a comparative analysis of crystal structures of mitochondrial cytochrome bc1 with bound substrate and inhibitors at the Qi site.* Biochemistry, 2003. **42**(30): p. 9067-80.
37. Crofts, A.R., et al., *Mechanism of ubiquinol oxidation by the bc(1) complex: different domains of the quinol binding pocket and their role in the mechanism and binding of inhibitors.* Biochemistry, 1999. **38**(48): p. 15807-26.
38. Bartoschek, S., et al., *Three molecules of ubiquinone bind specifically to mitochondrial cytochrome bc1 complex.* J Biol Chem, 2001. **276**(38): p. 35231-4.
39. Ding, H., et al., *Cytochrome bc1 complex [2Fe-2S] cluster and its interaction with ubiquinone and ubihydroquinone at the Qo site: a double-occupancy Qo site model.* Biochemistry, 1992. **31**(12): p. 3144-58.
40. Ding, H., et al., *Ubiquinone pair in the Qo site central to the primary energy conversion reactions of cytochrome bc1 complex.* Biochemistry, 1995. **34**(49): p. 15979-96.
41. Berry, E.A., et al., *X-Ray Structure of Rhodobacter Capsulatus Cytochrome bc (1): Comparison with its Mitochondrial and Chloroplast Counterparts.* Photosynth Res, 2004. **81**(3): p. 251-75.
42. Zhang, H., et al., *Exposing the complex III Qo semiquinone radical.* Biochim Biophys Acta, 2007. **1767**(7): p. 883-7.
43. Muller, F.L., et al., *Architecture of the Qo site of the cytochrome bc1 complex probed by superoxide production.* Biochemistry, 2003. **42**(21): p. 6493-9.
44. Raha, S., et al., *Superoxides from mitochondrial complex III: the role of manganese superoxide dismutase.* Free Radic Biol Med, 2000. **29**(2): p. 170-80.
45. Page, C.C., et al., *Natural engineering principles of electron tunnelling in biological oxidation-reduction.* Nature, 1999. **402**(6757): p. 47-52.
46. Moser, C.C., et al., *Biological electron transfer.* J Bioenerg Biomembr, 1995. **27**(3): p. 263-74.
47. Hong, S., et al., *The energy landscape for ubihydroquinone oxidation at the Q(o) site of the bc(1) complex in Rhodobacter sphaeroides.* J Biol Chem, 1999. **274**(48): p. 33931-44.
48. Osyczka, A., C.C. Moser, and P.L. Dutton, *Fixing the Q cycle.* Trends Biochem Sci, 2005. **30**(4): p. 176-82.

49. Snyder, C.H., E.B. Gutierrez-Cirlos, and B.L. Trumpower, *Evidence for a concerted mechanism of ubiquinol oxidation by the cytochrome bc1 complex.* J Biol Chem, 2000. **275**(18): p. 13535-41.
50. Crofts, A.R., et al., *The Q-cycle reviewed: How well does a monomeric mechanism of the bc(1) complex account for the function of a dimeric complex?* Biochim Biophys Acta, 2008. **1777**(7-8): p. 1001-19.
51. Osyczka, A., et al., *Role of the PEWY glutamate in hydroquinone-quinone oxidation-reduction catalysis in the Qo Site of cytochrome bc1.* Biochemistry, 2006. **45**(35): p. 10492-503.
52. Rich, P.R., *The quinone chemistry of bc complexes.* Biochim Biophys Acta, 2004. **1658**(1-2): p. 165-71.
53. Crofts, A.R., et al., *Proton-coupled electron transfer at the Q(o) site: what type of mechanism can account for the high activation barrier?* Biochim Biophys Acta, 2000. **1459**(2-3): p. 456-66.
54. Takamiya, K.I. and P.L. Dutton, *Ubiquinone in Rhodopseudomonas sphaeroides. Some thermodynamic properties.* Biochim Biophys Acta, 1979. **546**(1): p. 1-16.
55. de Vries, S., et al., *A new species of bound ubisemiquinone anion in QH2: cytochrome c oxidoreductase.* J Biol Chem, 1981. **256**(23): p. 11996-8.
56. Ohnishi, T. and B.L. Trumpower, *Differential effects of antimycin on ubisemiquinone bound in different environments in isolated succinate . cytochrome c reductase complex.* J Biol Chem, 1980. **255**(8): p. 3278-84.
57. Junemann, S., P. Heathcote, and P.R. Rich, *On the mechanism of quinol oxidation in the bc1 complex.* J Biol Chem, 1998. **273**(34): p. 21603-7.
58. Robertson, D.E., et al., *Thermodynamic properties of the semiquinone and its binding site in the ubiquinol-cytochrome c (c2) oxidoreductase of respiratory and photosynthetic systems.* J Biol Chem, 1984. **259**(3): p. 1758-63.
59. Dutton, P.L., D.F. Wilson, and C.P. Lee, *Oxidation-reduction potentials of cytochromes in mitochondria.* Biochemistry, 1970. **9**(26): p. 5077-82.
60. Engstrom, G.J., et al., *The use of ruthenium labeled cytochrome c in the kinetic characterization of electron transfer between cytochrome c and cytochrome c1 in the cytochrome bc1 complex.* Biophysical Journal, 2002. **82**(1): p. 289A-290A.

Chapter 2: Mutations to heme c_1 binding site residues reveal *R. sphaeroides* Complex III activity is robust

It is becoming increasingly clear that electron transfer chains in natural proteins are not finely tuned, but robustly designed to transfer electrons between catalytic sites and survive the many obstacles of mutational change during evolution and natural selection. In this chapter, mutational work at heme c_1 has revealed that the reversible electron transfer chain in *R. sphaeroides* Complex III is engineered to withstand large changes in active site residues and midpoint potential to preserve turnover. The impact of altering these motifs in *R. sphaeroides* was tested as a means to explain how heme c_1 can maintain its function in response to massive changes in *R. sphaeroides* ligation, while the midpoint potential of *R. capsulatus* c_1 cannot avoid collapsing to a dysfunctional level. This work is part of a first-author manuscript in preparation to *Biochemistry* [1].

2.1 Introduction

A critical part of maintaining the productive energy-conversion observed in Complex III is the protection against electronic and protonic short circuits between reactive intermediates subsequent to charge separation [3, 4]. By promoting macroscopically reversible energy coupling, Complex III has several unproductive short circuits to defend against within the Qo site, and cannot rely upon the high driving force and practical irreversibility used by photosynthetic reaction centers as a defense.

2.1.1 Mutations at the heme c_1 binding site. Though the seemingly complicated Qo bifurcation electron transfer reaction should have specific thermodynamic requirements for the rest of the redox cofactors in Complex III in order to avoid these short circuit reactions, surprisingly, Complex III turnover is rarely affected by substantial midpoint potential changes within the high potential chain. While the CXXCH motif found in *R. sphaeroides* is the consensus motif for high potential class I *c*-type cytochromes, previous work has demonstrated that the heme c_1 found in this system is very tolerable to changes in its sixth axial ligand methionine [5]. This tolerance was described as a gradual decrease in the midpoint potential of heme c_1 as the methionine residue is varied, with only a M185H mutant rendering the midpoint potential too low for Complex III to remain functional.

Both *R. capsulatus* and *R. sphaeroides* c_1 subunits contain a disulfide-secured loop near the heme binding site that has been identified to support high c_1 midpoint potentials [2, 5, 6]. However, surprisingly, the threshold for making changes to the c_1 sixth ligand in *R. capsulatus* is significantly lower than that of *R. sphaeroides*. It has been proposed that the β–branched amino acid that directly precedes the heme ligating

position in *R. sphaeroides* increases both solvent inaccessibility and protein packing within the c_1 subunit and helps to maintain a higher c_1 midpoint potential even after changes to the methionine residue are introduced. In fact, adding a β-branched amino acid motif to *R. capsulatus* can repair incompetent midpoint potentials caused by breaking the disulfide loop [6].

2.1.2 Inhibition of heme c_1. Adding inhibitors to the quinone sites has been used to isolate electron transfer reactions in the low-potential chain of Complex III and control the flow of electrons. Stigmatellin [7, 8] and myxothiazol [9] can be added to inhibit Qo oxidation, and antimycin inhibits Qi reduction [10]. However, these inhibitors do block Qo and Qi from their active sites, making it impossible to isolate and describe specific quinone catalytic events when inihibitors are bound.

Reversible inhibition of the hemes in Complex III would allow the isolation of sequential electron transfers to be extended to the high-potential chain of Complex III without sabotaging Qo site oxidation. Photo-dissociable small ligands, such as carbon monoxide (CO) are ideal inhibitors of heme c_1 because their dissociation rate from heme c_1 would be on the same timescale as enzyme turnover, enabling normal electron transfer between the FeS cluster and heme c_1. Additionally, the formation of a heme c_1-CO complex would provide a unique experimental opportunity to light-activate Complex III in the absence of other chromatophore proteins, such as the reaction center. This would simplify current light-activation experiments that involve chromatophore membranes that contain several redox proteins (that can have overlapping spectral properties). Though a heme c_1-CO complex has never been formed in wild type Complex III, heme c_1 has proven to be amendable to ligation with other small molecules. Oxidized heme c_1 in *R.*

capsulatus Complex III has been demonstrated to reversibly bind cyanide with high affinity and shift the heme midpoint potential dramatically [11].

2.2 Materials and Methods

2.2.1 Bacterial strains and growth. Mutations to Complex III heme c_1 binding site residues were constructed by Haibo Zhang using the Quikchange site-directed mutagenesis system (Stratagene) as described previously [12]. These mutants were stored as glycerol stocks at -80 º C.

50 μL of *R. sphaeroides* glycerol stocks were plated on agar plates with Sistrom's Minimal Media A and 10 μM tetracycline. Plates were incubated for 2 days at 37 º C. 25 mL of autoclaved Sistrom's Minimal Media A with tetracycline added was inoculated with a single colony from the plate, and these flasks were agitated in the dark at 37 º C and 200 rpm overnight. 10 mL of this culture were transferred to 1 L of growth media and agitated in the dark for an additional day at 37 º C and 200 rpm.

2.2.2 Chromatophore membrane / protein purification. Growth media was centrifuged at 5000 rpm for 30 minutes and cell pellets were collected. Cell pellets were resuspended in 90 mL of equilibration buffer (100 mM NaCl, 50 mM Tris pH 8, 20% glycerol). Phenylmethanesulfonylfluoride (PMSF) (Sigma) was added to the solution at a final concentration of 2 μM, and the solution was French pressed to break the cell membranes. Cells were centrifuged at 10,000 rpm for 45 minutes, and the supernatant was collected for ultracentrifugation. The solution was spun at 45,000 rpm for 2 hours, and the chromatophore pellet was collected and resuspended in 25 mL of equilibration buffer for purification.

Complex III proteins were purified from chromatophore membranes using a BioGel A DEAE ion-exchange column (Bio-Rad). The column was equilibrated with five column volumes of equilibration buffer and 10 mL of the protein sample was loaded onto the column. The column was washed with two column volumes of equilibration buffer and then a 200 mL salt gradient of 150 mM to 600 mM NaCl was used to elute Complex III (buffers also contained 50 mM Tris pH 8 and 20% glycerol). Complex III eluted between 375 – 400 mM NaCl. The fractions that contained Complex III were pooled and dialyzed against a low salt buffer overnight and then concentrated to 5 mL of purified protein. Reduced minus oxidized UV-visible difference absorption spectra (Figure 2.1) were collected for each of the Complex III mutant proteins in this study.

2.2.3 Flash-induced single turnover kinetics. Flash-induced single-turnover time-resolved kinetics were performed according to [13] using chromatophore membranes and a double-wavelength spectrophotometer (Biomedical Instrumentation

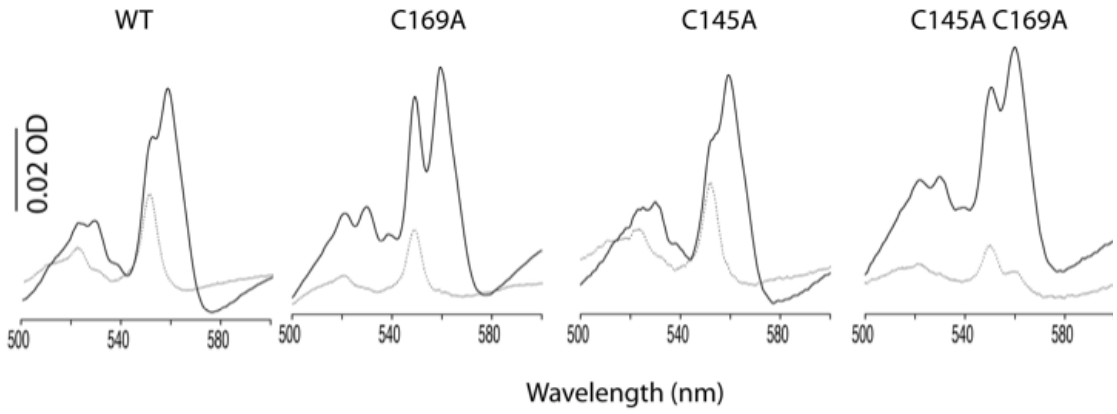

Figure 2.1: Difference UV-visible absorption spectra of Complex III wild type and heme c_1 mutant proteins. Both spectra are the difference in absorption between reduced Complex III and oxidized (using potassium ferricyanide). The dotted line represents the samples reduced with ascorbate and the solid line represents samples reduced with dithionite.

Group, University of Pennsylvania, Philadelphia, PA) in the presence of 2.5 μM valinomycin, 8 μM 2,3,5,6-tetramethyl phenylenediamine, 2.5 μM phenazine methosulphate, 2.5 μM phenazine ethosulfate, 6 μM 1,2 naphthoquinone, 6 μM 2-hydroxy-1,4-naphthoquinone, 100 μM ferrocyanide and 70 μM benzyl viologen. Transient cytochrome *c* re-reduction kinetics initiated by a short saturating flash (8 μs) from a xenon lamp was followed at 552-540 nm. The concentration of antimycin, myxothiazol and stigmatellin used were 5, 5 and 1 μM, respectively, and the ambient potential was poised at 100 mV or 250 mV.

2.2.4 Redox titrations of heme c_1 mutants. Equilibrium redox potentiometry was used as a functional analysis of the oxidation and reduction of heme c_1 [14]. Redox titrations were performed in an anaerobic 1 mL cuvette (Starna Cells) equipped with a silver / silver chloride and platinum combination electrode (Microelectrodes Inc.). All of the potentials reported are in reference to the normal hydrogen electrode (NHE). The reduction potential of the cuvette solution was adjusted by adding microliter aliquots of freshly prepared solutions of either sodium dithionite (for reducing) or potassium ferricyanide (for oxidizing). 20 μL of a stock solution containing the following redox mediator dyes was also added to the solution (final concentrations reported): 2.5 μM valinomycin, 8 μM 2,3,5,6-tetramethyl phenylenediamine, 2.5 μM phenazine methosulphate, 2.5 μM phenazine ethosulfate, 6 μM 1,2 naphthoquinone, 6 μM 2-hydroxy-1,4-naphthoquinone, 100 μM ferrocyanide and 70 μM benzyl viologen. After equilibration at each midpoint potential, the UV-visible spectrum of Complex III was recorded, monitoring in particular the increase in the sharp α-band absorption at 550 nm relative to a 540 nm reference wavelength.

2.2.5 CO binding. 3 mL of 5 μM Complex III was added to a UV-visible quartz cuvette and purged with argon. A concentrated dithionite solution was titrated in 1 μL at a time until the protein was fully reduced (5-6 μL). 10 mL of CO gas was added to the cuvette in the hood with a gas-tight syringe. The solution was monitored for up to two hours to determine the extent of CO ligation, if any.

2.2.7 Reduction of decylubiquinone (DBH) substrate. Quinols were prepared from the oxidized quinone using the method described by Peter Rich [15]. 0.25 g decylubiquinone was dissolved in 50 mL diethyl ether and placed in a separatory funnel. A solution of 1 g sodium dithionite in 50 mL water was added and the mixture was shaken together. The quinone could be seen to initially increase in yellow color due to semiquinone formation, but eventually became colorless as full reduction to quinol occurred. The ethereal layer was shaken with a second 50 mL solution of sodium dithionite to ensure completion of the reduction reaction. After removal of the dithionite solution, the ethereal layer was washed twice with a saturated sodium chloride solution. The ethereal layer containing quinol was then passed through 30 g anhydrous sodium sulfate in a sintered glass funnel to remove any residual water, and the ethereal solution was then dried down by rotovaporization at 25°C. The resulting white powder was dissolved in an acidic ethanol solution (95% ethanol containing 10 mM hydrochloric acid) and flash frozen in 500 mL aliquots.

2.2.8 Steady-state measurement of Complex III activity. Complex III activity was measured using a standard assay developed by Trumpower *et al* [16]. A solution of 25 mM horse heart cytochrome *c* (Sigma) in redox buffer (50 mM potassium phosphate and 100 mM potassium chloride at pH 8) and 10 μM decylubiquinone was incubated in a

3 mL cuvette saturated with CO gas and stirred for one minute, after which CO-inhibited Complex III was introduced into the cuvette in nanomolar concentrations (10-100 nM). Using an extinction coefficient of 18.5 $mM^{-1}cm^{-1}$ for the 551 nm – 540 nm difference absorption, cytochrome *c* reduction was monitored over time until the amount of cytochrome *c* reduced reached a constant maximum.

2.3 Results

Sixth ligand mutagenesis of heme c_1 caused electron tunneling at heme c_1 to become the rate limiting step in ubiquinone oxidation at the Qo site, establishing an unfavorable redox equilibrium limit (three to four orders of magnitude) for Complex III catalysis [5]. However, Complex III can tolerate a remarkably wide range of energy barriers before turnover is halted, demonstrating that electron transfer reactions carried out by long chains of cofactors are undeniably robust. This work explored whether the disulfide loop residues found in the *R. sphaeroides* binding site are responsible for stabilizing heme c_1 midpoint potential. Mutations C145A, C169A, and C145AC169 did not significantly impact Complex III activity or heme c_1 midpoint potential, indicating that these residues do not play an active role in stabilizing the midpoint potential of heme c_1 or modulating the thermodynamics of FeS cluster to heme c_1 electron transfer. Table 2.1 summarizes the general characteristics for each of the disulfide mutants. Representative flash kinetic traces and redox titrations for the mutant proteins are reported as C145A data.

2.3.1 Flash kinetics of cytochrome c_1 + cytochrome c_2. Using light-activated chromatophores, the kinetics of specific redox reactions within Complex III can be monitored following a short flash. The electrons delivered from the flash of light activate

Table 2.1 Mutagenesis of cysteine residues in *Rb. sphaeroides* Complex III

Mutation	Phenotype [(a)]	Em7 (mV) [(b)]	b_H reduction rate (s^{-1}) [(c)]	CO binding [(d)]	Reversion to $Ps^{+(e)}$
Wild type	PS+	281	856	-	N/A
C145A	PS+	276	836	-	N/A
C169A	PS+	278	892	-	N/A
C145A_C169A	PS+	285	840	+	N/A

(a) Ps+ and Ps- indicate photosynthetic competence and incompetence, respectively. (b) Midpoint redox potential of cytochrome c_1 in purified Complex III. (c) b_H reduction rates were determined by flash kinetics at the ambient potential of 100 mV at pH 7.0 by recording the absorbance changes at 560-570 nm, and fitting them to a single exponential equation. (d) (+) and (-) indicate the ability of ferrocytochrome c_1 in isolated Complex III to binding carbon monoxide. (e) Spontaneous site suppressor mutations in cytochrome c_1 that restore photosynthetic activity of the cells.

the photosynthetic reaction center and go on to create the two substrates of Complex III, oxidized cytochrome c_2 and hydroquinone, within microseconds.

Figure 2.2 compares the flash-induced cytochrome *c* oxidation and re-reduction in wild type and the C145A mutant measured under the conditions which preset cytochrome *c* and FeS reduced and the quinone pool half-reduced before activation at 100 mV. Kinetic traces without any inhibitor and with two potent Qo site inhibitors, myxothiazol and stigmatellin, are shown. In all cases, the flash-induced cytochrome *c* oxidation (cytochrome c_1+c_2, which is not resolved in the experiment) is rapid, with a time constant beyond the resolution of the instrument.

The Qo site inhibitors provide a useful means of measuring the levels of different phases of cytochrome reduction. Stigmatellin, which completely inhibits the Qo site activity as well as fixes the FeS cluster in its *b*-position docked onto cytochrome *b* [17, 18], reveals the full level of oxidation of cytochrome *c* by flash activated reaction center

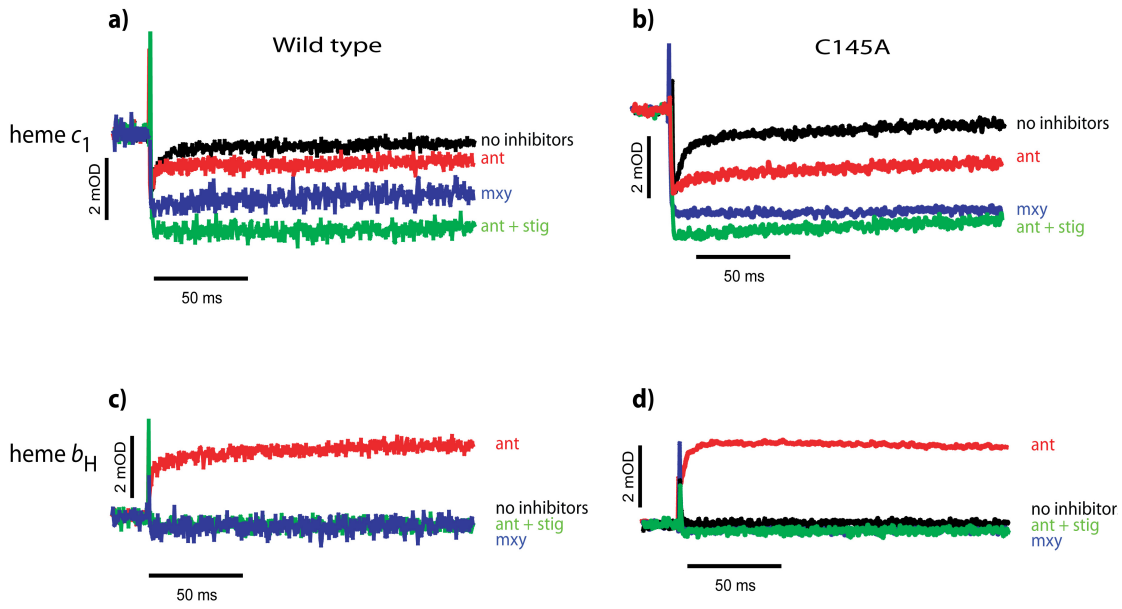

Figure 2.2: Flash kinetics of heme b_H and cytochrome *c* in chromatophores from wild type Complex III and a C145A mutant. The ambient redox potential was poised at 100 mV at pH 7.0. The kinetics of the flash-induced cytochrome *c* were followed at 551-540 nm (a, c), and the kinetics of the flash-induced heme b_H were followed at 560-570 nm (b, d). The kinetic traces completed in the absence of inhibitors are shown in black. The Qi site reaction was inhibited with antimycin (red), the Qo site was inhibited with myxothiazol (blue), and in the control experiment, both Qi and Qo site activity were inhibited with antimycin and stigmatellin (green).

(green traces in Figure 2.2). Myxothiazol, which also inhibits the Qo site but has no effect on the FeS cluster movement, normally does not reveal the portion of cytochrome that becomes rapidly reduced by pre-reduced FeS cluster. Thus, the offset in the amplitude of cytochrome *c* oxidation with the stigmatellin and myxothiazol, seen clearly in wild-type Complex III, is attributed to this initial phase of the cytochrome *c* re-reduction. C145A displays very similar heme c_1 kinetics as the wild-type Complex III protein. With no inhibitors present, the re-reduction of heme c_1 occurs at 143 s^{-1} in the C145A mutant, in comparison to 167 s^{-1} for wild-type Complex III.

2.3.2 Flash kinetics of heme b_H. Using antimycin to completely inhibit electron transfer at the Qi site [10] sets up a sensitive test for how changing the binding site residues at heme c_1 impact the rate of the Qo site bifurcation reaction and subsequent redox equilibrium. Figures 2.2 and 2.3 shows the time-course of flash-induced heme b_H reduction in wild-type Complex III and the C145A mutant at two different driving force conditions by changing the ambient redox potential prior to activation.

First, the redox potential of the chromatophores was poised at 100 mV, which creates a state where the Q-pool is half-reduced and close to the potential of the Qo site prior to the flash. In the presence of antimycin, the reduction of heme b_H takes place on a millisecond timescale in both wild type Complex III and the C145A mutant. In a second experiment, chromatophores were poised at 250 mV prior to the flash. Under this

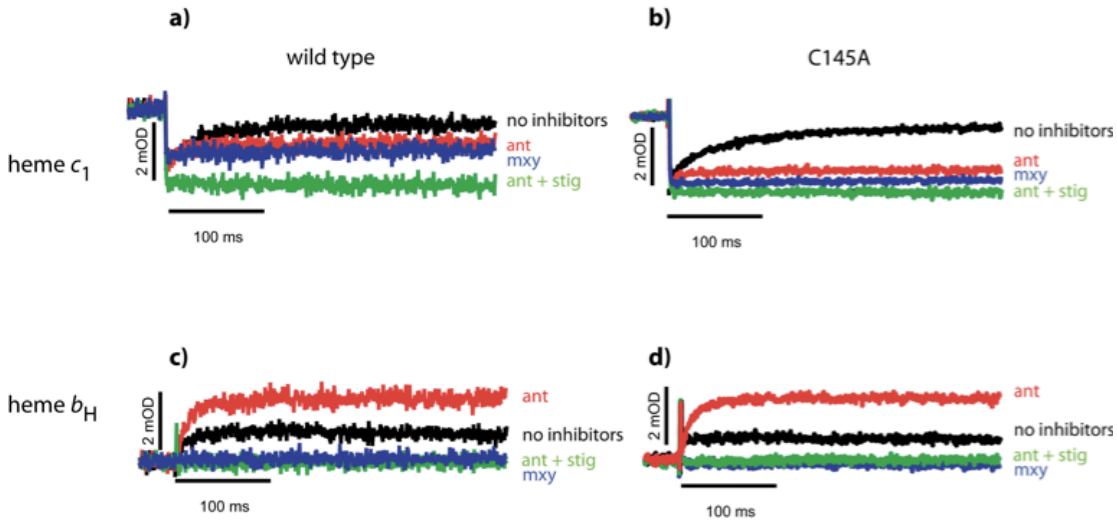

Figure 2.3: Flash kinetics of heme b_H and cytochrome c in chromatophores from wild type Complex III and a C145A mutant. The ambient redox potential was poised at 250 mV at pH 7.0. The kinetics of the flash-induced cytochrome c were followed at 551-540 nm (a, c), and the kinetics of the flash-induced heme b_H were followed at 560-570 nm (b, d). The kinetic traces completed in the absence of inhibitors are shown in black. The Qi site reaction was inhibited with antimycin (red), the Qo site was inhibited with myxothiazol (blue), and in the control experiment, both Qi and Qo site activity were inhibited with antimycin and stigmatellin (green).

condition, the Q-pool is fully oxidized and reduced quinone is only available after flash activation of the reaction centers, diffusing through the Q-pool before binding to the Qo site. For wild type, this diffusion is the rate-limiting step in the overall reaction at this high redox potential, and heme b_H reduction is slowed relative to when the system is poised at lower redox potential. C145A actually demonstrates slightly faster b_H reduction kinetics under these condtions, with a rate of 119 s^{-1} compared to 77 s^{-1} in the wild-type Complex III.

2.3.3 Heme c_1 – CO. The ability of the mutant proteins to bind CO was tested to determine if any of the heme ligands were disrupted by eliminating the disulfide bridge.

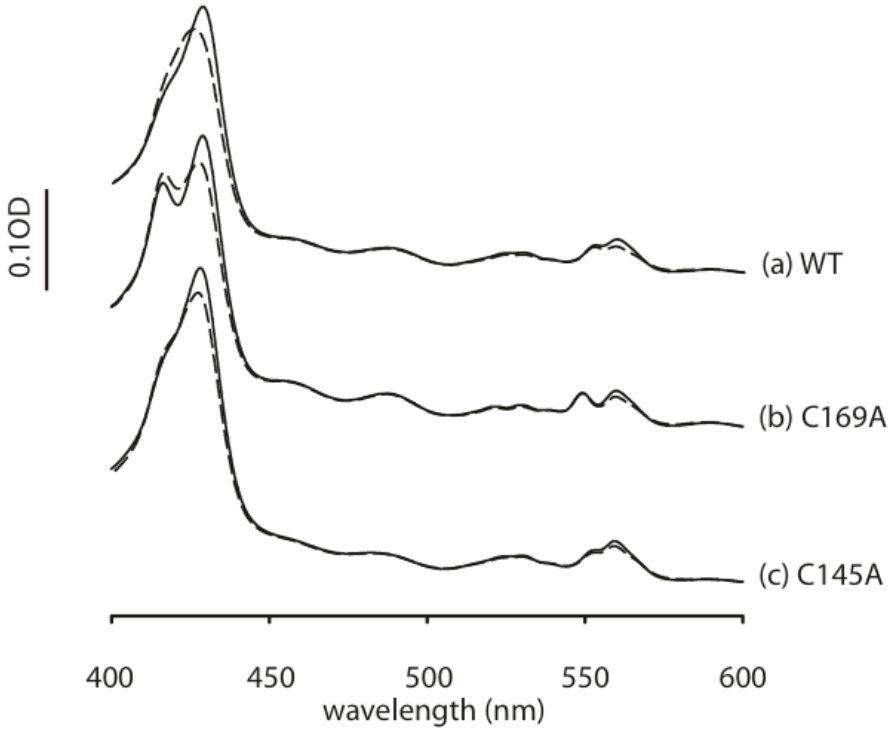

Figure 2.4: UV-visible spectra for reduced wild-type (a) and two cysteine mutant proteins, C169A (b) and C145A (c), before (solid line) and after (dashed line) the addition of CO to the cuvette.

Figure 2.4 shows the UV-visible absorbance spectra for wild-type, C145A, and C169A proteins before (solid line) and after (dashed line) treatment with CO. The difference between the dithionite reduced + CO spectra minus the dithionite reduced spectra is equivalent for all of the proteins, indicating that the ligands of heme c_1 are not affected by mutating the disulfide bridge residues. This is disappointing because of the experimental advantages that could be gained from a light-activatable ligand in the high potential chain, but not surprising given the mutants behaved so similarly to wild-type heme c_1.

If left under a constant stream of CO gas for two or more hours, reduced wild-type Complex III does begin to demonstrate more significant spectral changes due to the presence of CO in the cuvette. The Soret band blue shifts 5 nm from the reduced Soret band found at 424 nm, and the characteristic *b*-heme α-band signature also begins to decrease. These samples were tested for Complex III activity using the steady-state assay developed by Trumpower *et al* [16] and were found to have diminished Complex III activity even after the CO has been removed from the sample. Therefore, even on longer timescales, it is not likely that wild-type heme c_1 ligates a CO molecule to heme c_1. Instead, these changes could either be associated with a slow re-oxidation of the protein or gradual destruction of the *b*-hemes by CO.

2.4 Discussion

2.4.1 Heme c_1 binding motifs are not required for midpoint potential stability. Not surprisingly, just as *R. sphaeroides* is more resilient to changes in its disulfide loop region, it can also withstand mutations to its β-branched amino acid without losing functionality. Single and double cysteine mutants that break the disulfide bridge within the c_1 heme-binding motif are still photosynthetically competent and retain

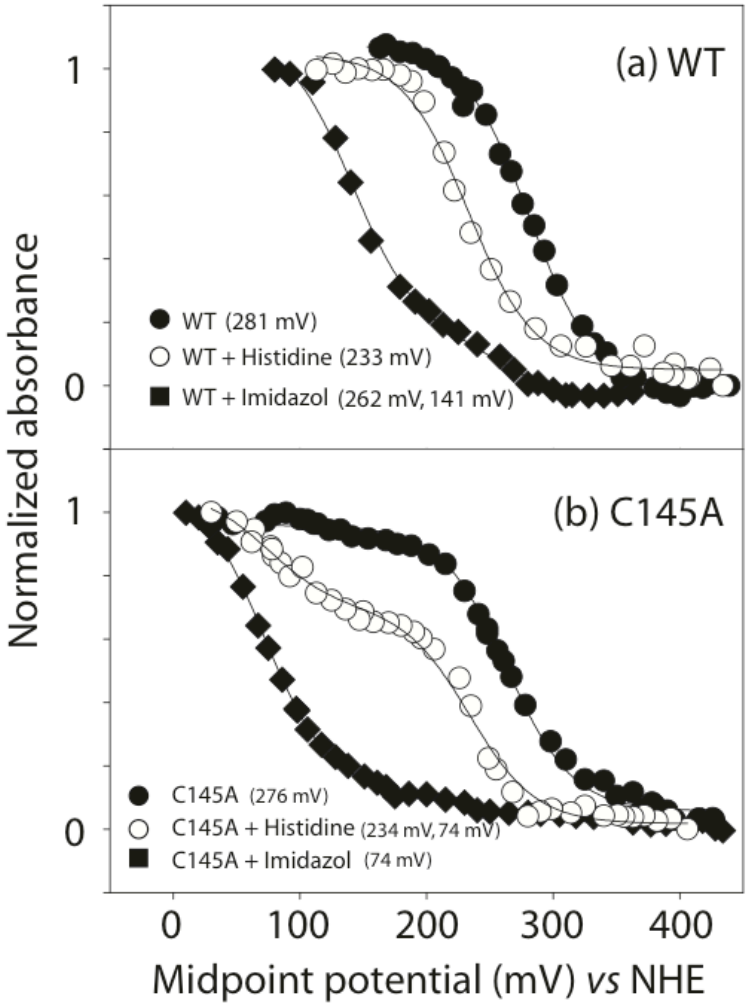

Figure 2.5: Redox titrations of wild-type and C145A Complex III proteins in different buffer conditions. These titrations are meant to reproduce the buffer conditons used by Elberry *et al* [2]. The sample represented by the closed circles was prepared in the same equilibration buffer used for purifying Complex III, and is the standard buffer used by the Dutton laboratory. The open circles represent the same protein sample with 50 mM histidine added to the redox buffer.

high c_1 midpoint potentials (Table 2.1). Additionally, a double mutant that breaks the disulfide loop and eliminates the β-branched isoleucine is also surprisingly still physiologically competent [2].

Elberry *et al*. also reported experimental mutations in disulfide bridge residues still resulted in Complex III functionality [2]; however, they report extremely low heme

c_1 midpoint potentials of approximately +50 mV that fall outside of the well-defined thermodynamic threshold for heme c_1 [5] If their midpoint potentials were correct, Complex III would be unable to function because the thermodynamic barrier for FeS cluster to heme c_1 electron transfer would be insurmountable. This discrepancy can be explained by their use of an imidazole buffer for protein purification and a histidine buffer in their redox titration experiments. As shown in figure 2.5, the presence of histidine and/or imidazole can lower midpoint potentials of heme cofactors by over 50 mV. Eliminating this artifact from their experiments would raise their reported midpoint potential values to lie within the thermodynamic range previously defined for heme c_1 and within the midpoint potentials determined in this chapter.

2.5 Conclusion

The specific engineering element of *R. sphaeroides* Complex III responsible for the robustness of its heme c_1 active site must include other interactions beyond those provided by residues neighboring the active site, or may not be structurally related to the heme c_1 active site. It could be that electrostatic interactions with the FeS cluster (when it is rotated proximal to the heme c_1 active site) are enough to stabilize the midpoint potential of *R. sphaeroides* heme c_1 and preserve turnover of the high potential chain.

2.6 References

1. Chobot, S.E., Zhang, H., Marshall, D.A., Osyczka, A., Moser, C.C., Dutton, P.L., *Presenting a simple model for Complex III electron transfer.* in preparation - to be submitted to Biochemistry, 2010.
2. Elberry, M., L. Yu, and C.A. Yu, *The disulfide bridge in the head domain of Rhodobacter sphaeroides cytochrome c(1) is needed to maintain its structural integrity.* Biochemistry, 2006. **45**(15): p. 4991-4997.
3. Osyczka, A., C.C. Moser, and P.L. Dutton, *Fixing the Q cycle.* Trends Biochem Sci, 2005. **30**(4): p. 176-82.

4. Chobot, S.E., et al., *Breaking the Q-cycle: finding new ways to study Qo through thermodynamic manipulations.* Journal of Bioenergetics and Biomembranes, 2008. **40**(5): p. 501-507.
5. Zhang, H., et al., *Resilience of Rhodobacter sphaeroides cytochrome bc1 to heme c1 ligation changes.* Biochemistry, 2006. **45**(48): p. 14247-55.
6. Osyczka, A., et al., *Controlling the functionality of cytochrome c(1) redox potentials in the Rhodobacter capsulatus bc(1) complex through disulfide anchoring of a loop and a beta-branched amino acid near the heme-ligating methionine.* Biochemistry, 2001. **40**(48): p. 14547-56.
7. von Jagow, G. and T. Ohnishi, *The chromone inhibitor stigmatellin--binding to the ubiquinol oxidation center at the C-side of the mitochondrial membrane.* FEBS Lett, 1985. **185**(2): p. 311-5.
8. Lancaster, C.R., et al., *A Comparison of Stigmatellin Conformations, Free and Bound to the Photosynthetic Reaction Center and the Cytochrome bc(1) Complex.* J Mol Biol, 2007.
9. Thierbach, G. and H. Reichenbach, *Myxothiazol, a new inhibitor of the cytochrome b-c1 segment of th respiratory chain.* Biochim Biophys Acta, 1981. **638**(2): p. 282-9.
10. Ohnishi, T. and B.L. Trumpower, *Differential effects of antimycin on ubisemiquinone bound in different environments in isolated succinate . cytochrome c reductase complex.* J Biol Chem, 1980. **255**(8): p. 3278-84.
11. Osyczka, A., C.C. Moser, and P.L. Dutton, *Novel cyanide inhibition at cytochrome c1 of Rhodobacter capsulatus cytochrome bc1.* Biochim Biophys Acta, 2004. **1655**(1-3): p. 71-6.
12. Yun, C.H., et al., *Cloning and DNA sequencing of the fbc operon encoding the cytochrome bc1 complex from Rhodobacter sphaeroides. Characterization of fbc deletion mutants and complementation by a site-specific mutational variant.* Eur J Biochem, 1990. **194**(2): p. 399-411.
13. Osyczka, A., et al., *Reversible redox energy coupling in electron transfer chains.* Nature, 2004. **427**(6975): p. 607-12.
14. Dutton, P.L., *Redox potentiometry: determination of midpoint potentials of oxidation-reduction components of biological electron-transfer systems.* Methods Enzymol, 1978. **54**: p. 411-35.
15. Rich, P.R., *Electron transfer reactions between quinols and quinones in aqueous and aprotic media.* Biochimica et Biophysica Acta, 1981. **637**: p. 28-33.
16. Trumpower, B.L. and C.A. Edwards, *Purification of a reconstitutively active iron-sulfur protein (oxidation factor) from succinate . cytochrome c reductase complex of bovine heart mitochondria.* J Biol Chem, 1979. **254**(17): p. 8697-706.
17. Iwata, S., et al., *Complete structure of the 11-subunit bovine mitochondrial cytochrome bc1 complex.* Science, 1998. **281**(5373): p. 64-71.
18. Zhang, Z., et al., *Electron transfer by domain movement in cytochrome bc1.* Nature, 1998. **392**(6677): p. 677-84.

Chapter 3: Design and characterization of an amphiphilic maquette, AP6

The maquette approach uses simplified versions of natural proteins to investigate the basic protein engineering necessary to reproduce functional elements of biological energy transduction. The first maquette family, which had a hydrophilic (HP) exterior, established the design principles for iron-protoporphyrin IX (FePPIX) binding and demonstrated proton coupling to oxidation/reduction. However, hydrophilic maquettes cannot unravel design principles for protein assembly into membranes. Therefore, a second maquette family was designed to be amphiphilic (AP), meaning it contains both HP and lipophilic (LP) domains, and can assemble inside membranes. In this chapter, a new member of the AP family of maquettes is fully characterized, AP6. These experiments reveal the full potential of AP6 to serve as a model system for studying complicated transmembrane proteins, such as Complex III. The results contained within this chapter are a part of two manuscripts in preparation [7, 8].

3.1 Introduction

A century before this thesis work began, Emil Fischer won the Nobel Prize and 'foresaw a time in which physiological chemistry will not only make greater use of natural enzymes, but will actually resort to creating synthetic ones' [9, 10]. Fischer's prediction was remarkably astute, as the field of *de novo* protein design has indeed created robust protein-cofactor complexes that serve as simple models (or as the Dutton laboratory has named them, maquettes) for much more complicated natural oxidoreductases. Protein designers have established the principles for assembling water-soluble α-helical bundles [1, 11-16], transmembrane α-helical proteins [2, 17], and basic β-sheet proteins [18, 19]; however, translating any particular protein function into a successful synthetic protein construction remains challenging.

Part of what makes reproducing protein function difficult is an incomplete understanding of the mechanisms of complicated oxidoreductases, such as Complex III. These proteins have a built-in complexity arising from Darwin's principle of multiple-utility [20], which states that each amino acid in a protein is naturally selected for multiple and overlapping roles. Therefore, one of the engineering challenges protein designers face is paring down this complexity to focus on one or two functional roles for their model system and progressively build up these functions, one amino acid at a time.

The design strategy for recreating structure and function in membrane-bound synthetic proteins is achieved in three main steps: 1) extract the basic engineering requirements from membrane oxidoreductases and reproduce them in hydrophilic (HP) maquettes; 2) provide a structural basis for lipophilic (LP) maquette assembly into a membrane; and 3) integrate properties from the HP and LP proteins designed in steps one

and two into an amphiphilic (AP), transmembrane maquette. This work built upon from established maquette families existing in the Dutton laboratory and published from other sources to accomplish the third step – applying what has already been learned through HP and LP designs towards reproducing transmembrane proton-coupled electron transfer function into a simplistic AP maquette design, named AP6.

3.1.1 Step 1: reproducing membrane protein function in HP maquettes.

As outlined in chapter one, the main functional elements of biological energy transduction are conversion of light or chemical redox energy into electron transfer, coupling electron transfer to proton translocation, and coupling protonmotive forces with conformational changes. As the mechanism of Complex III contains all of these functional elements, the first step of protein design was to re-establish the hydrophobic di-heme *b* subunit from Complex III as a HP four-helix maquette [16, 21].

Through the binary patterning of polar and non-polar residues, Regan and DeGrado were the first to demonstrate that soluble four α-helix bundles could be assembled from simple heptad repeat peptides [22]. In their work, polar residues were positioned on the protein surface, and non-polar residues were aligned in the core of the protein, creating hydrophobic interactions that drove the assembly of the helices into a four-helix bundle protein. This simple design proved to be easily manipulated, creating a family of HP maquettes able to bind many different types of cofactors, including hemes [1, 3, 5, 16, 21, 23, 24], quinones [25, 26], flavins [27], iron-sulfur clusters [28], redox-active tyrosine and tryptophan radicals [15, 29, 30], carboyxlate-bridged dimetal clusters [31, 32], chlorophylls [33], and chlorins [34, 35].

However, creating a peptide sequence that facilitates cofactor ligation and function is not enough to create a successful maquette protein; all successful maquette designs also have singular structures. Though the first HP maquettes relied upon global hydrophobic sequestering rather than specific residue-residue contacts, design of native-like singular structures in maquettes has now been approached by many different methods [14, 16, 36-38]. The Dutton laboratory has relied upon iterative design to attain successful structural resolution for the HP maquette family. This design process progresses from the assembly of a generic protein helical bundle, to insertion of cofactor ligating amino acids, and finally towards iteratively testing and redesigning to engineer function and singular structure.

As shown in Figure 3.1, Dutton laboratory maquette design began with the design of H10H24, which was derived from three and half repeats of the LLKKLLE heptad sequence. A tryptophan residue was incorporated near the N-terminus of the protein on the exterior surface to facilitate optical detection using UV-visible spectroscopy methods. Cofactor binding in this protein was achieved through replacement of two leucine residues (Leu 10 and Leu 24) in the interior of the protein with histidine residues, and N-terminal disulfide-forming loops (CGGG) were incorporated between sets of helices to reduce the possibilities for overall protein assembly to just two conformations – *syn* (all helices parallel) and *anti* (helices anti-parallel, or facing in opposite directions). Variants of this protein, such as H10A24, were also successfully created and characterized, and were found to have allosterically regulated conformational switches (from all-*syn* to all-*anti*) upon redox change of the bound heme cofactors [12].

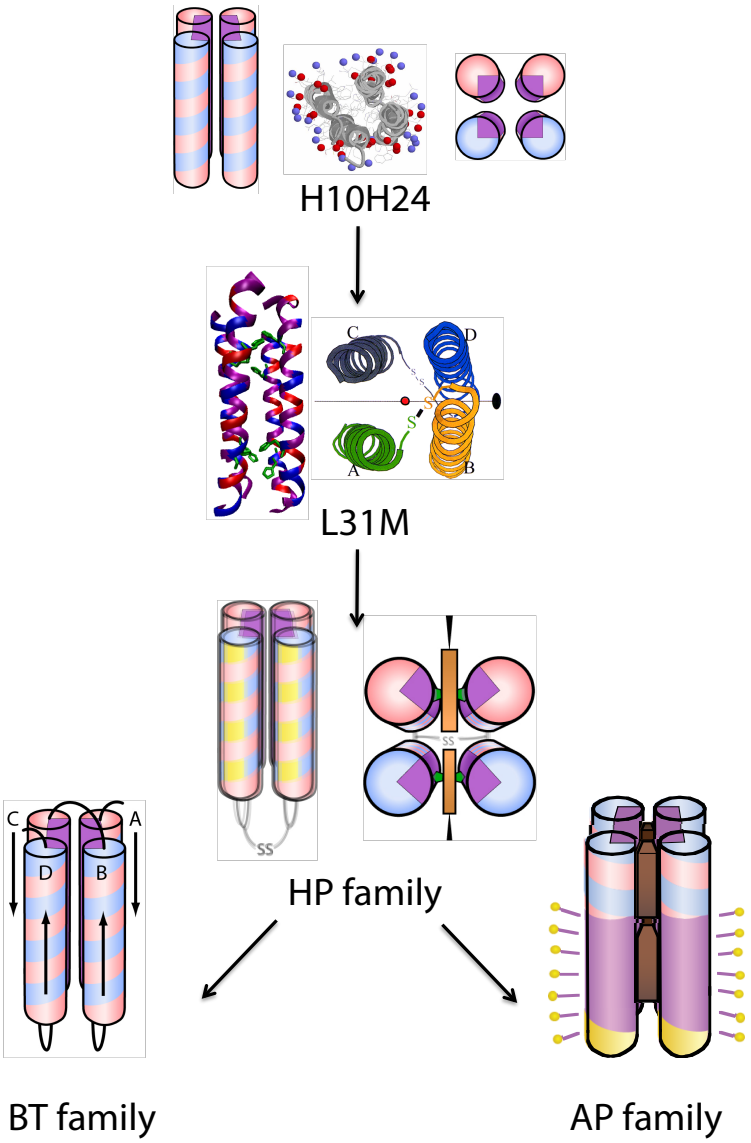

Figure 3.1: The Dutton laboratory maquette family tree [1-5]. Purple regions of the protein cartoons depict the locations of hydrophobic residues, red regions correspond to acidic residues, blue regions represent basic residues, and yellow regions indicate the placement of amino acids with carboxyamide functional groups.

This mobility between conformations was eliminated in the apomaquette L31M, which incorporated β-branched amino acids in the interior of the protein to solidify a singular structure. L31M was characterized by NMR [4] and by x-ray crystallography [37] and then redesigned as HP-1, a disulfide-bridged two-α-helix peptide with two histidines for heme ligation [3]. This peptide retained the singular structure of L31, as it self-assembled to form an *anti* four-helix bundle, and also maintained the strong coupling between heme redox reactions and glutamate acid-base transitions initially designed in H10H24.

With a basic heme-binding HP scaffold in place, the HP design evolved through a series of iterative modifications to create HP7, an oxygen transport protein with properties and function remarkably similar to neuroglobin [1]. Unlike its predecessors H10H24 and HP1, HP7 only binds two hemes, with the histidine at residue 24 replaced with a phenylalanine. Another structural difference that is the key to HP7 function is the N-terminal loops are linked into a monomeric 'candelabra' structure, further constraining water access to the heme binding site. Additionally, the rotation of three glutamate residues into the protein core destabilizes one of the iron-histidine ligations, producing a population of penta-coordinate heme that is then free to bind exogenous ligands such as carbon monoxide or oxygen [1].

3.1.2 Step 2: Modifying HP designs to create proteins that can assemble in detergent micelles or phospholipid bilayers. As the HP proteins have been progressively designed to shield water from their active site in order to stabilize the formation of an oxy-ferrous state, some of the key design strategies employed by the HP family of maquettes was applied towards the design of LP and AP maquettes. The same

hydrogen bonding pattern in the HP protein core that forms its α-helical secondary structure was also used in designs of membrane-associated peptides.

Once the secondary structure is formed, it must be inserted into a membrane interface. Hydrogen bonding residues have sufficient thermodynamic driving force for membrane helix association [39, 40]; however, the degree of stabilization in the membrane is strongly dependent on the position of those residues within the membrane interface. When asparagine is positioned in the middle of a membrane, it has been shown to provide more stability than when it is located directly at the membrane-solvent interface [41]. Additionally, certain sequence motifs have been demonstrated to aid assembly of peptides in membranes. For example, Lear *et al*. demonstrated that the incorporation of multiple serine residues in specific motifs drives the association of simple transmembrane α-helices into higher oligomers that were then functional as ion channels [42, 43]. Subsequently, Engelman *et al*. also confirmed that the incorporation of multiple serine and threonine motifs drives transmembrane assembly [44].

The length of the peptide assembling into the membrane can also affect peptide-lipid interactions [45]; however, hydrophobic mismatch between the membrane interface and the peptide can be compensated for in peptide designs. Charged residues with long and/or aromatic side chains (such as lysine or phenylalanine) can overcome hydrophobic mismatch by partitioning into the headgroup region of the bilayer [46]. Additionally, peptides with larger tilt angles can also accomplish membrane assembly with slightly shorter lengths [45].

3.1.3 Step 3: Integrate properties from the HP and LP proteins into an AP maquette. The design and construction of the AP family of maquettes was intended to

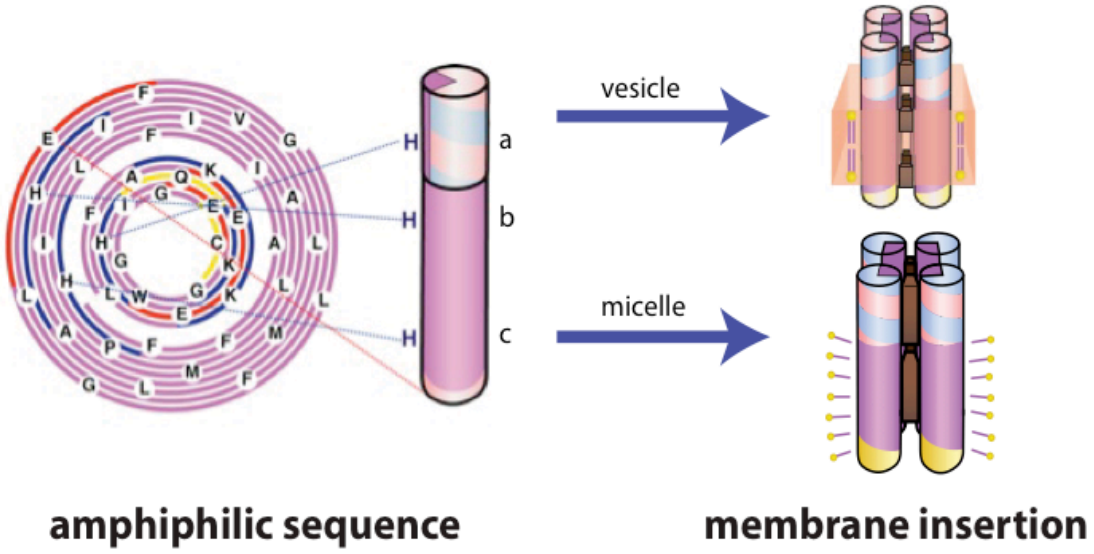

Figure 3.2: Polar plot diagram for the AP6 peptide. There are three histidines in the AP6 peptide sequence for heme ligation – histidine 10 (binding site "a"), histidine 21 (binding site "b"), and histidine 35 (binding site "c"). AP6 assembles as a four α-helix bundle in either lipid vesicles (top right) or detergent micelles (bottom right).

provide a simplistic platform for achieving functions typically carried out by more complicated biological enzymes across a membrane interface. Three existing AP family members were characterized previous to this work – AP1, AP2, and AP3 [2, 17]. AP1 combined 14 residues from HP1 with 24 residues from the membrane domain of the natural M2 channel from the influenza virus through a flexible linking sequence (GGNG). This peptide assembled as a *syn* four helix bundle, and each assembled maquette bound up to two heme cofactors via histidine ligation located in the HP domain. Two variants of this maquette, AP2 and AP3, were created to explore heme-binding characteristics in the LP domain. These maquettes removed the heme-ligating histidine from the HP domain of AP1, and modeled their LP domain sequences after the transmembrane helices found in the *b*-subunit of Complex III. These two variants were

the first examples of successful cofactor binding sites within a designed peptide that were located in a LP domain.

Selection of the primary sequence for AP6 was aided in part by what is known about previously designed maquettes in the HP [1, 5, 12] and AP families [2, 17]. AP6 incorporates characteristics of many of its predecessors, as it has a HP-based domain taken from HP7 and an LP-based domain built upon those tested in AP2 and AP3. AP6 has multiple heme binding sites (one within the HP domain and two within the LP domain). This design, shown in cartoon form in Figure 3.2, was meant to combine the best engineering elements learned from previous maquettes to become the first *de novo* designed protein to establish transmembrane electrochemical and proton gradients akin to those that occur in more complicated natural systems, such as Complex III.

3.2 Materials and Methods

3.2.1 Peptide synthesis and purification. Table 3.1 outlines the sequences of AP6 and its mutants AP6a, AP6b, AP6c, AP6ab, AP6bc, and AP6ac. The peptides described in Table 3.1 were synthesized on a continuous-flow solid-phase synthesizer (CEM) using a standard Fmoc/tBu protection strategy on a Fmoc-PEG-PAL-PS resin (NovaBioChem) on a 0.2 mmol scale. The peptides were purified on a reversed-phase C18 HPLC column (Vydac) using a 65%-70% gradient of acetonitrile (Fisher) and water both containing 0.1% (v/v) trifluoroacetic acid (Sigma). The purity and molecular weight of the acetylated peptides were confirmed by matrix-assisted laser desorption/ionization mass spectrometry (MALDI-MS), and the molecular weights of the mutant peptides are listed in Table 3.1. Peptide yields were comparable to water-soluble peptides of similar length [1].

Table 3.1 Summary of the sequences and MW of AP6 and AP6 variants

Protein	MW (g/mol)	Sequence
AP6	5022	CGGGEIWKQH_{10}EEALKKFFAFH_{21} FILPFIIMAIAMVH_{35}LLFLFGEG
AP6a	5042	CGGGEIWKQH_{10}EEALKKFFAFF_{21} FILPFIIMAIAMVF_{35}LLFLFGEG
AP6b	5042	CGGGEIWKQF_{10}EEALKKFFAFH_{21} FILPFIIMAIAMVF_{35}LLFLFGEG
AP6c	5042	CGGGEIWKQF_{10}EEALKKFFAFF_{21}F ILPFIIMAIAMVH_{35}LLFLFGEG
AP6ab	5032	CGGGEIWKQH_{10}EEALKKFFAFH_{21} FILPFIIMAIAMVF_{35}LLFLFGEG
AP6ac	5032	CGGGEIWKQH_{10}EEALKKFFAFF_{21} FILPFIIMAIAMVH_{35}LLFLFGEG
AP6bc	5032	CGGGEIWKQF_{10}EEALKKFFAFH_{21} FILPFIIMAIAMVH_{35}LLFLFGEG

With the exception of pH dependent experiments, all experiments were performed in buffered solutions containing 100 mM potassium chloride and 50 mM potassium phosphate (pH 8.0). The word maquette refers to the desired total assembly of four peptide helices. As such, our peptide concentrations reported here are for assembled four-helix bundles. Peptide concentrations were determined by UV-visible absorbance spectroscopy at 280 nm with an extinction coefficient of 22,400 M^{-1} cm^{-1} $bundle^{-1}$

calculated from the AP6 sequence using the Swiss Institute of Bioinformatics' EXPASY server (http://us.expasy.org/cgi-bin/protparam).

3.2.2 Peptide Solubilization. Water-insoluble AP6 peptides and their assembled maquettes need a detergent for solubilization in aqueous buffers. We have determined that, in general, common detergents near or above the critical micelle concentration (CMC) readily solubilize AP6 maquette family members. In these experiments, dodecylphosphocholine (DPC) or Zwittergent was used to solubilize AP6 at a final concentration of 2 mM. AP6 can also be incorporated into phospholipids vesicles. Gregory Wiedman and Paul O'Brien pursued this line of solubilization. Vesicles were prepared from a 9:1 mixture of 1-palmitoyl-2-oleoylphosphatidylcholine (POPC) and 1-palmitoyl-2-oleoylphosphatidylserine (POPS). The lipid mixture was dried under nitrogen gas and then overnight under vacuum. The dry lipids were co-dissolved with a solution of AP6 in detergent, and then dialyzed against a buffer solution without detergent.

3.2.3 Heme binding. A 1 mM stock solution of hemin (Sigma) was prepared in 20 mM potassium hydroxide and its concentration was verified using a standard hemochrome difference spectrum, as described by Berry *et al* [47]. The aliquot of hemin to be added was then determined based upon the concentration of the hemin stock and the concentration of the AP6 solution. Then, the aliquot of hemin was added and stirred for one minute, after which complete heme incorporation into AP6 was observed by a spectral shift in the heme absorbance from unbound heme (380 nm) to bound, oxidized heme (412 nm). Aliquots were titrated in until the desired amount of heme was incorporated into the protein.

Solutions of millimolar zinc porphyrin were made in DMSO, and the exact concentration of these solutions was also determined using a reduced – oxidized absorbance differences and the extinction coefficient at 412 nm, 22,100 $M^{-1}cm^{-1}$. It was important when measuring the concentration of the zinc porphryin solution that the stock was not too concentrated, as the absorbance of millimolar solutions are difficult to measure accurately. Therefore, though stock solutions for titrations were still millimolar in concentration to limit the volume of porphryin added to the AP6 solution, this stock was diluted by 10- or 100-fold in order to accurately determine the true concentration.

3.2.4 Analytical ultracentrifugation. A Beckman XLA/I analytical centrifuge in the DeGrado laboratory was used to determine the molecular weight of self-assembled AP6 complexes with and without hemin bound. The molecular weight of the complex was assessed in a 5 mM DPC solution, and density was matched with D_2O (51%) so that the contribution of the detergent solution to the buoyant molecular weight of the peptide complex would be negligible. Sedimentation equilibrium experiments in density-matched D_2O solutions were done at 25 °C at four speeds (30,000, 35,000, 40,000, and 45,000 rpm) and two wavelengths (280 nm and 412 nm). Data analysis was completed using the WatFitter4 program designed by Dr. James Lear in the DeGrado laboratory .

3.2.5 Circular dichroism (CD). Gregory Wiedman measured CD spectra of AP6 to determine its secondary structure. The CD trace shown was taken at 15 °C.

3.2.6 Oxygen binding determination. Stopped flow analysis of predominantly mono-exponential binding kinetics of O_2 and CO ligating with ferrous hemin in AP6 were followed spectroscopically in collaboration with J.L.Ross Anderson according to published methods [1]. Rapid stopped-flow mixing of AP6 with CO gas concentrations

from 2% to 50% saturation at 15 °C was completed using an Olis RSM 1000 spectrometer. Three different solubilization conditions for AP6 were used to determine if the detergent/lipid composition had any effect on ligand binding: 2 mM DPC, 2 mM Zwittergent, and incorporation into phospholipid vesicles comprised of 2-oleoylphosphatidylcholine (POPC) and 1-palmitoyl-2-oleoylphosphatidylserine (POPS). The Olis machine scans both the α-band and Soret band absorptions 1,000 times per second, which was then followed by SVD analysis of the kinetic components at each wavelength.

3.2.7 Midpoint potential determination. Equilibrium redox potentiometry was used as a functional analysis of the oxidation and reduction of hemes bound to AP6 [48]. Redox titrations were performed in an anaerobic 1 mL cuvette (Starna Cells) equipped with a silver / silver chloride and platinum combination electrode (Microelectrodes Inc.). All of the potentials reported are in reference to the normal hydrogen electrode (NHE). The reduction potential of the cuvette solution was adjusted by adding 1 μL aliquots of freshly prepared solutions of either sodium dithionite (for reducing) or potassium ferricyanide (for oxidizing). 20 μL of a stock solution containing the following redox mediator dyes was also added to the solution (final concentrations reported): 5 μM 1,2-naphthoquinone, 5 μM 1,4- naphthoquinone, 20 μM duroquinone, 10 μM pyocyanine, 5 μM indigotrisulfonate, 10 μM 2-hydroxy-1,4-naphthoquinone, 1 μM indigocarmine, 10 μM anthraquinone-2-sulfonate, and 5 μM benzyl viologen. After equilibration at each midpoint potential, the UV-visible spectrum of the AP6-heme complex was recorded, monitoring in particular the increase in the sharp α-band absorption at 559 nm relative to a 575 nm reference wavelength.

3.3 Results

3.3.1 AP6 assembly. The molecular weight of the AP6 complex in DPC was determined by analytical ultracentrifugation. The absorbance vs. radius data collected for each sample was fit using the WatFitter4 program to determine the experimental molecular weight for each sample. The aggregation number of AP6 was calculated by dividing this experimental molecular weight by the molecular weight of a single AP6 peptide. In experiments where hemes were added, the aggregation number was determined by the following formula:

$$N = (MW - 652m) / 5022 \qquad \text{Equation 3.1}$$

where m is the number of hemes added per tetramer. The aggregation number for both the apo and holo forms of AP6 was 4, indicating that AP6 assembles cleanly in micelles as a tetramer. Experiments completed by Paul O'Brien and Gregory Wiedman also confirmed tetrameric assembly of AP6 in lipid vesicles [8].

As shown in Figure 3.3, the weight fraction of over a range of concentrations indicates that apo-AP6 assembles predominantly as a tetramer at millimolar concentrations, but the population of AP6 is split between half monomer and half dimer at micromolar concentrations of apo protein. Upon the addition of a heme, all other species are eliminated, and AP6 assembles entirely as a tetramer. This suggests that heme binding stabilizes the assembly of the four helix bundle.

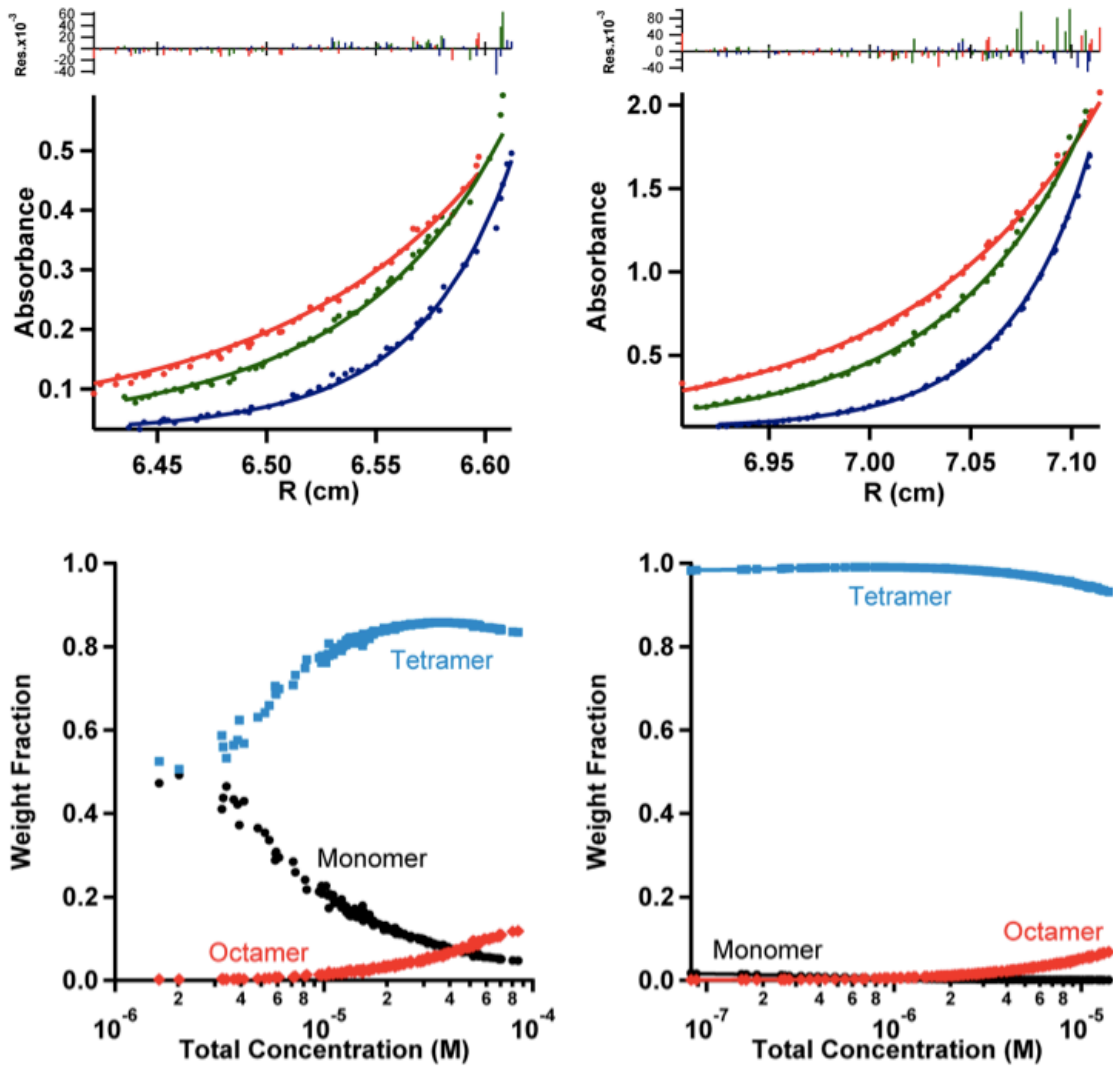

Figure 3.3: Analytical ultracentrifugation data for AP6 in its apo (left) and holo (right) forms. Shown in top panels are the absorbances at 280 nm at different radii from the center of the ultracentrifugation cell. Each trace represents a different speed: 40,000 rpm (red), 45,000 rpm (green), and 50,000 rpm (blue). This data was fit using the WatFitter4 program to obtain the MW of the AP6 complex. The bottom panels depict the weight fraction analysis of AP6 samples. AP6 assembles as a tetramer (blue trace) at millimolar concentrations without heme, and its assembly is aided by adding heme equivalents. With one heme equivalent bound, AP6 is solely a tetramer even at nanomolar concentrations.

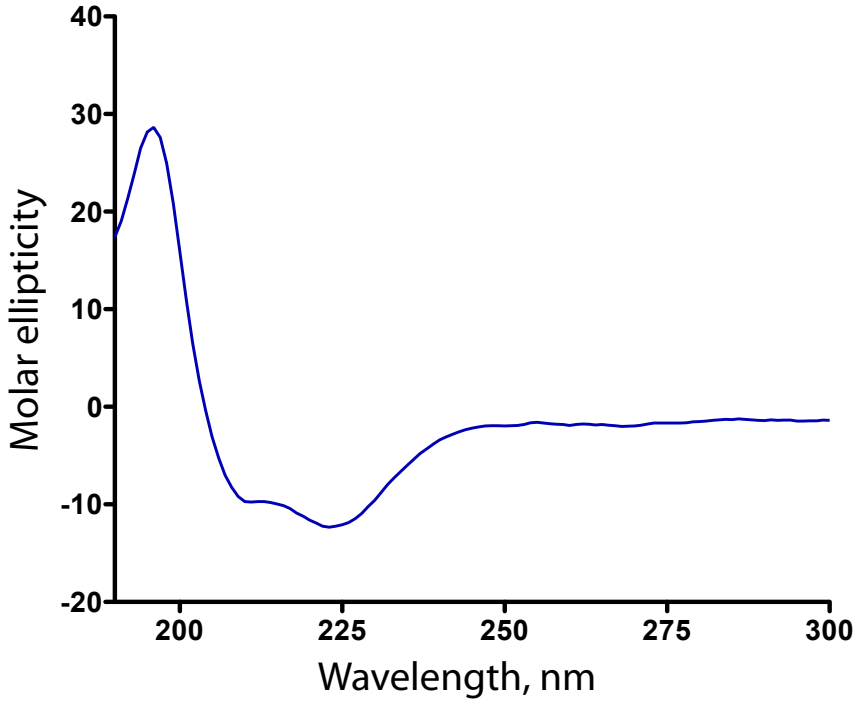

Figure 3.4 A CD spectrum of 4 μM AP6 at 15 °C (data collected by Gregory Wiedman). Secondary structure can be determined by CD spectroscopy in the far-UV spectral region (190-250 nm), and AP6 displays spectral properties characteristic of a helical structure. Helical content can be calculated using the molar ellipticity of AP6 at 222 nm, and from these calculations, AP6 is 92% helical.

Though analytical ultracentrifugation experiments verified the tetrameric assembly of AP6, circular dichroism (CD) confirmed the secondary structure of the AP6 design to be comprised of stable alpha helices (Figure 3.4). The alpha-helical content of a protein can be calculated by the following equation:

$$\% \text{ a-helix } = ([\theta]_{222\text{ nm}} - \theta_C) / (\theta_H - \theta_C) \qquad \text{Equation 3.2}$$

where θ_{222nm} is the molar ellipticity at 222 nm, θ_H and θ_C are the baseline ellipticities for the helix and random coil respectively. Using the empirical values of Rohl and Baldwin [49]:

$$\theta_H = 2220 - 53T \qquad \text{Equation 3.3}$$

$$\theta_C=(-44000 + 250T)(1-3/N_r) \quad \text{Equation 3.4}$$

where T is temperature (in ºC) and N_r is the number of amino acid residues, tetrameric AP6 is 92% helical at 15 ºC.

3.3.2 Heme binding in AP6. AP6 was designed to bind up to six bis-histidine ligated porphryns. The binding site ligated to histidine 10 in the HP region is referred to the "a" binding site, whereas the two sites located in the LP region at histidines 24 and 35 are named "b" and "c" respectively. Figure 3.5 shows a hemin titration of 2 μM AP6 in 2 mM DPC. The Soret absorbance of heme increases linearly with heme additions until one heme per bundle is bound. This indicates that the first dissociation constant (K_{d1}) is below the 5 nM resolution level of this experimental assay. The linear relationship between the initial points can be used to estimate the extinction coefficient of the bound heme, which reduces the number of unknowns in the Mathematica (Wolfram Research) program used for fitting the heme titration data to heme dissociation constants. The AP6 binding data shown in Figure 3.5 were fit to six independent binding sites with equilibrium binding constants of $K_{d1} < 5$ nM, $K_{d2} = 70$ nM, $K_{d3} = 1.4$ μM $K_{d4} = 2.1$ μM, K_{d5}, $K_{d6} > 5$ μM in 2 mM DPC. AP6 variants were fit to binding constants based upon the number of available hisitidine binding sites. All of the K_d values for AP6 proteins are listed in Table 3.2.

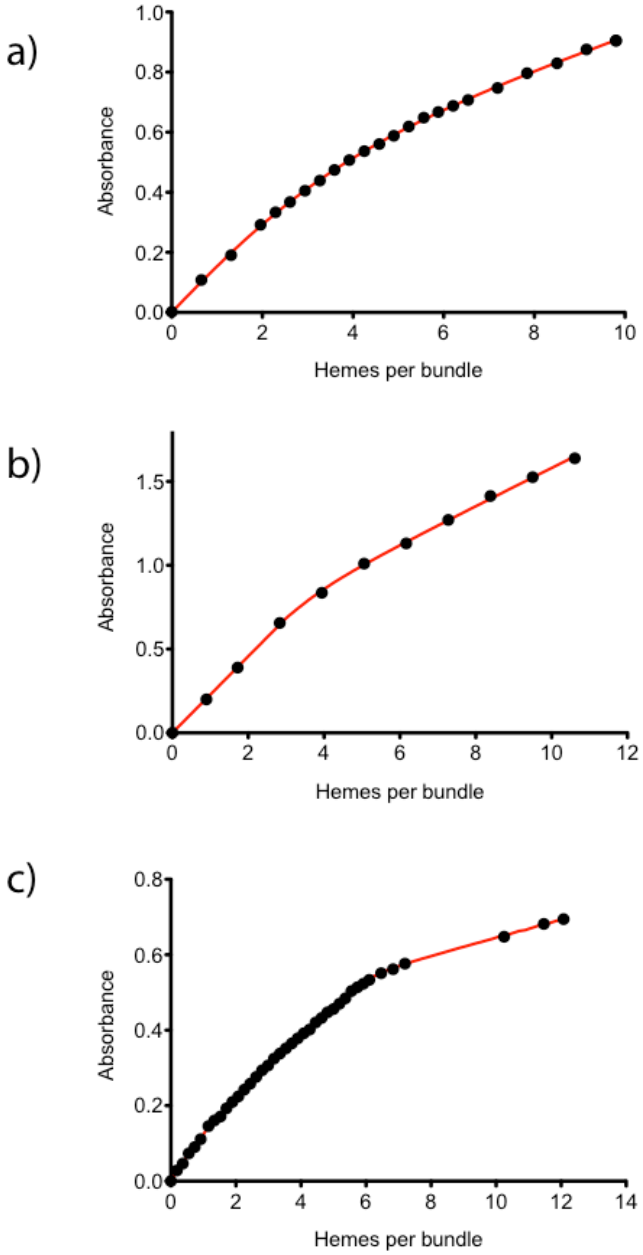

Figure 3.5: Heme binding to a) 1.53 μM AP6 in 2 mM DPC b) 2 μM AP6 in DCM, and c) 1 μM AP6 in POPC vesicles (completed by Gregory Wiedman). The curve in a) can be fit to six different binding constants, representing all six binding sites found in AP6. Those constants are: $K_{d1} < 5$nM, $K_{d2} = 70$ nM, $K_{d3} = 1.4\ \mu$M, $K_{d4} = 2.1\mu$M, K_{d5}, $K_{d6} > 5\ \mu$M.

Table 3.2: Summary of K_d values for hemes bound to AP6 and AP6 variants

Protein	Hemes bound	Kd
AP6	6	K_{d1} < 5nM, K_{d2} = 70 nM, K_{d3} = 1.4 μM, K_{d4} = 2.1μM, K_{d5} & K_{d6} >5 μM
AP6a	2	50 nM, 1 μM
AP6b	2	100 nM, 3 μM
AP6c	Not measured	Not measured
AP6ab	2	50 nM, 3 μM
AP6ac	4	7 nM, 150 nM, 2 μM, 4.2 μM
AP6bc	4	200 nM, 1 μM, K_{d3} & K_{d4} > 5μM

Binding porphyrins that contain zinc is advantageous because these porphyrins are then photoactivatable, allowing for the investigation of light-initiated electron- and energy-transfer events between chromophores in multi-cofactor maquettes. Initial ZnPPIX binding titrations were completed using AP6 solubilized in 2 mM DPC. Previous maquette designs have demonstrated single-histidine axial ligation of ZnPPIX [50], and fully assembled AP6 also adopts this coordination upon cofactor binding. As shown by the initial linear dependence of bound heme absorbance to heme:bundle in Figure 3.6, AP6 is able to bind up to seven ZnPPIX cofactors at nanomolar affinity before the cofactor binding strength weakens.

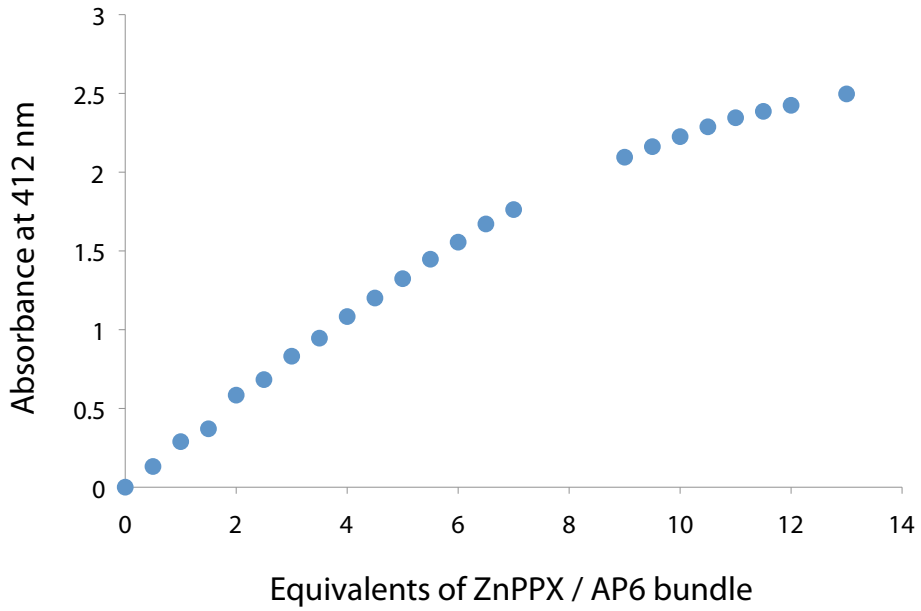

Figure 3.6 Titrations of a millimolar ZnPPX solution (in DMSO) added to 1 μM AP6 in 2 mM DPC (data obtained by Gregory Wiedman).

3.3.3 Redox potentials of hemes bound to AP6. Figure 3.7 illustrates redox titrations of AP6 with varying equivalents of heme bound. The titrations reveal a splitting in redox potential that originates from a difference in heme environment due to

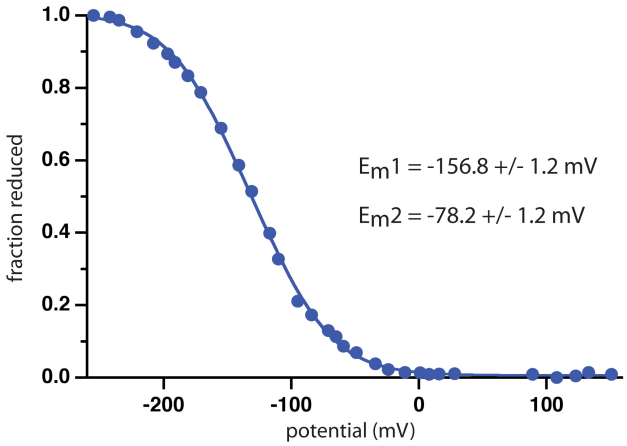

Figure 3.7 Redox titration of 4 μM AP6 in 2 mM DPC with two heme equivalents added.

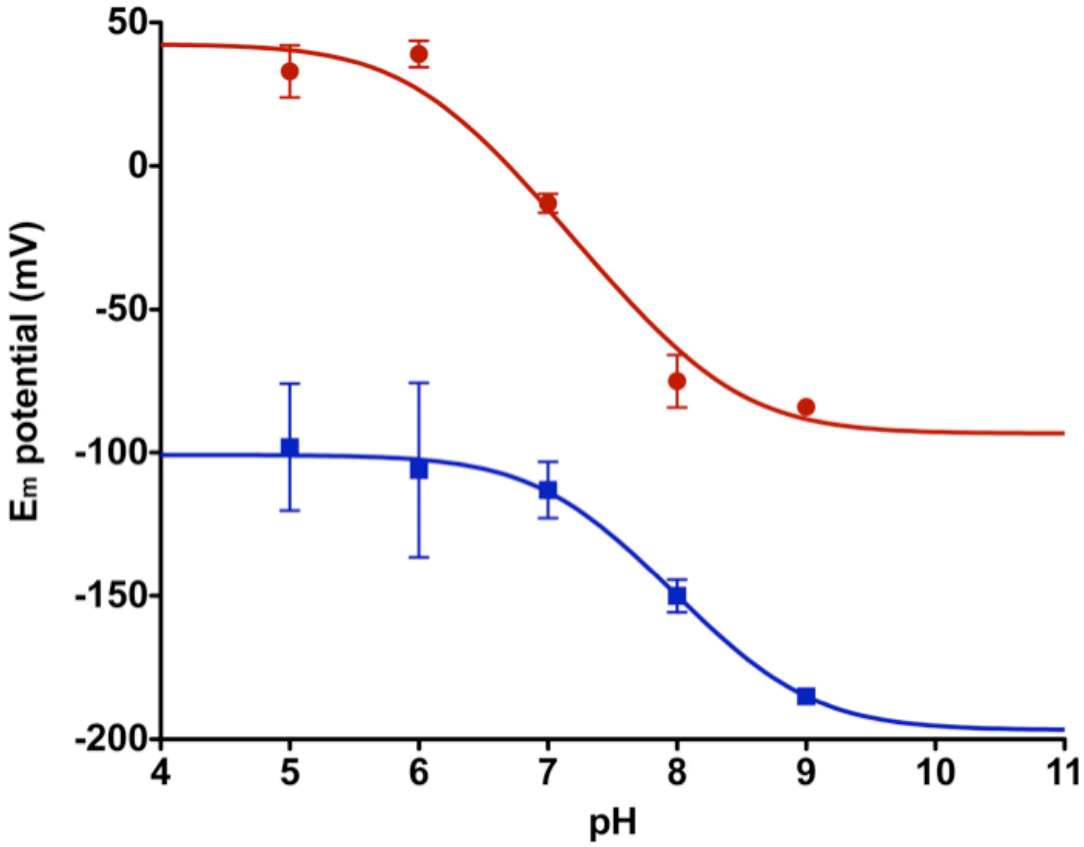

Figure 3.8 Determination of the pK_{red} and pK_{ox} for each of the AP6 heme *b* midpoint potentials. Data was fit to Equation 3.7.

heme-heme charge interactions. The relationship between midpoint potential and pH was explored for the hemes bound to AP6 and is shown in Figure 3.8. The higher potential heme had a pKox of 6.1 and a pKred of 8.3. Over a modest pH range from pH 6.1 to pH 8.3, the slope was -57 mV/pH unit, indicative of a 1 e^- / 1H^+ relationship. The low potential heme displayed a pKox of 7.2 and a pKred of 8.8. Interestingly, between those pH ranges, this heme did not display the same 1 e^- / 1H^+ relationship shown for the higher potential heme, but instead had a slope of -37 mV/pH unit.

3.3.4 Generation of the oxy-ferrous state in AP6. AP6 with reduced hemes bound was tested to see if the hemes could ligate CO or O_2. It was expected that since

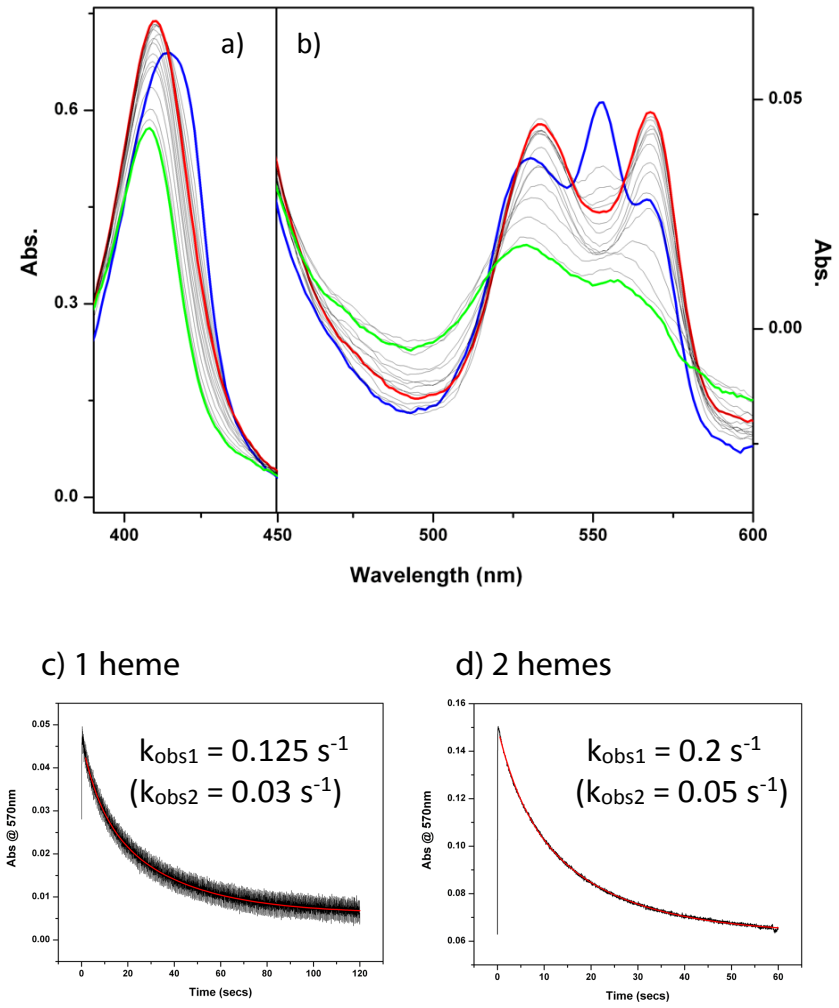

Figure 3.9: Forming the oxy-ferrous intermediate in 5 μM AP6 in 2 mM Zwittergent. Panels a (Soret) and b (a-bands) depict the spectral changes associated with oxidized (green), reduced (blue), and oxy-ferrous generation (red). Panels (c) and (d) reflect the auto-oxidation rate of heme *b* from the oxy-ferrous state (Fe^{2+}-O_2) to the oxidized form (Fe^{3+}). These experiments were completed in collaboration with J.L. Ross Anderson.

the HP domain of AP6 was based on the successful oxygen-binding HP7 protein [1], any reduced hemes bound to this domain should also be able to ligate oxygen. Surprisingly, AP6 only bound oxygen when solubilized in Zwittergent; DPC and phospholipid vesicles were not successful environments for AP6-heme oxygen binding.

Figure 3.8 (a) and (b) depict the stopped-flow spectral changes for mixing

reduced AP6 proteins with oxygen at 15 ° C. The Soret (a) and α-band (b) spectra show the transformation of the reduced heme *b* (blue) to the oxy-ferrous state (red), which eventually becomes oxidized (green). Intermediate states are shown in gray. The auto-oxidation rates from an AP6 oxy-ferrous state (Fe^{2+}-O_2) to its oxidized state (Fe^{3+}) were measured with 1 (c) and 2 (d) hemes bound.

3.3.5 AP6 variants. Six variants of AP6 were created using solid phase peptide synthesis to learn more about the individual characteristics of each heme binding site. The heme binding properties of these mutants – AP6a, AP6b, AP6c, AP6ab, AP6ac, and AP6bc – are listed in Table 3.2. The names of these mutants correspond with the binding sites present as labeled in Figure 3.2; for example, AP6a retains the histidine at residue

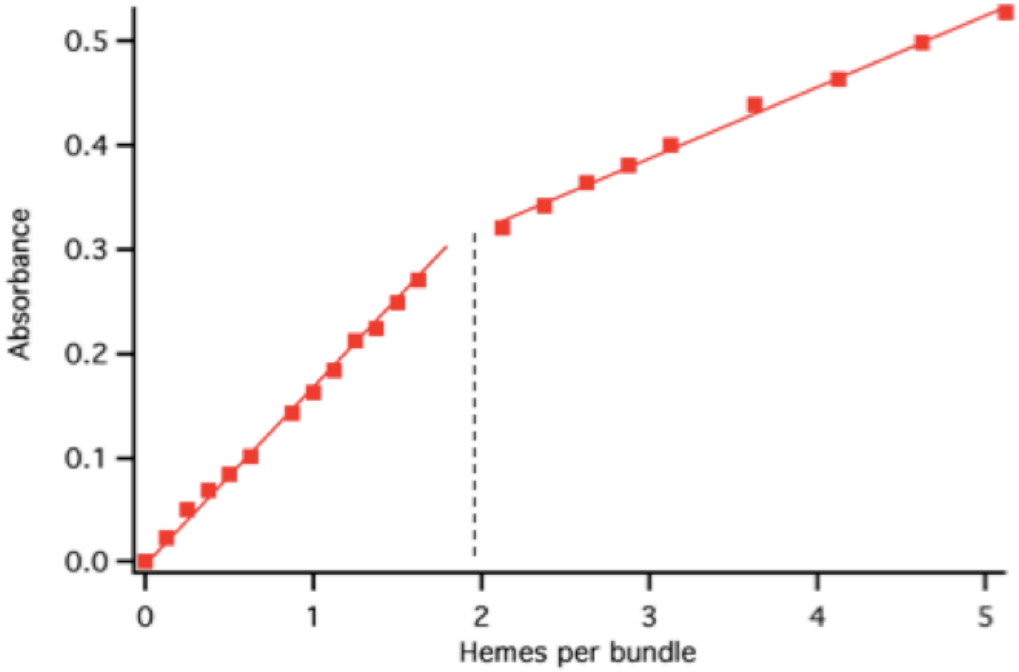

Figure 3.10 Heme titration with 1.25 μM AP6ab. Though it has four binding sites available, this AP6 variant very clearly binds only two tightly from the break in the linear binding relationship that occurs after 2 hemes per bundle were added to the solution. K_d values were determined to be $K_d1 < 5$ nM and $K_d2 = 120$ nM.

10, but not at residues 24 and 35, where phenylalanine was substituted.

The variants were first analyzed by analytical ultracentrifugation to determine if all of the heme binding sites were required for tetrameric assembly of AP6. AP6 does not require all three heme binding sites to be present for tetrameric assembly. All of the AP6 variant proteins containing single or multiple binding sites assembled as tetramers except AP6c, which aggregated as an octomer in both its apo- and holo-forms.

The heme binding characteristics of the AP6 variants varied considerably from the binding patterns associated with AP6, and are outlined in Table 3.2. Though the mutants with a single heme binding site (AP6a and AP6b; AP6c was not tested since it did not assemble as a four-helix bundle) both bound up to two hemes tightly, the mutants that contained four heme binding sites (APab, APac, APbc) did not all bind up to four hemes. AP6ab bound two hemes that were fit to binding constants around the nanomolar constraint of the assay (Figure 4.10). AP6bc bound hemes weakly, with much of the heme equivalents added remaining unbound.

3.4 Discussion

3.4.1 Design characteristics. The main principle of AP6 construction was the same structured assembly driven by Regan and DeGrado [22] and its AP predecessors [2, 17] – a well-developed exterior pattern of polar and non-polar residues exposed along the axis of the four-helix bundle. However, it was important that these external interactions did not conflict with the interior amino acids that make up the helix interface. Additionally, a reasonably accurate prediction of the location of each residue was needed to ensure that the metal porphyrin-ligating histidine residues within the interior were properly aligned to ensure tight cofactor binding. The HP and LP domains each have

their own amphiphilic exterior and interior patterns and specific interior residues that need to be aligned with respect to one another in one helix. As shown in Figure 3.2, the alignment of the two domains within the AP6 sequence was accomplished by plotting the sequence on polar graphs that emphasize the angular position of each residue in the sequence according to the following equation:

$$\theta = 360° / r \qquad \text{Equation 3.6}$$

where r is the number of residues per turn. Since the value of r cannot be determined without structural characterization, polar plots were created using an r-value assumed from the related protein structure of HP7 (3.58 residues per turn) and assuming an ideal, straight a-helix with 3.6 residues per turn for the transmembrane portion, or a $\theta = 100°$.

The sequence of the HP domain found in AP6 is 15 residues in length and incorporates the bis-histidine ligating sequence from HP7 that was successful for tight cofactor binding. The LP domain is based on the native hydrophobic heme binding sequences from Complex III [6]. Complex III enzymes contain a conserved four-helix bundle that ligates b_L and b_H between four histidine residues on helices *b* and *d*. As shown in Figure 3.11, unlike the structure surrounding the b_L site, where the diameter of the four-helix bundle increases around the heme binding site to allow for interactions with additional helical segments, the helical structure around the heme b_H binding site (residues 188-200) is a more ideal alpha helix. In the AP(2-3) designs, Complex III residues 188-200 around the heme b_H binding site served as a template for their LP domain. The new AP6 design extends the sequence of the LP domain to 29 residues, but does still maintain high homology with the sequence found in Complex III. In addition, a four residue helix-capping sequence, GEGL, was used at the C-terminus to promote

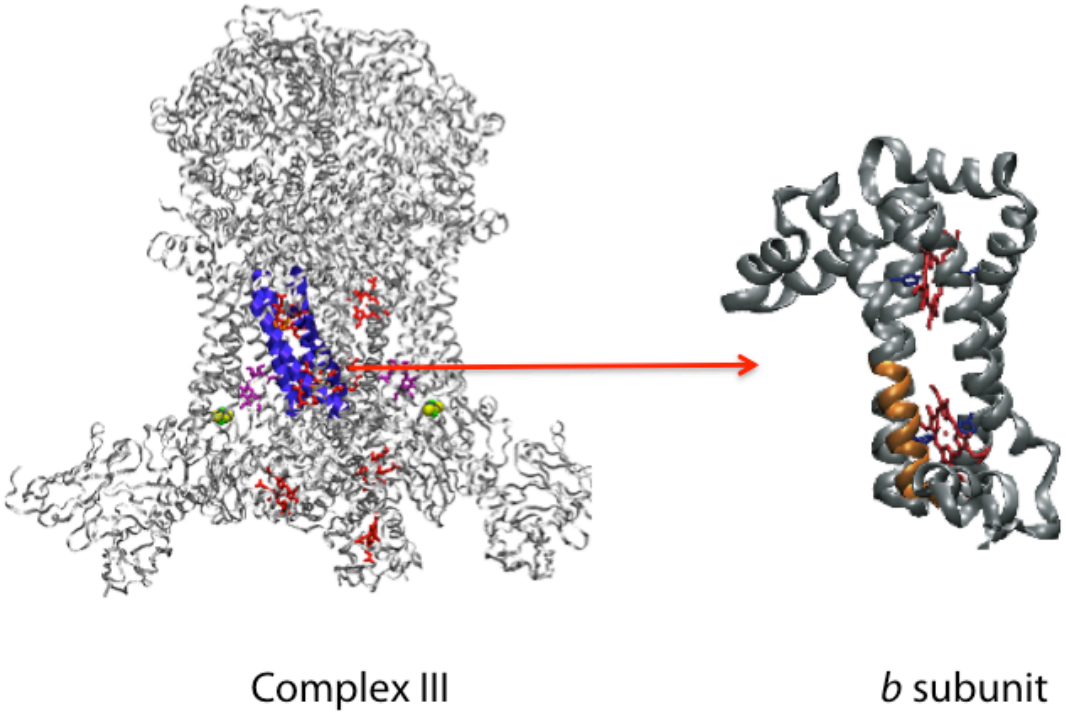

Figure 3.11 Crystal structures of native Complex III depicting its b subunit in blue (left) and zoomed in (right). Shown in yellow are residues 188 – 200, where the Complex III helix is the most ideal. The LP domain found in AP6 is based upon this section of Complex III. This figure was drawn from PDB file 1BE3 [6] using Pymol (DeLano Scientific and Schröedinger) software.

hydrogen bonding interactions that can be lost at the end of a peptide sequence. One factor that simplified the AP6 design was that the tilt angle of the HP7 helix (5.1°) closely matches the tilt angle calculated for Complex III (8.5°); therefore, the flexible linking sequence found in the earlier AP1 design was not necessary in this design to link the two domains. However, two phenylalanine residues were placed between the HP and LP domains, because phenylalanine can successfully partition between polar and non-polar interfaces due to its aromatic character.

3.4.2 AP6 may require additional structural constraints. Though the structure of AP6 is not yet known on a molecular scale, much is still known about AP6

secondary structure and assembly. CD experiments reveal that AP6 is highly helical in nature, and that its helical structure is stable over a wide range of temperatures and denaturant concentrations [8]. High stability in the LP domain was expected for AP6 (as was demonstrated by predecessor AP family members [2]) because disrupting hydrogen bonds of alpha helices in a hydrophobic environment is energetically unfavorable. Not surprisingly, the helical nature of the HP domain has been demonstrated in earlier HP proteins [51], and is most likely further stabilized in AP6 by the LP domain.

AP6 assembles as a tetramer in its apo-form, and binding hemes stabilizes four-helix bundle formation at higher concentrations. AP6 variants that lack one or more of the three histidine binding residues are not able to maintain heme binding at all remaining available sites in some cases. These results suggest that without all of the porphryn coordinating histidines present in its sequence, AP6 may adopt different conformations that do not promote heme binding, even though it is still assembled as a tetramer. Also, removing the tightest binding site "a" in AP6bc may interrupt cooperative heme binding, lowering the binding affinity for the "b" and "c" sites such that they no longer bind hemes as tightly.

3.4.3 Heme properties in AP6. The observation of redox potential splitting upon addition of just one heme cofactor demonstrates cooperative cofactor binding. In this scenario, binding one heme in one binding site increases the affinity for the other heme to bind in a binding site within the same maquette. When one heme is added, the redox titrations are measuring the redox potential of a heterogeneous mixture of AP6 maquettes, where the half of the maquette population is comprised of apo-proteins and half of the AP6 proteins have two heme equivalents bound. Therefore, the best

experimental conditions for redox titrations are to bind at least two hemes so that the maquette population is homogenous.

The assembly topology of the maquette dictates the heme-heme distances, and therefore heme-heme charge interactions, in maquettes with at least two hemes bound [2, 12]. AP6, like many previous maquette designs [1, 2, 5, 12, 17], assembles with a *syn* topology (Figure 3.2). Maquettes with a *syn* topology, such as AP1 [2], H10A24 [5, 12], or AP6, ligate two hemes in close proximity, leading to an electrostatic interaction between the two cofactors. In AP6, a single midpoint potential value for that binding site is split by ~75 mV when two hemes are added. This dramatic potential split is consistent with an electric field effect – the heme with the -156 mV potential is titrated while influenced by the electric field of an uncharged ferrous heme, while the heme with the -78 mV potential was titrated while in the presence of the electric field from the other charged ferric heme.

The redox splitting information can be used to assign cofactor binding constants to specific binding sites. In order for the hemes to have charge-charge interactions, the hemes need to be in close proximity to one another. Therefore, the first two hemes equivalents added need to either be bound to two identical binding sites (*i.e.* both hemes bound at this bis-histidine 10 site) or in two sites directly adjacent to one another (*i.e.* one heme bound at the histitine 10 site and one heme bound at the histidine 24 site). The large splitting of ~75 mV in midpoint potential represents the same field strength and charge-charge interaction energy observed in the H10A24 maquette [12], suggesting that the interaction is derived from two hemes parallel to one another in identical binding sites as they are in H10A24. As AP6a binds hemes more tightly than the other AP6 variants

(Table 3.2), it is likely that the first two hemes in AP6 bind to the two binding sites at histidine 10 before binding to the membrane-associated sites.

Successful formation of an AP6 oxy-ferrous state confirmed that construction and assembly of AP6 maintains the symmetric rotation of key glutamate residues into the maquette interior required in HP maquettes for oxygen binding, excluding water from the redox active site. However, this occurs only in certain membrane interfaces. The heme binding affinity must change when AP6 assembles in different membrane interfaces, as it is the affinity of the heme that drives the rotation of the glutamates into the bundle interior and weakens one of the histidine ligands enough to promote oxygen ligation [1]. Therefore, AP6 assembly varies when solubilized in different detergents (and lipid compositions, though that was not explored in this thesis work).

3.4.4 Proton coupling to heme midpoint potential. Proton coupling to heme oxidation and reduction requires that the pK value of an acidic or basic group on the cofactor (or on a residue within the active site) shifts according to this thermodynamic scheme:

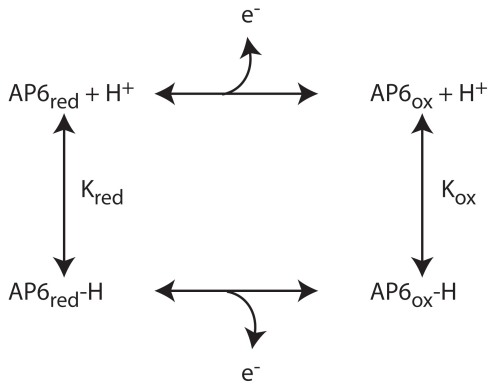

Scheme 3.1

Oxidizing the cofactor increased its positive charge, decreasing the proton affinity (pK_{ox}) of the acidic/basic group. Likewise, under reduced conditions, the proton affinity (pK_{red})

is increased as the cofactor increases its negative charge. In regions between the pK_{ox} and pK_{red}, the midpoint potential of the cofactor will depend upon the protonation state of the acidic/basic group, decreasing as the pH increases. For every proton coupled to one electron from a cofactor, the slope of its pH dependence will be -59 mV. These conditions were evaluated for AP6 to determine the pK_{ox} and pK_{red} for each of the hemes bound. The heme oxidation / reduction when coupled to protonatable residues is described according to the following equation:

$$E_m = E_0 + \frac{RT}{nF} \log\left(\frac{10^{-pK_{red}} + 10^{-pH}}{10^{-pK_{ox}} + 10^{-pH}}\right)$$

Equation 3.7

where E_0 is the midpoint potential of the heme at low pH when all of the influencing residues are protonated.

As shown in Figure 3.8, the high potential heme is dependent on a single proton group, as its slope between its pKox and pKa red is -57 mV/pH unit, which is very close to the ideal slope of -59 mV / pH for a 1 e^- / 1 H^+ process. The proton coupled to this midpoint potential could either be associated with either of its bis-histidine ligands, or glutamate residue 11, which is located within the heme binding site between the bundle's interior and exterior. There is some precedent for proton coupling with a glutamate residue for hemes bound to AP maquettes; glutamate residues in AP1 were found to raise the pK_{red} above pH 8 in its ferrous state [2]. The lower potential heme displays a modest proton dependence of -37 mV / pH unit between its pK_{ox} and pK_{red}. This reflects more than a full proton equivalent coupled to a single electron transfer, and could mean that the

charge-charge interaction between the two hemes also affects its coupling to glutamate proton exchange.

3.5 Conclusion

In this chapter, the maquette approach was applied to design a new member of the AP maquette family, AP6. AP6 contains both a HP and a LP domain and assembles as tetrameric α-helical bundles in detergents, organic solvents, or in lipid vesicles. Six FePPIX binding sites are distributed within the AP6 sequence to create a transmembrane cofactor chain, with two hemes binding in the HP domain (histidine 10), two hemes binding at the solvent/membrane interface (histidine 21), and two hemes binding within the LP domain (histidine 35). The hydrophobic environment of the membrane increases the redox potential of the bis-histidine bound hemes (in comparison to hemes bound to the HP maquettes) and AP6 can withstand significant electrostatic interactions between two bound heme cofactors. Furthermore, AP6 has proton coupling to heme oxidation/reduction over a modest pH range.

However common it might be for the Complexes within the mitochondrial respiratory chain, complexity is not an essential requirement for enzymatic activity. This simple AP6 design was created as a model system for studying the basic functions carried out by the enzymes of the respiratory chain, such as Complex III: transmembrane electron transfer, electron transfer with aqueous proteins, and proton-coupled electron transfer. In chapter four, the extent of AP6 quinol-cytochrome *c* oxidoreductase activity will be tested using standard Complex III steady-state activity assays.

3.6 References

1. Koder, R.L., et al., *Design and engineering of an O(2) transport protein*. Nature, 2009. **458**(7236): p. 305-9.
2. Discher, B.M., et al., *Design of amphiphilic protein maquettes: controlling assembly, membrane insertion, and cofactor interactions*. Biochemistry, 2005. **44**(37): p. 12329-43.
3. Huang, S.S., et al., *The HP-1 maquette: from an apoprotein structure to a structured hemoprotein designed to promote redox-coupled proton exchange*. Proc Natl Acad Sci U S A, 2004. **101**(15): p. 5536-41.
4. Gibney, B.R., et al., *Hydrophobic modulation of heme properties in heme protein maquettes*. Biochemistry, 2001. **40**(35): p. 10550-61.
5. Shifman, J.M., et al., *Heme redox potential control in de novo designed four-alpha-helix bundle proteins*. Biochemistry, 2000. **39**(48): p. 14813-21.
6. Iwata, S., et al., *Complete structure of the 11-subunit bovine mitochondrial cytochrome bc1 complex*. Science, 1998. **281**(5373): p. 64-71.
7. Chobot, S.E., Wiedman, G.R., Moser, C.C., Discher, B.M., Dutton, P.L., *Demonstrating quinol-cytochrome c oxidoreductase kinetic activity by an amphiphilic maquette protein*. Biochemistry, 2010. **submitted**.
8. Wiedman, G.R., O'Brien, P.A., Chobot, S.E., Parekh, V.P., Karunakaran, V., Anderson, J.L.R., Moser, C.C., Dutton, P.L., Discher, B.M., *Building a Function into Simplified Protein Structures: Amphiphilic Maquettes with Multiple Cofactor Binding Sites*. Biochemistry, 2010. **submitted**.
9. Fischer, E., *Synthesen in der Purin- und Zuckergruppe*. In Les Prix Nobel en 1902, 1905.
10. Discher, B.M., et al., *Hydrophilic to amphiphilic design in redox protein maquettes*. Curr Opin Chem Biol, 2003. **7**(6): p. 741-8.
11. Hecht, M.H., et al., *De novo design, expression, and characterization of Felix: a four-helix bundle protein of native-like sequence*. Science, 1990. **249**(4971): p. 884-91.
12. Grosset, A.M., et al., *Proof of principle in a de novo designed protein maquette: an allosterically regulated, charge-activated conformational switch in a tetra-alpha-helix bundle*. Biochemistry, 2001. **40**(18): p. 5474-87.
13. Di Costanzo, L., et al., *Toward the de novo design of a catalytically active helix bundle: a substrate-accessible carboxylate-bridged dinuclear metal center*. J Am Chem Soc, 2001. **123**(51): p. 12749-57.
14. Wei, Y., et al., *Stably folded de novo proteins from a designed combinatorial library*. Protein Sci, 2003. **12**(1): p. 92-102.
15. Dai, Q.H., et al., *Structure of a de novo designed protein model of radical enzymes*. J Am Chem Soc, 2002. **124**(37): p. 10952-3.
16. Ghirlanda, G., et al., *De novo design of a D2-symmetrical protein that reproduces the diheme four-helix bundle in cytochrome bc1*. J Am Chem Soc, 2004. **126**(26): p. 8141-7.

17. Noy, D., et al., *Design of amphiphilic protein maquettes: enhancing maquette functionality through binding of extremely hydrophobic cofactors to lipophilic domains*. Biochemistry, 2005. **44**(37): p. 12344-54.
18. Silverman, J.A., R. Balakrishnan, and P.B. Harbury, *Reverse engineering the (beta/alpha)8 barrel fold*. Proc Natl Acad Sci U S A, 2001. **98**(6): p. 3092-7.
19. Ramirez-Alvarado, M., F.J. Blanco, and L. Serrano, *De novo design and structural analysis of a model beta-hairpin peptide system*. Nat Struct Biol, 1996. **3**(7): p. 604-12.
20. Darwin, C., *Origin of the Species*. 1862.
21. Robertson, D.E., et al., *Design and synthesis of multi-haem proteins*. Nature, 1994. **368**(6470): p. 425-32.
22. Regan, L. and W.F. DeGrado, *Characterization of a helical protein designed from first principles*. Science, 1988. **241**(4868): p. 976-8.
23. Gibney, B.R., et al., *Self-assembly of heme A and heme B in a designed four-helix bundle: implications for a cytochrome c oxidase maquette*. Biochemistry, 2000. **39**(36): p. 11041-9.
24. Bender, G.M., et al., *De novo design of a single-chain diphenylporphyrin metalloprotein*. J Am Chem Soc, 2007. **129**(35): p. 10732-40.
25. Lichtenstein, B.R., et al., *Reversible proton coupled electron transfer in a peptide-incorporated naphthoquinone amino acid*. Chem Commun (Camb), 2009(2): p. 168-70.
26. Hay, S., K. Westerlund, and C. Tommos, *Redox characteristics of a de novo quinone protein*. J Phys Chem B, 2007. **111**(13): p. 3488-95.
27. Sharp, R.E., et al., *Design, synthesis, and characterization of a photoactivatable flavocytochrome molecular maquette*. Proc Natl Acad Sci U S A, 1998. **95**(18): p. 10465-70.
28. Kennedy, M.L. and B.R. Gibney, *Proton coupling to [4Fe-4S](2+/+) and [4Fe-4Se](2+/+) oxidation and reduction in a designed protein*. J Am Chem Soc, 2002. **124**(24): p. 6826-7.
29. Tommos, C., et al., *De novo proteins as models of radical enzymes*. Biochemistry, 1999. **38**(29): p. 9495-507.
30. Westerlund, K., et al., *Exploring amino-acid radical chemistry: protein engineering and de novo design*. Biochim Biophys Acta, 2005. **1707**(1): p. 103-16.
31. Maglio, O., et al., *Preorganization of molecular binding sites in designed diiron proteins*. Proc Natl Acad Sci U S A, 2003. **100**(7): p. 3772-7.
32. Summa, C.M., et al., *Computational de novo design, and characterization of an A(2)B(2) diiron protein*. J Mol Biol, 2002. **321**(5): p. 923-38.
33. Noy, D., C.C. Moser, and P.L. Dutton, *Design and engineering of photosynthetic light-harvesting and electron transfer using length, time, and energy scales*. Biochim Biophys Acta, 2006. **1757**(2): p. 90-105.
34. Razeghifard, M.R. and T. Wydrzynski, *Binding of Zn-chlorin to a synthetic four-helix bundle peptide through histidine ligation*. Biochemistry, 2003. **42**(4): p. 1024-30.

35. Mennenga, A., et al., *Effects of noncovalently bound quinones on the ground and triplet states of zinc chlorins in solution and bound to de novo synthesized peptides*. Phys Chem Chem Phys, 2006. **8**(46): p. 5444-53.
36. Springs, S.L., et al., *A multigeneration analysis of cytochrome b(562) redox variants: evolutionary strategies for modulating redox potential revealed using a library approach*. Biochemistry, 2002. **41**(13): p. 4321-8.
37. Huang, S.S., et al., *X-ray structure of a maquette scaffold*. J Mol Biol, 2003. **326**(4): p. 1219-25.
38. Gibney, B.R., Rabanal, F., Skalicky J.J., Wand, A.J., Dutton, P.L., *Iterative protein redesign*. J Am Chem Soc, 1999. **121**: p. 4952-4960.
39. Choma, C., et al., *Asparagine-mediated self-association of a model transmembrane helix*. Nat Struct Biol, 2000. **7**(2): p. 161-6.
40. Bowie, J.U., *Understanding membrane protein structure by design*. Nat Struct Biol, 2000. **7**(2): p. 91-4.
41. Lear, J.D., et al., *Position-dependence of stabilizing polar interactions of asparagine in transmembrane helical bundles*. Biochemistry, 2003. **42**(21): p. 6400-7.
42. Lear, J.D., Z.R. Wasserman, and W.F. DeGrado, *Synthetic amphiphilic peptide models for protein ion channels*. Science, 1988. **240**(4856): p. 1177-81.
43. DeGrado, W.F., H. Gratkowski, and J.D. Lear, *How do helix-helix interactions help determine the folds of membrane proteins? Perspectives from the study of homo-oligomeric helical bundles*. Protein Sci, 2003. **12**(4): p. 647-65.
44. Dawson, J.P., J.S. Weinger, and D.M. Engelman, *Motifs of serine and threonine can drive association of transmembrane helices*. J Mol Biol, 2002. **316**(3): p. 799-805.
45. Killian, J.A., *Hydrophobic mismatch between proteins and lipids in membranes*. Biochim Biophys Acta, 1998. **1376**(3): p. 401-15.
46. Strandberg, E. and J.A. Killian, *Snorkeling of lysine side chains in transmembrane helices: how easy can it get?* FEBS Lett, 2003. **544**(1-3): p. 69-73.
47. Berry, E.A. and B.L. Trumpower, *Simultaneous determination of hemes a, b, and c from pyridine hemochrome spectra*. Anal Biochem, 1987. **161**(1): p. 1-15.
48. Dutton, P.L., *Redox potentiometry: determination of midpoint potentials of oxidation-reduction components of biological electron-transfer systems*. Methods Enzymol, 1978. **54**: p. 411-35.
49. Rohl, C.A. and R.L. Baldwin, *Comparison of NH exchange and circular dichroism as techniques for measuring the parameters of the helix-coil transition in peptides*. Biochemistry, 1997. **36**(28): p. 8435-42.
50. Sharp, R.E., Diers, J.R., Bocian, D.F., Dutton, P.L, *Differential binding of iron(III) and zinc(II) protoporphyrin IX to synthetic four-helix bundles*. J Am Chem Soc, 1998. **120**: p. 7103-7104.
51. Gibney, B.R. and P.L. Dutton, *Histidine placement in de novo-designed heme proteins*. Protein Sci, 1999. **8**(9): p. 1888-98.

Chapter 4: Demonstrating quinol-cytochrome *c* oxidoreductase kinetic activity by AP6

Given its sequence and heme binding capabilities, the AP6 design outlined in chapter three could accomplish a variety of potential functions, including: transmembrane electron transfer, electron transfer with aqueous proteins, and/or proton-coupled electron transfer. In this chapter, AP6 is tested as a potential quinol-cytochrome *c* oxidoreductase (Complex III) enzyme. As determined using standard Complex III activity assays, AP6 is the first example of a synthetic maquette with enzymatic activity within two orders of magnitude of a natural protein. AP6 quinol-cytochrome *c* oxidoreductase activity can be generated with a variety of reduced quinone substrates, and is dependent on the concentration of cytochrome *c* present. With no obvious quinone-binding site included in our protein design, AP6 provides clear evidence that an elaborate quinone-binding site within a membrane protein is not essential for generating significant quinol-cytochrome *c* oxidoreductase enzymatic activity from a heme protein. A version of the work in this chapter is in preparation for submission to *Biochemistry* [1].

4.1 Introduction

As outlined in chapters one and two, diffusible redox cofactors that link together multiple protein complexes are critical to the design of Complex III. Catalytic sites for oxidation and reduction of otherwise stable substrates, including quinone molecules together with chains of redox cofactors, add speed and direction to electron transfer and proton translocation to turn the free energy of oxidation-reduction reactions into a transmembrane $\Delta\mu_H+$. These electron transfer reactions have been studied extensively; however, an understanding of energy coupling as it relates to specific electron transfer mechanisms within Complex III remains elusive. In order to address this problem, a basic understanding of the structure, specificity, and functionality of membrane proteins needs to be achieved. In chapter four, the maquette approach [2, 3] was applied to engineer a simple transmembrane protein, AP6, to perform the same types of electron transfer mechanisms found in more complicated protein systems. AP6 was engineered to contain all of the benefits of a transmembrane cofactor chain capable of accelerating electron and proton transfer without the structural or functional complexities that plague our understanding of natural Complex III.

Complex III is a complicated redox enzyme with many aspects of its mechanism undefined, but reproducing its quinol-oxidoreductase function should not be out of reach for a transmembrane maquette protein. Quinones are present in high cellular concentrations (millimolar) and are also extremely mobile and reactive [4]. Even without specific binding pockets for decylubiquinone explicitly designed, the hydrophobicity of the quinone molecules coupled with excess concentrations in the cuvette works to promote quinone association with the detergent micelle and hydrophobic AP6 maquette.

Though no other protein has ever been specifically designed to mimic Complex III activity specifically, AP6 is not the first example of a maquette protein designed for catalysis. In 2004, Kaplan and DeGrado designed di-iron oxidoreductase mimics that catalyzed the two-electron oxidation of 4-aminophenol (k_{cat} / K_m = 1500 $M^{-1}s^{-1}$) to the corresponding quinone monoamine using a bound diiron cofactor [5]. The sequence of this non-natural enzyme was designed using a computational method that considered stabilizing known structural properties of previously designed dueferri (DF) family of proteins, as well as destabilizing likely alternative protein folds. The catalytic efficiency of this protein was sensitive to the size of the methyl group in the active site of the protein, suggesting that the active site design was specifically engineered to maximize catalysis. Addtionally, *de novo* designed retro-adolase enzymes were created using computational and directed evolution enzyme design strategies [6]. Recently, Röthlisberger *et al*. applied those same techniques to create enzymes that catalyze the Kemp elimination reaction, a model reaction for proton transfer from carbon, with multiple turnovers on a seconds timescale [7]. Although the turnover rates for these enzymes are lower than the rates of many natural proteins, all of these enzymes successfully applied known structures towards the design of natural function and signified the advancement of the protein design field. However, one plausible reason for their lowered turnover rates could be that these proteins were designed to recreate a singular structure of the active natural enzyme, ignoring any transition states that may be required to fully reproduce the enzyme's function. Therefore, one of the benefits of the AP6 design is that its assembly and structure is controlled but not static, allowing for

subtle structural movements that would be required for substrate interactions and subsequent electron transfer reactions.

4.2 Materials and methods

4.2.1 Complex III growth and purification. Growth of the *R. sphaeroides* strains was done as described in chapter two [8]. Chromatophore membranes and purified Complex III were isolated and purified as described using a DEAE-sepharose column (Amersham Pharmacia) [9, 10].

4.2.2. Peptide synthesis and purification. The peptide sequence of AP6 is: CGGGEIWKQ**H**EEALKKFFAF**H**FILPFIIMAIAMA**H**LLFLFGEGL. AP6 peptides were synthesized on a continuous-flow solid-phase synthesizer (CEM) using a standard Fmoc/tBu protection strategy on a Fmoc-PEG-PAL-PS resin (NovaBioChem) at 0.2 mmol scale. The peptides were purified on a reversed-phase C18 HPLC column (Vydac) using gradients of acetonitrile (Fisher) and water both containing 0.1% (v/v) trifluoroacetic acid (Sigma). The purity and molecular weight of the acetylated AP6 peptide was confirmed by matrix-assisted laser desorption/ionization mass spectrometry (MALDI-MS) to be 5022 g/mol. The peptides were purified without difficulty with yields comparable to water-soluble peptides of similar length [2, 11].

Unless noted otherwise, all experiments were performed in buffered solutions containing 100 mM potassium chloride and 50 mM potassium phosphate (pH 8.0). As shown previously [12], the maquettes reported here assemble as tetramers; therefore, the word maquette refers to the total assembly of four peptide helices. As such, our peptide concentrations reported here are for assembled four-helix bundles. Peptide concentrations were determined by UV-visible absorbance spectroscopy at 280 nm assuming an

extinction coefficient of 22400 M^{-1} cm^{-1} $bundle^{-1}$ calculated from the AP6 sequence using the Swiss Institute of Bioinformatics' EXPASY server (http://us.expasy.org/cgi-bin/protparam).

4.2.3 Peptide solubilization. Water-insoluble AP6 peptides and their assembled maquettes need a detergent for solubilization in aqueous buffers. We have determined that, in general, common detergents near or above the critical micelle concentration (CMC) readily solubilize AP6 maquette family members [3, 12]. In these experiments, we used dodecylphosphocholine (DPC) at a final concentration of 2 mM to solubilize AP6.

4.2.4 Heme binding. A 1 mM stock solution of hemin (Sigma) was prepared in 20 mM potassium hydroxide and its concentration was verified using a standard hemochrome difference spectrum, as described by Berry *et al* [13]. Though AP6 has been shown previously to bind up to six hemes [12], in these experiments we chose to bind four hemes, as the last two hemes were determined in chapter three to bind with micromolar rather than nanomolar affinity. A 4:1 ratio of hemin to protein was added and stirred for one minute, after which complete heme incorporation into AP6 was observed by a spectral shift in the heme absorbance from unbound heme (380 nm) to bound, oxidized heme (412 nm).

4.2.5 Reduction of decylubiquinone (DBH) substrate. Quinols were prepared from the oxidized quinone using the method described by Peter Rich [14] and detailed in chapter two. 0.25 g decylubiquinone was dissolved in 50 mL diethyl ether and placed in a separatory funnel. A solution of 1 g sodium dithionite in 50 mL water was added and the mixture was shaken together. The quinone could be seen to initially increase in

yellow color due to semiquinone formation, but eventually became colorless as full reduction to quinol occurred. The aqueous layer was removed, but the ethereal layer was shaken with a second 50 mL solution of sodium dithionite to ensure completion of the reduction reaction. After removal of the dithionite solution, the ethereal layer was washed twice with a saturated sodium chloride solution. The ethereal layer containing quinol was then passed through 30 g anhydrous sodium sulfate in a sintered glass funnel to remove any residual water, and the ethereal solution was then dried down by rotovaporization at 25°C. The resulting white powder was dissolved in an acidic ethanol solution (95% ethanol containing 10 mM hydrochloric acid) and flash frozen in 500 μL aliquots.

4.2.6 Enzyme steady state activity measurements. Maquette functionality as a quinol-cytochrome *c* oxidoreductase was measured via its reduction of cytochrome *c* in the presence of excess decylubiquinol [15]. A solution of 25 μM horse heart cytochrome *c* (Sigma) in redox buffer (50 mM potassium phosphate and 100 mM potassium chloride at pH 8) and 10 μM decylubiquinone (DBH) was incubated anaerobically in a 3 mL cuvette and stirred for one minute, after which a maquette protein was introduced into the cuvette in nanomolar concentrations (10-100 nM). Using an extinction coefficient of 18.5 $mM^{-1}cm^{-1}$ for the 551 nm – 540 nm difference absorption, cytochrome *c* reduction was monitored over time until the amount of cytochrome *c* reduced reached a constant maximum.

This cuvette assay was modified for anaerobic stopped flow experiments to obtain the initial velocity for AP6 activity. An Olis multiwavelength stopped flow spectrometer was used to measure cytochrome *c* reduction over 200 s. 100 μL from a syringe containing 20 mM decylubiquinone in reaction buffer and DMSO was mixed with 100

μL from a syringe containing 25 nM AP6 and 50 μM cytochrome *c*.

4.2.7 Computational work. As described in the Appendix, the Dutton laboratory has developed an electron transfer rate expression that offers a simple way to examine parameters that directly relate to the oxidoreductase activity of a particular mitochondrial enzyme. The electron tunneling rates of the decylubiquinone, AP6, and cytochrome *c* redox centers were simulated using Equation A.1 in user-written programs constructed in Mathematica (Wolfram Research) to create a model for quinone semiquinone stability and electron transfer distances [16, 17].

4.3 Results

The maquette approach enables the construction of useful synthetic proteins with applications in the material science and medical fields. This approach has been so successful because only the basic protein engineering requirements needed to obtain enzymatic activity are applied to the designs, which have so far proven to be relatively simple. To design AP6 to have quinol-cytochrome *c* oxidoreductase activity, the main elements of these electron transfer reactions in Complex III were extracted and incorporated into AP6: simple α-helical structure to promote membrane association, both hydrophilic and hydrophobic sections of amino acids to promote interactions with both the membrane and soluble molecules, multiple histidine sites for heme ligation, and a tryptophan molecule for convenience when determining AP6 concentration.

4.3.1 Quinol-cytochrome c oxidoreductase activity of AP6. We demonstrated quinol-cytochrome *c* oxidoreductase activity in AP6 using a steady-state turnover assay previously designed to determine Complex III activity (Figure 4.1) [15]. In this assay, a pool of reduced quinone reduces the hemes in the transmembrane protein,

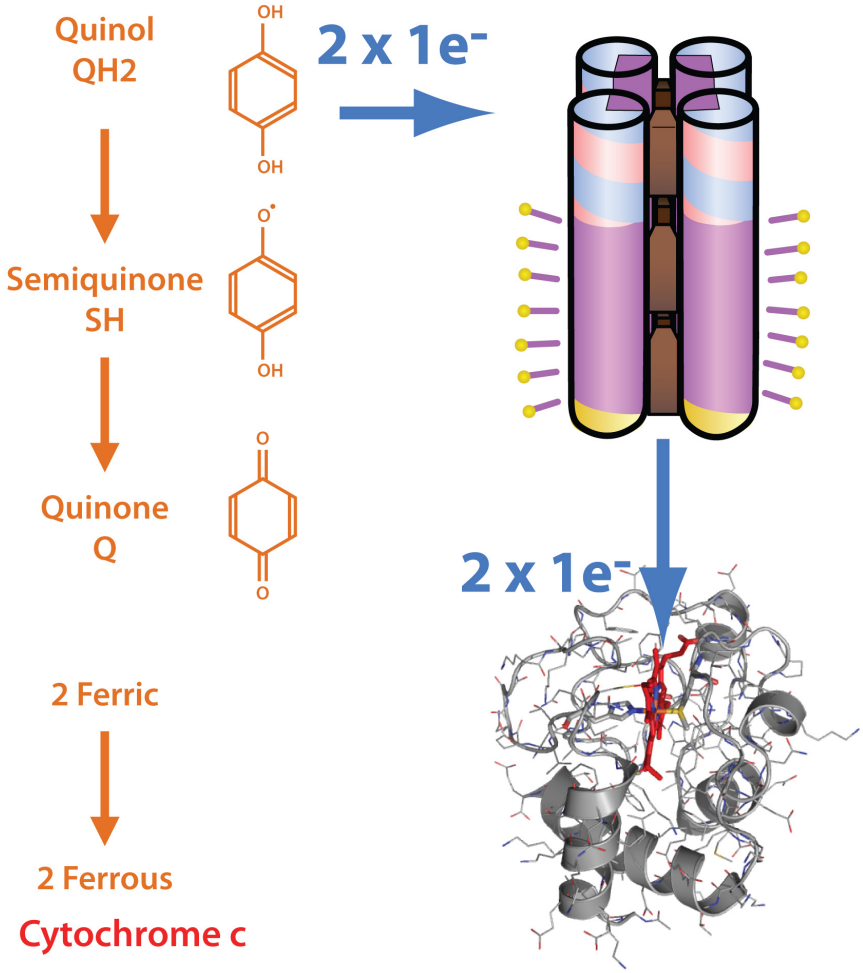

Figure 4.1: Cartoon representations of the components of the assay. Reduced quinol molecules diffuse within reasonable electron transfer distances of both AP6 hemes and cytochrome *c*, though reactions with AP6 occur on a much faster timescale than those with cytochrome *c* (background rate). The two electron reduction of AP6 results in two, one electron reductions of cytochrome *c* molecules.

transferring electrons across the membrane interface (Figure 4.1). The reduced protein can then transfer electrons to the oxidized cytochrome *c* inside the soluble portion of the detergent micelle. The transition from oxidized to reduced cytochrome *c* is monitored in this assay, with activity traces reflecting the total amount of cytochrome *c* reduced over time.

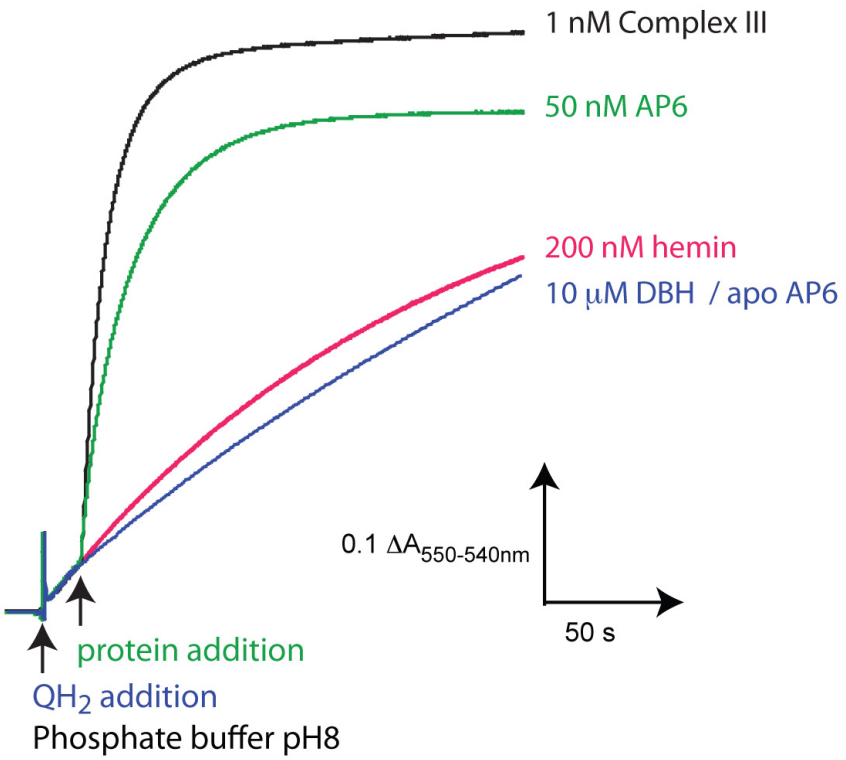

Figure 4.2: Demonstration of quinol / cytochrome c oxidoreductase activity for AP6 in a standard Complex III activity assay, which monitors the reduction of cytochrome c (as indicated by a difference in it 550-540 nm abosrabnce) over the time after AP6 is added. In the presence of 10 μM reduced DBH, 50 nM AP6 (green) reduces 25 μM cytochrome *c* in a 2 mM DPC detergent solution over two orders of magnitude better than free hemin (red), or the background rate when apo-AP6 is present (blue). The rate of AP6 reduction is approximately 100 fold slower than Complex III (black).

As shown in Figure 4.2, decylubiquinone is significantly reactive with cytochrome *c* even without the aid of a catalytic protein, such as Complex III. We left the background rate in the initial time points visible in this figure so that any changes induced by protein additions would be more evident; however, this rate was subtracted from the data to determine the true rate of cytochrome *c* reduction caused by the addition of AP6. The rate of cytochrome *c* reduction is unchanged when apo-AP6 is added;

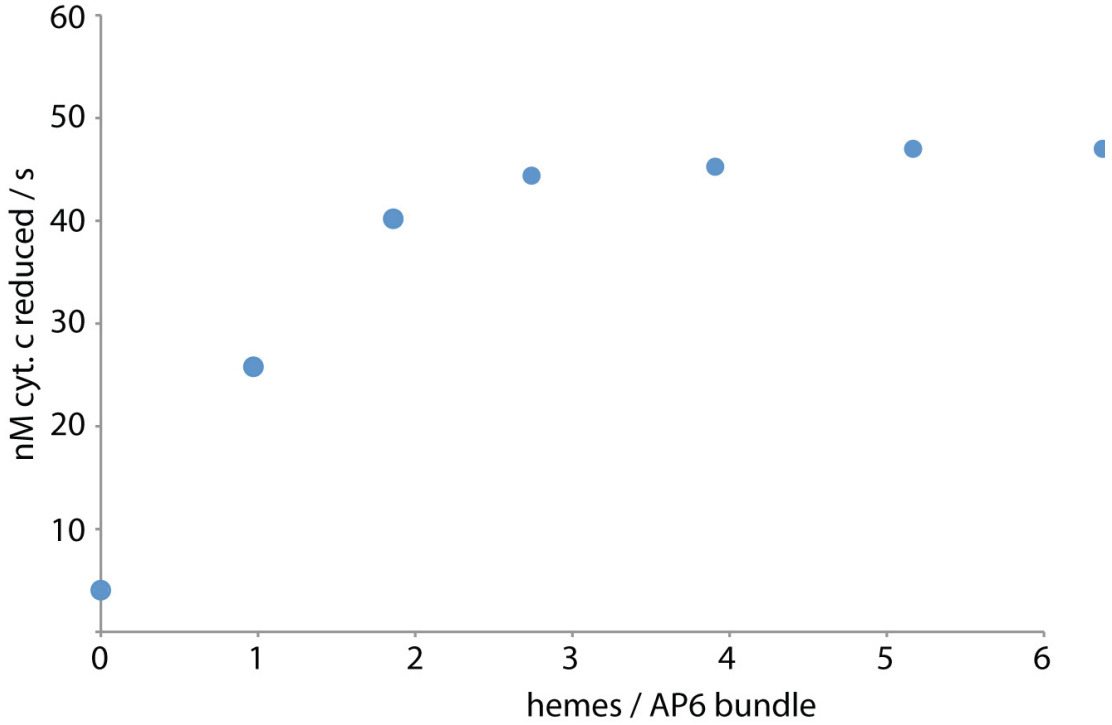

Figure 4.3: Rates of cytochrome *c* reduction of 10 nM AP6 with varying ratios of hemes bound per bundle as reported by stopped flow data with 25 μM cytochrome c and 10 μM DBH present.

adding hemin alone only stimulates this background rate slightly. However, upon the addition of AP6 with just two heme equivalents bound, cytochrome *c* reduction takes off, occurring at a rate ~500-fold faster than the background rate and within 100-fold of the rate of *R. capsulatus* Complex III. Though the design of AP6 supports up to six hemes bound per maquette bundle, only two hemes are needed to achieve this maximal enzymatic activity (Figure 4.3).

In complementary stopped-flow experiments, the cytochrome *c* substrate concentration is varied to resolve kinetic parameters for the various proteins tested in this assay (Table 4.1, Figure 4.4). As expected, AP6 activity increased with increasing amounts of cytochrome *c*, reaching a maximal activity of 62 nM / s. The K_m for

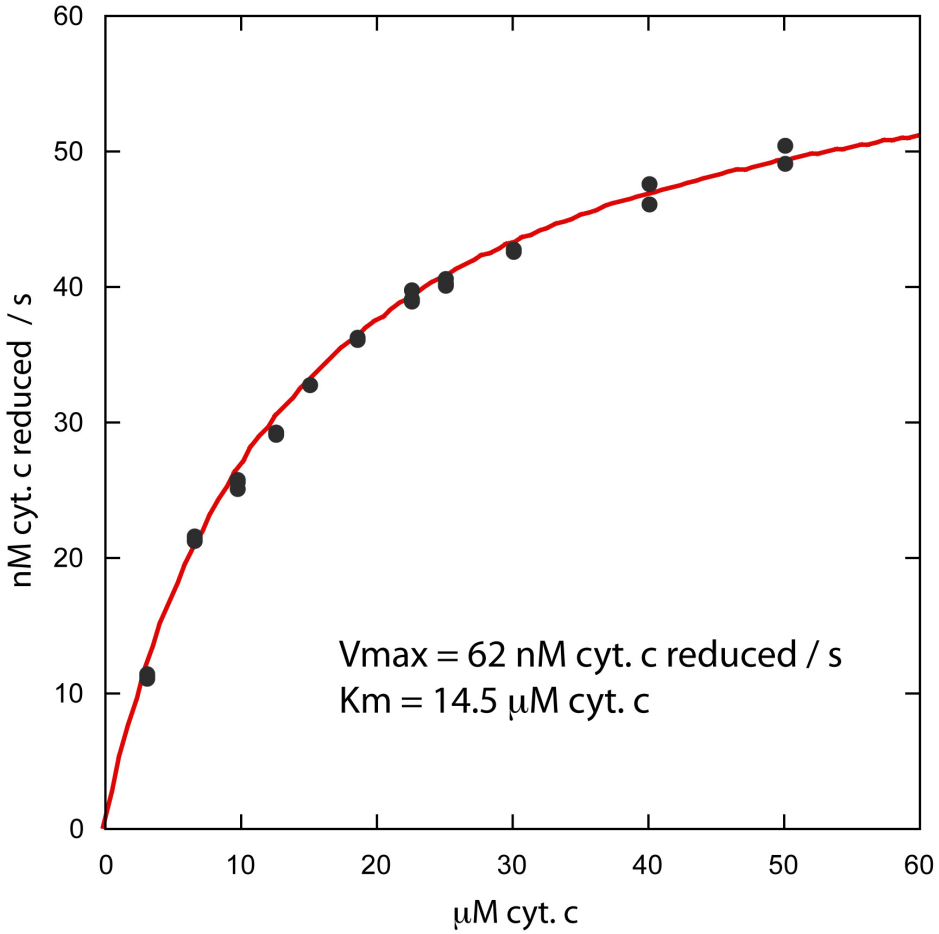

Figure 4.4: Solutions containing 25 nM AP6 with 4 hemes bound and varying cytochrome *c* concentrations were mixed with equal volumes of a solution containing 20 μM decylubiquinone. Data was fit to steady state kinetics of an enzyme with a single substrate to determine initial velocities and kinetic parameters.

cytochrome *c* association with AP6 was 14.5 μM, which is almost identical to the K_m for cytochrome *c* with Complex III of 13.4 μM [18]. In contrast, the concentration of decylubiquinone in these assays does not have any affect on AP6 activity once the background rate is accounted for because quinone levels are already saturating in this assay.

4.3.2 Testing AP6 activity with alternative quinone substrates Successful reduction of AP6 by a quinone pool is not specific to an excess of ubiquinone present;

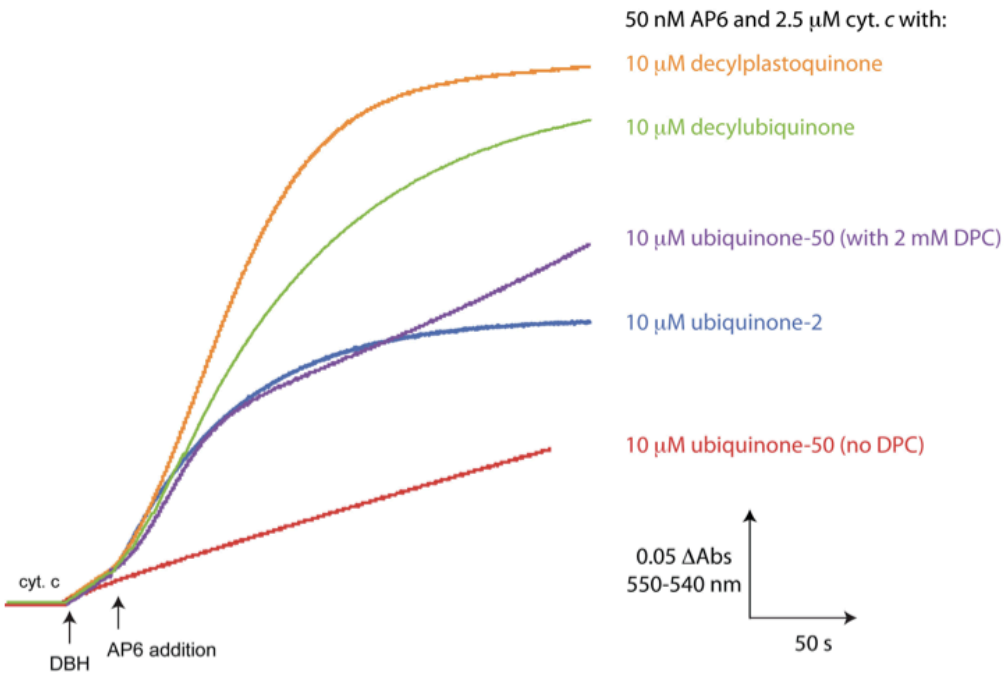

Figure 4.5: Varying the quinone substrate: decylubiquinone (green), decylplastiquinone is added (orange), and ubiquinone-2 (blue). Ubiquinone-50 in organic solvents was inactive (red), but did show activity when solubilized in a solvent and 2 mM DPC mixture (purple).

several other quinone molecules are able to successfully initiate AP6 turnover (Figure 4.5). We have determined that, like cytochrome b_6f found in chloroplasts and cyanobacteria [19], decylplastoquinone yields AP6 turnover that is slightly faster than the turnover reported for decylubiquinone. In addition to varying the R-groups on the quinone ring, the isoprene tail of the molecule can also be varied to some degree with successful enhancement of the background rate. Ubiquinone-2 does reduce AP6, though at a slower rate than the decylquinone molecules. However, it was more difficult to add the extremely water-insoluble ubiquinone-50, which is the natural substrate for Complex III in chromatophore membranes. Adding the UQ-50 with DPC detergent side steps some of these solubility issues and leads to enhanced activity in the presence of AP6.

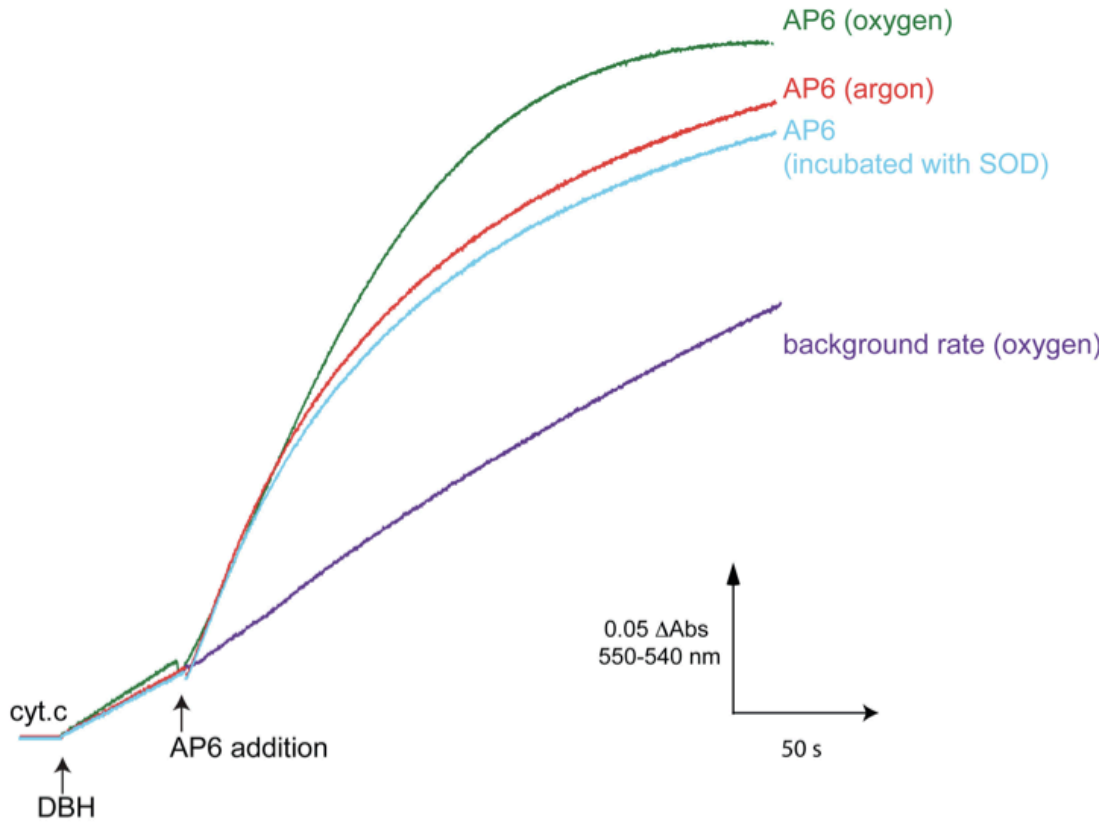

Figure 4.6: The assay was completed under aerobic conditions to see if oxygen was required for AP6 activity. Though the presence of oxygen does increase the number of turnovers AP6 can complete (green), it does not change the turnover rate observed in anaerobic conditions (red). However, adding superoxide dismutase prior (blue) or after (purple) the addition of AP6 does not limit AP6 activity, suggesting superoxide is not formed in this reaction in high enough quantities to have an effect on the reaction rate.

4.3.3 Observing changes in AP6 activity in the presence of oxygen. The experiments described above were performed anaerobically to minimize the role played by oxygen. However, when AP6 activity assays were performed in the presence of oxygen, the addition of SOD does not change the amount of cytochrome c reduced (Figure 4.6); this indicates that reduction of cytochrome *c* by quinol via AP6 in the presence of oxygen is not dominated by a superoxide-mediated mechanism.

Table 4.1 Summary of AP6 activity

Protein	E_m (mV)	k_{cat} (s^{-1})	K_m (μM)	k_{cat} / K_m	hemes bound
Complex III	FeS +280 b_L - 200	200	13.2	1.63×10^7	2
AP6	heme1 -156 heme2 -78	4.1	14.5	3.12×10^5	4

4.4 Discussion

As shown in Figure 4.2 and Table 4.1, AP6 clearly demonstrates significant quinol-cytochrome *c* oxidoreductase turnover, being the first maquette protein to match near-natural levels of activity. Here we outline a model for how AP6 functions so well and suggest a role for our designs in understanding more complicated electron transfer systems in the mitochondria.

4.4.1 Developing a model for AP6 heme reactivity. There are several possible combinations for heme binding in AP6 when four hemes are bound, and it is certainly possible that our assays actually contain a mixture of AP6 proteins that have different arrangements of heme binding. However, based on the heme affinity studies completed in chapter four, we assume that the AP6 that is most populated in this assay has two hemes bound in the heme binding site located in the water soluble extension of the 4-helix bundle (histidine 10) and two hemes bound in the nearest membrane binding site (histidine 24). Even without a heme in the third membrane binding site (histidine 35), the electron transfer distance between the second heme and cytochrome *c* would be

approximately 8.5 Å, which is still allows for electron transfer reactions to occur on the millisecond timescale we observe in these experiments.

Figure 4.3 illustrates that AP6 activity is halved when only one heme is bound. Due to cooperative heme binding in AP6, when one heme equivalent is added, there are two distinct populations of AP6 present – 50% apo-protein, and 50% of AP6 with two hemes bound. Therefore, as the concentration of active AP6 is cut in half, it is not surprising that AP6 can only reduce cytochrome *c* at half the rate. Additionally, apo-proteins present will interact with cytochrome *c* substrate molecules, impacting the amount of substrate available to active AP6.

It is known that oxygen can interact with reduced quinones to produce superoxide intermediates that can in turn reduce cytochrome *c*. Indeed, the presence of oxygen leads to substantial background rates when quinone and cytochrome *c* (but not AP6) are present. In order to eliminate oxygen from contributing to the background rate and/or the measured enzymatic rate, the assays were conducted under anaerobic conditons. Additionally, AP6 was exclusively solubilized in DPC, a detergent micelle system that does not allow for the formation of an AP6 oxy-ferrous intermediate state. However, as the natural Complex III can generate superoxide upon turnover (under certain redox conditions), it was necessary to test whether or not AP6 quinol-cytochrome *c* turnover also generated superoxide in the presence of oxygen, and if limiting superoxide production in the aerobic assay caused a dramatic difference in AP6 turnover rate.

The turnover rate of AP6 was unaffected in the presence of oxygen, though the total amount of cytochrome *c* reduced was increased (Figure 4.6). However, the addition of SOD to the reaction cuvette did not limit AP6 activity or quench turnover. This

suggests either that the levels of superoxide generated in this assay are not high enough to activate SOD, or that the role of oxygen in this reaction is limited. It is also possible that any superoxide formed in the presence of oxygen is rapidly converted to hydrogen peroxide (and thus, not quenched in the presence of SOD); however, levels of hydrogen peroxide cannot be tested under these assay conditons because cytochrome *c* is an indirect redox partner for the horseradish peroxidase system commonly used to measure hydrogen peroxide concentrations.

4.4.2 Thermodynamic constraints on AP6 activity. The initial transition from quinol to semiquinone as an electron is transferred to AP6 is an uphill step, and is thermodynamically unfavorable (Figure 4.7). However, a similar uphill step is expected in native Complex III as a reduced quinol molecule at the Qo site transfers an electron to oxidized FeS [20, 21]. We expect the uphill step in AP6 to be much larger than in native Complex III, which may explain why the reaction is slower (Figure 4.7). Changing the thermodynamics of this very important electron transfer step may prove to enhance AP6 turnover. Work ongoing in the laboratory involves modifying AP6 to bind hemes with significantly higher midpoint potentials, such as heme *a*. In the meantime, altering the thermodynamics of this reaction was explored with HP7, which has already been engineered to accommodate a variety of heme cofactors, as detailed in chapter five.

4.4.3 AP6 activity is not decylubiquinone specific. It is not surprising that AP6 is able to receive electrons from a variety of quinone substrates, as a specific quinone binding pocket within the protein was not engineered. Also, though most Complex III proteins use pools of ubiquinone as substrates for the Qo and the Qi site, their activity is not dependent on ubiquinone specifically – Complex III activity is

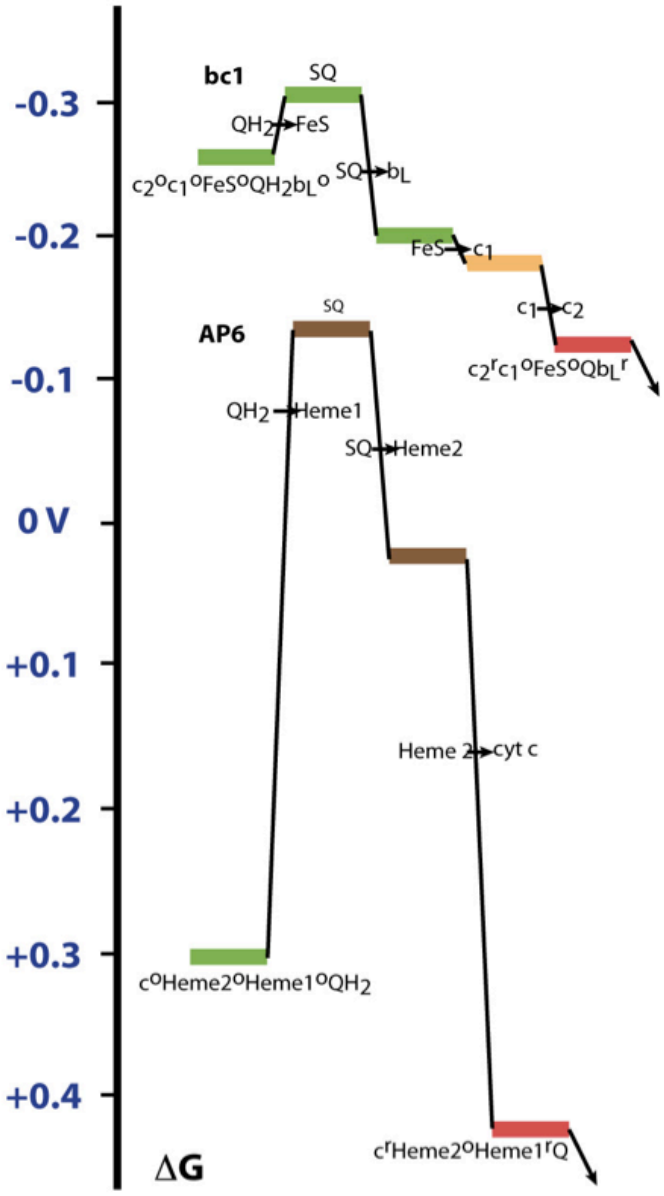

Figure 4.7: The thermodynamics of Complex III and AP6 electron transfer are structured in a similar way. Both Complex III (top) and AP6 (bottom) have reactions that are unfavorably uphill followed by favorable (downhill) reactions. In Complex III, the uphill step is the initial electron transfer reaction between the QH_2/SQ at the Qo site and the FeS cluster, and in AP6, the QH_2/SQ to heme *b* electron transfer step is unfavorable. Quinol reduction of AP6 is four times more unfavorable than the uphill step in Complex III, and could account for the difference in AP6 and Complex III activity.

maintained when alternative quinones are substituted into the Qo site [22]. Particularly since plastoquinone is used naturally by cytochrome $b_6 f$, a Complex III analog, it was expected that plastoquinone and ubiquinone would work equally well as electron donors in this assay.

Depending on the substituents or the length of the isoprene tail, different quinones will interact with AP6 differently. Based on the quinones tried in this work, the isoprene tail seems to dictate AP6 activity levels, presumably due to their regulation of quinol-AP6 proximity. Hydrophobic quinones such as decylplastoquinone and decylubiquinone will associate with the detergent micelle better because they have more isoprene groups, bringing the quinol closer to the *b* hemes bound to AP6. Not surprisingly, AP6 turnover is the essentially the same in the presence of either of these substrates. Though ubiquinone-2 is also capable of acting as an electron donor to AP6, it likely does not associate with the detergent as well due to a much shorter hydrophobic tail, limiting its electron transfer with AP6.

4.4.4 Estimating semiquinone stability of the "Q-pool" and Q-heme *b* electron transfer distances. The rate of electron transfer through AP6 is likely to be dependent on the individual one-electron redox couples of the two-electron quinone substrate—that is, on the stability constant of the quinone substrate. When the midpoint potential of the first electron added to fully oxidized quinone is more negative than the midpoint potential of the second electron, then the intermediate semiquinone is unstable and the stability constant is less than 1. Electron tunneling rate calculations give us some idea of what the tunneling distance and stability constants might be. Here we work with quinones that all have very similar semiquinone stability, but we can model the effect

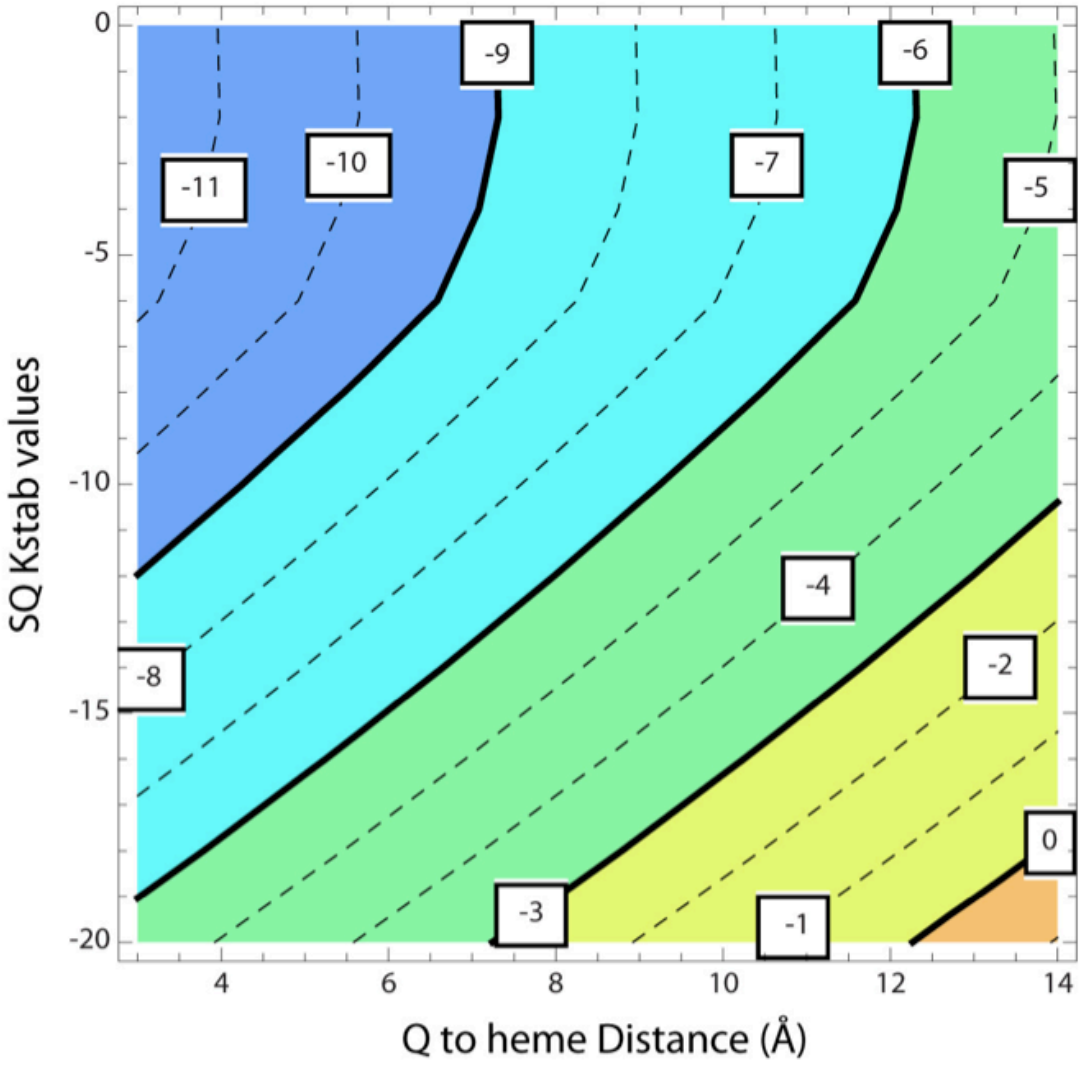

Figure 4.8: The Moser-Dutton equation for calculating electron transfer rates was used to model ranges of semiquinone stability and electron transfer distances that would produce AP6 turnover on a given timescale. Shown on the y-axis are values for the semiquinone stability constant on a logarithmic scale, and depicted on the x-axis are values for the electron transfer distance between the AP6 hemes and cytochrome c. Each line depicts a timescale (logarithmic scale), with the lines in bold indicating nanoseconds (-9 in box), microseconds (-6), milliseconds (-3), and seconds (0) and dashed lines indicating ranges in between these values. As the k_{cat} of AP6 indicates each turnover occurs on a millisecond timescale, we were particularly interested in the values falling within the light green range of the graph.

varying semiquinone stability would have when the midpoint potentials of the hemes in AP6 are fixed using the Moser-Dutton equation (Figure 4.8). In order to achieve the

reaction on a millisecond timescale, the semiquinone stability constant of the Q-pool would need to be between 10^{-9} to 10^{-20}, indicative of an unstable semiquinone intermediate. Therefore, it is most likely that the quinone here does not form an appreciable semiquinone intermediate at all, but transfers two electrons concertedly to two of the hemes bound to AP6. This also agrees with our observation that only two hemes are required to achieve maximal activity (Figure 4.3).

As no structural data exists for the substrate-AP6 complexes in this assay, the exact electron transfer distances between the cofactors are unknown and could also affect enzyme turnover. We can use the heme binding information known about AP6 along with docking studies of cytochrome c and Complex III [23] to assume the electron transfer distance between the *b*-hemes bound to AP6 and the *c*-heme in cytochrome *c* to be approximately 8.5 Å. This assumption allows us to model possible distances between the reduced quinol molecules and the AP6 hemes, which is more of an unknown because there is not a fixed binding site for quinol within AP6. As indicated by Figure 4.8, to achieve a reaction on a millisecond timescale (green section of graph), the distance between the quinol and heme *b* is limited to a range of 3.5 – 7.5 Å if the semiquinone is unstable. Short electron transfer distances between the heme and quinol could reasonably occur; the hydrophobicity of the quinone molecule allows it to partially associate with the DPC detergent micelle, shortening the distance the electron has to travel between the quinone and AP6's heme cofactors. Additionally, it is possible that the quinone pool in this experiment is associating with AP6 non-specifically, as this behavior has been observed for other synthetic proteins [24]. This would enable the quinone to partition into the hydrophobic core of the protein, promoting a stronger interaction with hemes

bound to AP6 at very short distances. Quinone/heme electron transfer appears quite possible using the simple enzymatic principle of proximity--securing quinone at a specific binding site or manipulating the quinone stability constant through specific interactions with the protein do not appear essential for catalysis. This simple proximity model for quinone reactivity with heme proteins is not an unrealistic representation of how these electron transfer processes occur in biological membranes; it is well-established that the ubiquinone at the Qo site is highly mobile, initiating Complex III turnover when it is bound. As no evidence for specific quinone-protein interactions have been established at Qo, it is reasonable to assume that our experiments demonstrate a very important piece of biological engineering – quinone concentrations need only to be in excess at a particular active site in order to generate substantial turnover.

This model could be tested through the development of an AP6 protein that contains a quinone amino acid fixed in position within the soluble region of the maquette. Previous experiments incorporating a napthoquinone amino acid, Naq, into a small peptide have demonstrated that Naq is spacially equivalent to a tryptophan residue [25]. Therefore, Naq can be readily added to the AP6 peptide sequence without large disruptions in protein assembly or heme binding. Fixing the quinone into one position in the maquette would answer definitively whether or not quinone-protein interactions are essential for maximal enzymatic turnover.

4.5 Conclusion

This work was able to translate a complicated mitochondrial redox enzyme into a simple, transmembrane electron transfer chain that still retained all of the necessary engineering elements to accomplish quinol-cytochrome *c* oxidoreductase activity within

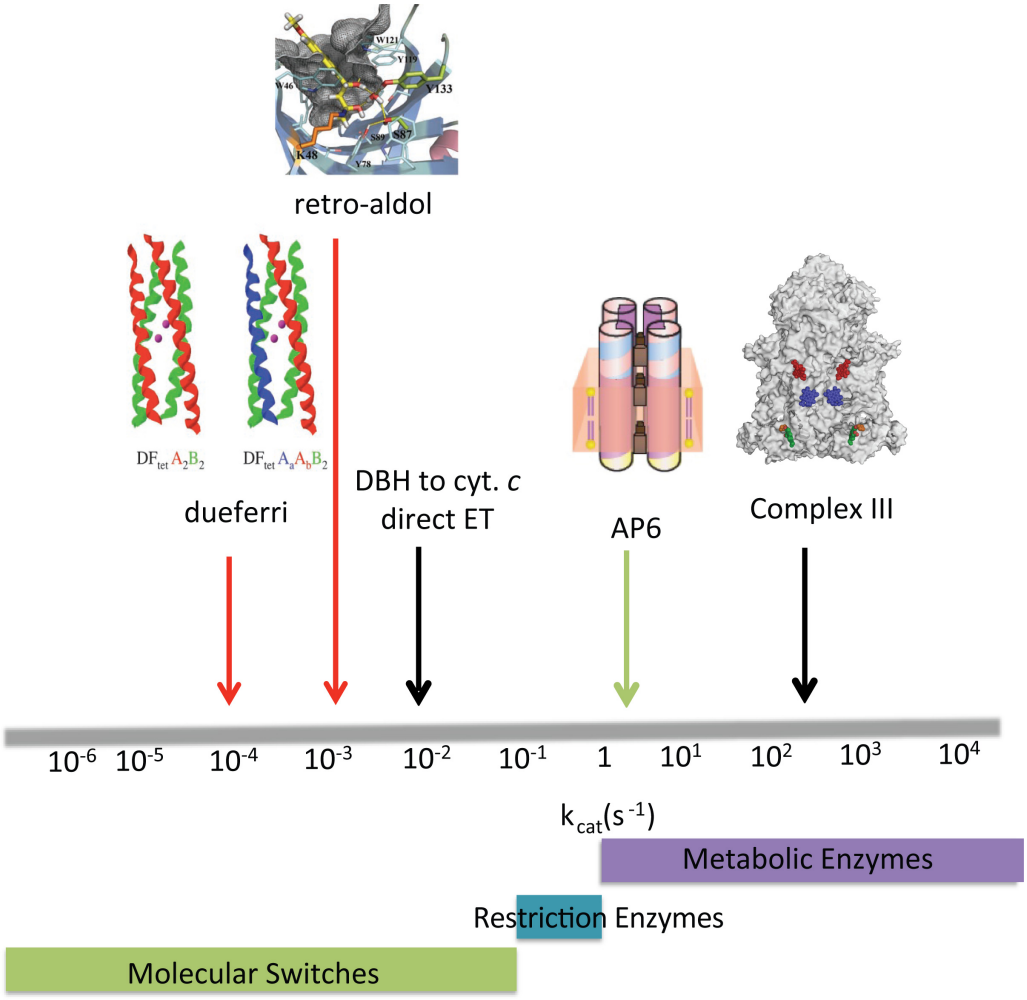

Figure 4.9 Comparing AP6 (green arrow) k_{cat} to other *de novo* designed enzymes (red arrows) [5-7], and natural turnover rates (black arrows).

two orders of magnitude of the natural rate. The hemes bound to AP6 were able to receive electrons from quinone substrates and reduce cytochrome *c* on a millisecond timescale. Figure 4.9 compares AP6 activity to the turnover rates for previous *de novo* designed enzymes [5-7], the background rate for quinol to cytochrome *c* electron transfer, and Complex III steady-state turnover rates. AP6 improves upon the catalytic rates of other designed oxidoreductases, and begins to bridge the gap between the rate of uncatalyzed cytochrome *c* reduction and the rate of Complex III turnover.

4.6 References

1. Chobot, S.E., Wiedman, G.R., Moser, C.C., Discher, B.M., Dutton, P.L., *Demonstrating quinol-cytochrome c oxidoreductase kinetic activity by an amphiphilic maquette protein*. Biochemistry, 2010. **submitted**.
2. Huang, S.S., et al., *The HP-1 maquette: from an apoprotein structure to a structured hemoprotein designed to promote redox-coupled proton exchange*. Proc Natl Acad Sci U S A, 2004. **101**(15): p. 5536-41.
3. Noy, D., et al., *Design of amphiphilic protein maquettes: enhancing maquette functionality through binding of extremely hydrophobic cofactors to lipophilic domains*. Biochemistry, 2005. **44**(37): p. 12344-54.
4. Crofts, A.R., et al., *Proton pumping in the bc1 complex: a new gating mechanism that prevents short circuits*. Biochim Biophys Acta, 2006. **1757**(8): p. 1019-34.
5. Kaplan, J. and W.F. DeGrado, *De novo design of catalytic proteins*. Proc Natl Acad Sci U S A, 2004. **101**(32): p. 11566-70.
6. Jiang, L., et al., *De novo computational design of retro-aldol enzymes*. Science, 2008. **319**(5868): p. 1387-91.
7. Rothlisberger, D., et al., *Kemp elimination catalysts by computational enzyme design*. Nature, 2008. **453**(7192): p. 190-5.
8. Yun, C.H., et al., *Cloning and DNA sequencing of the fbc operon encoding the cytochrome bc1 complex from Rhodobacter sphaeroides. Characterization of fbc deletion mutants and complementation by a site-specific mutational variant*. Eur J Biochem, 1990. **194**(2): p. 399-411.
9. Atta-Asafo-Adjei, E. and F. Daldal, *Size of the amino acid side chain at position 158 of cytochrome b is critical for an active cytochrome bc1 complex and for photosynthetic growth of Rhodobacter capsulatus*. Proc Natl Acad Sci U S A, 1991. **88**(2): p. 492-6.
10. Valkova-Valchanova, M.B., et al., *Isolation and characterization of a two-subunit cytochrome b-c1 subcomplex from Rhodobacter capsulatus and reconstitution of its ubihydroquinone oxidation (Qo) site with purified Fe-S protein subunit*. Biochemistry, 1998. **37**(46): p. 16242-51.
11. Gibney, B.R., et al., *Self-assembly of heme A and heme B in a designed four-helix bundle: implications for a cytochrome c oxidase maquette*. Biochemistry, 2000. **39**(36): p. 11041-9.
12. Wiedman, G.R., O'Brien, P.A., Chobot, S.E., Parekh, V.P., Karunakaran, V., Anderson, J.L.R., Moser, C.C., Dutton, P.L., Discher, B.M., *Building a Function into Simplified Protein Structures: Amphiphilic Maquettes with Multiple Cofactor Binding Sites*. Biochemistry, 2010. **submitted**.
13. Berry, E.A. and B.L. Trumpower, *Simultaneous determination of hemes a, b, and c from pyridine hemochrome spectra*. Anal Biochem, 1987. **161**(1): p. 1-15.
14. Rich, P.R., *Electron transfer reactions between quinols and quinones in aqueous and aprotic media*. Biochimica et Biophysica Acta, 1981. **637**: p. 28-33.
15. Trumpower, B.L. and C.A. Edwards, *Purification of a reconstitutively active iron-sulfur protein (oxidation factor) from succinate . cytochrome c reductase complex of bovine heart mitochondria*. J Biol Chem, 1979. **254**(17): p. 8697-706.

16. Moser, C.C., et al., *Biological electron transfer*. J Bioenerg Biomembr, 1995. **27**(3): p. 263-74.
17. Page, C.C., et al., *Natural engineering principles of electron tunnelling in biological oxidation-reduction*. Nature, 1999. **402**(6757): p. 47-52.
18. Sarewicz, M., et al., *Demonstration of short-lived complexes of cytochrome c with cytochrome bc1 by EPR spectroscopy: implications for the mechanism of interprotein electron transfer*. J Biol Chem, 2008. **283**(36): p. 24826-36.
19. Cramer, W.A., et al., *Transmembrane traffic in the cytochrome b6f complex*. Annu Rev Biochem, 2006. **75**: p. 769-90.
20. Mitchell, P., *The protonmotive Q cycle: a general formulation*. FEBS Lett, 1975. **59**(2): p. 137-9.
21. Mitchell, P., *Possible molecular mechanisms of the protonmotive function of cytochrome systems*. J Theor Biol, 1976. **62**(2): p. 327-67.
22. Cape, J.L., et al., *Substrate redox potential controls superoxide production kinetics in the cytochrome bc complex*. Biochemistry, 2009. **48**(45): p. 10716-23.
23. Sarewicz, M., et al., *Estimation of binding parameters for the protein-protein interaction using a site-directed spin labeling and EPR spectroscopy*. Eur Biophys J, 2008. **37**(4): p. 483-93.
24. Razeghifard, M.R. and T. Wydrzynski, *Binding of Zn-chlorin to a synthetic four-helix bundle peptide through histidine ligation*. Biochemistry, 2003. **42**(4): p. 1024-30.
25. Lichtenstein, B.R., et al., *Reversible proton coupled electron transfer in a peptide-incorporated naphthoquinone amino acid*. Chem Commun (Camb), 2009(2): p. 168-70.

Chapter 5: Testing the thermodynamic limits of maquette quinol-cytochrome *c* oxidoreductase activity

As shown in chapter four, the electron transfer between a quinol molecule and the AP6 maquette is a drastic uphill reaction, and limits the rate at which AP6 can turnover. However, if the midpoint potential in the maquette were raised, the thermodynamic barrier for quinol to heme electron transfer would be lowered. In this chapter, the effect of modulating maquette midpoint potential on the rate of cytochrome *c* reduction is determined. For these studies, a library of soluble maquettes was chosen, primarily because they are able to bind a variety of heme-based cofactors in addition to heme *b*, yielding a wider range of midpoint potentials to test. From measuring the activity of proteins that have a range of different midpoint potentials, the thermodynamic limit for quinol-cytochrome *c* activity by a soluble maquette was determined for this assay. HP7 maquettes that contain hemes with measured midpoint potentials lower than -150 mV are inactive, indicating that the quinol/semiquinone to heme electron transfer step has reached an insurmountable thermodynamic barrier.

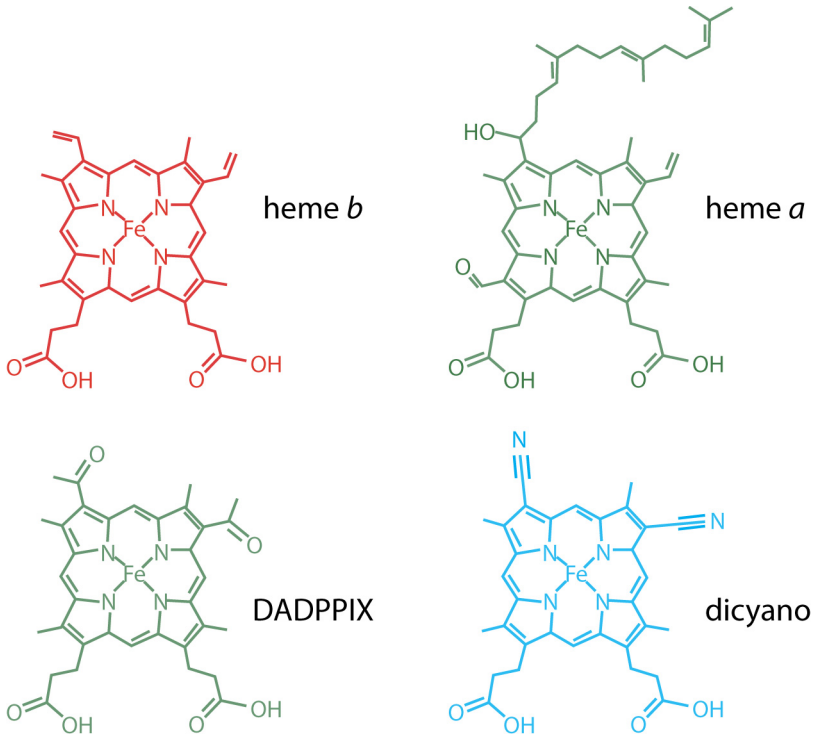

Figure 5.1: Structures of heme-based cofactors available to bind to HP7. Heme *b* (in the form of protoporphyrin IX) is shown in red, heme *a* and diacetyldeuterioporphyrin IX (a heme *a* mimic) in green, and iron(III)-dicyanodeuteroporphryin in teal.

5.1 Introduction

Chapter four revealed AP6 to be the first synthetic enzyme to achieve near-natural levels of Complex III enzymatic activity. However, one potential limitation on its turnover rate is the uphill electron transfer step between quinol and AP6. In order for this electron transfer reaction to become more favorable, the midpoint potential of hemes bound to AP6 needs to be raised. One convenient way to lower the thermodynamic barrier for quinol to maquette-cofactor electron transfer is to substitute the FePPIX cofactor bound with hemes that have higher midpoint potentials. However, though AP6

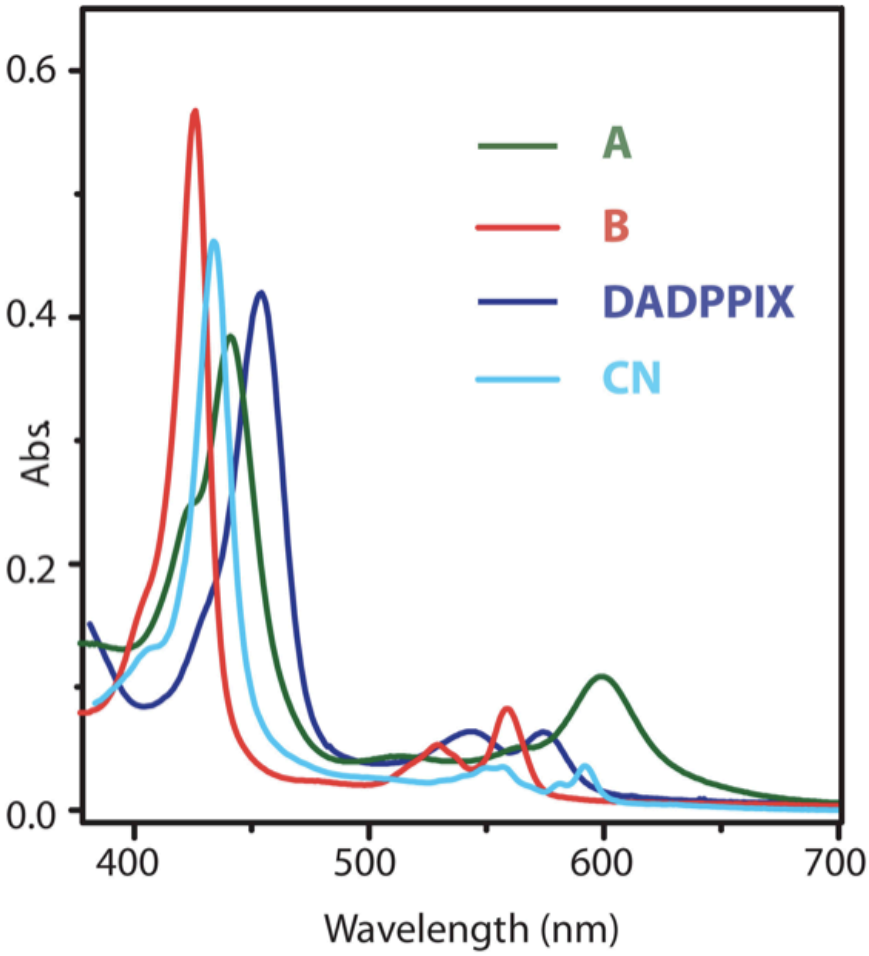

Figure 5.2: Absorbance spectra for HP7 with 1 cofactor equivalent bound. Shown in green is HP7 with heme *a* bound, in red HP7 with heme *b*, in blue HP7 with iron-2,4-diacetyldeuterioporphyrin IX (data courtesy of Ross Anderson) and in teal HP7 with iron(III)-dicyanodeuteroporphryin.

can successfully bind Fe- and ZnPPIX [1], its binding sites have not demonstrated tight binding with other porphyrin-based cofactors.

Soluble maquettes have been modified to bind a variety of different heme cofactors [2-8]. HP7 was chosen for this study because it is extremely well characterized [6] and shares sequence identity with the HP domain found in AP6. Shown in Figure 5.1 are the structures of four cofactors that can bind tightly to HP7 – heme *b*, heme *a*, iron(III)-dicyanodeuteroporphyrin (dicyano), and iron-2,4-diacetyldeuterioporphyrin IX

(DADPPIX) – and Figure 5.2 depicts characteristic absorbance spectra for each of the HP7-heme complexes. In heme *a*, the FePPIX C-8 methyl group is oxidized into a formyl group, and the vinyl group on C-2 is converted into a hydroxyethylfarnesyl side chain. DADPPIX is a heme *a* analog that substitutes the two vinyl groups found in FePPIX for acetyl groups. The dicyano heme is very similar in structure to DADPPIX, with the acetyl groups replaced by nitrile groups. A *c*-type HP7 protein also exists; however, heme *c* was not chosen for this work because its absorbance profile overlaps with that of the natural cytochrome c monitored in the assay (Figure 5.2).

Electron withdrawing groups present in heme *a* and DADPPIX have been shown to be responsible for raising the midpoint potential of maquettes upon binding, in comparison to when heme *b* is bound. For example, the presence of the electron withdrawing formyl group in heme *a* has been shown to raise the midpoint potential of soluble maquettes by destabilization of the ferric state [2, 4]. The midpoint potential of FePPIX in HP7 [6] (Table 5.1) is considerably lower than has been observed for its soluble maquette predecessors [4, 9], and it was expected that the midpoint potential of HP7 would be substantially increased by the introduction of electron withdrawing substituents on the heme because HP7 has a net charge of -14. The range of midpoint potentials available within the HP7 design allows for the direct control of quinol to heme electron transfer thermodynamics, yielding an opportunity to directly test whether manipulating maquette midpoint potential is enough to dictate its enzymatic function.

5.2 Materials and methods

5.2.1 Maquette preparation. All soluble maquette proteins were designed and synthesized by other members of the laboratory, and concentrated stocks of each protein

were donated for the completion of this work. Stocks of HP7 were obtained from Ross Anderson and BT3 was obtained from Tammer Farid and Bruce Lichtenstein. All concentrated stocks were diluted to their final concentrations with a 250 mM pH 9 borate buffer containing 100 mM potassium chloride, as both of the soluble maquettes required alkaline pH conditions to bind heme cofactors.

5.2.2. Heme stock preparation. A 1 mM stock solution of hemin (Sigma) was prepared in 20 mM potassium hydroxide and its concentration was verified using a standard hemochrome difference spectrum, as described by Berry *et al* [10]. Stocks of dicyano in DMSO were obtained from syntheses completed by Bruce Lichtenstein [11]. Stocks of heme *a* in DMSO were obtained from Ross Anderson.

5.2.3 Heme binding. Each of the soluble maquettes has the capacity to bind up to two heme cofactors. Based on the concentration of the protein stock, the concentration of the heme stock needed to add 0.1 aliquot was determined. Hemes were titrated into the maquettes in 0.1 aliquots until the desired number of equivalents was added into the solution. Then, the maquettes were passed down a PD-10 desalting column to separate unbound heme from the maquette-heme complex. This procedure was modified from a protocol published previously [6]. Samples of HP7 with DADPPIX bound were obtained from a frozen stock made by Ross Anderson, and did not require this step.

5.2.4 Midpoint potential determination. Equilibrium redox potentiometry was used as a functional analysis of the oxidation and reduction of hemes bound to HP7. Redox titrations were performed in a similar fashion to those completed in previous chapters using an anaerobic 1 mL cuvette (Starna Cells) equipped with a combination electrode (Microelectrodes Inc.). All of the potentials reported are in reference to the

normal hydrogen electrode (NHE). The reduction potential of the cuvette solution was adjusted by adding microliter aliquots of freshly prepared solutions of either sodium dithionite (for reducing) or potassium ferricyanide (for oxidizing). 20 μL of a stock solution containing the following redox mediator dyes was also added to the solution (final concentrations reported): 5 μM 1,2-naphthoquinone, 5 μM 1,4- naphthoquinone, 20 μM duroquinone, 10 μM pyocyanine, 5 μM indigotrisulfonate, 10 μM 2-hydroxy-1,4-naphthoquinone, 1 μM indigocarmine, 10 μM anthraquinone-2-sulfonate, and 5 μM benzyl viologen. After equilibration at each midpoint potential, the UV-visible spectrum of the maquette was recorded, monitoring in particular the increase in the sharp *a*-band absorption for each heme relative to a reference wavelength. The data were analyzed using the Nernst equation, fitting to an n=1 electron transfer process.

5.2.5 Enzyme steady state activity measurements. As described in chapter five, maquette functionality as a quinol-cytochrome *c* oxidoreductase was measured via its reduction of cytochrome *c* in the presence of excess decylubiquinol [12]. A solution of 25 μM horse heart cytochrome *c* (Sigma) in redox buffer (50 mM potassium phosphate and 100 mM potassium chloride at pH 8) and 10 μM decylubiquinone was incubated anaerobically in a 3 mL cuvette and stirred for one minute, after which a maquette protein was introduced into the cuvette in nanomolar concentrations (100 nM). Using an extinction coefficient of 18.5 $mM^{-1}cm^{-1}$ for the 551 nm – 540 nm difference absorption, cytochrome *c* reduction was monitored over time until the amount of cytochrome *c* reduced reached a constant maximum.

For HP7 maquette complexes that demonstrated activity, this cuvette assay was modified for anaerobic stopped flow experiments. An Olis multiwavelength stopped

flow spectrometer was used to measure cytochrome *c* reduction over 200 s. 100 mL from a syringe containing 20 mM decylubiquinone in reaction buffer and DMSO was mixed with 100 mL from a syringe containing 200 nM HP7 and 50 μM cytochrome *c*.

Table 5.1 Midpoint potentials and k_{cat} values at pH 8

Protein	E_{m8} (mV)	E_{m8} reference	k_{cat} (s^{-1})
HP7 FePPIX	-280	Ron Koder [6]	0.0062
HP7 heme *a*	-72	This work	0.54
HP7 dicyanoheme	+62	This work	0.63
HP7 DADPPIX	-147	Ross Anderson [13]	0.21
dicyano heme	n.d.	n.d.	1.2
AP6	-150, -75	This work	4.1

5.3 Results

5.3.1 Determining the midpoint potentials of alternative hemes bound to HP7.

The midpoint potentials of hemes bound HP7 are reported in Table 5.1. The acetyl groups found in DADPPIX were found to raise the midpoint potential of HP7 by 133 mV through weakening

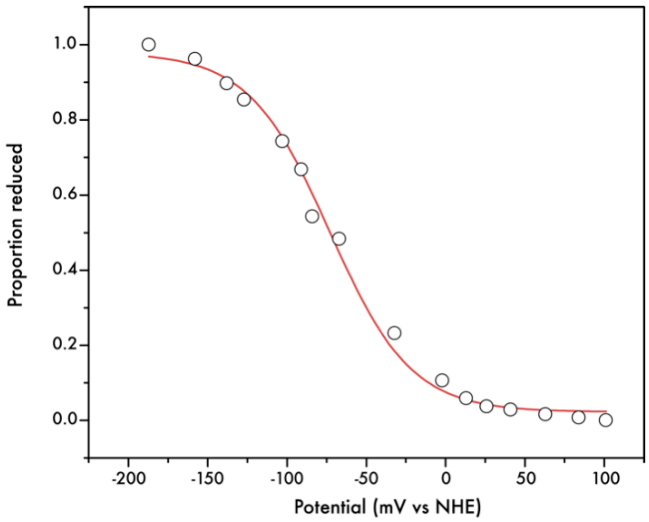

Figure 5.3: Redox titration of 5 μM HP7 with 1 equivalent of heme *a*. Data was fit using the Nernst equation with Igor Pro (Wavemetrics Inc.) software.

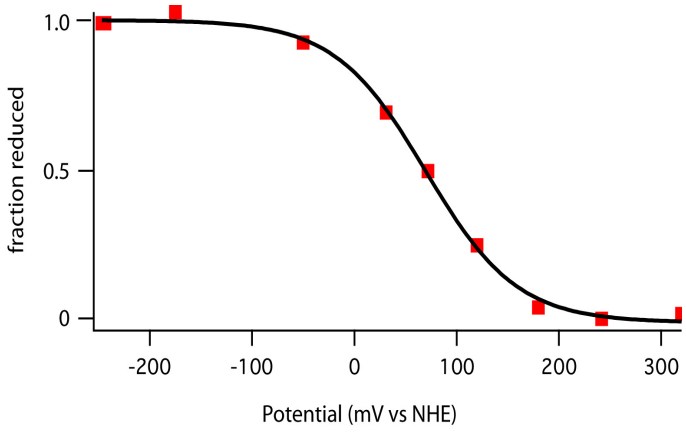

Figure 5.4: Redox titration of 5 μM HP7 with 1 equivalent of iron(III)-dicyanodeuteroporphryin. Data was fit using the Nernst equation with Igor Pro (Wavemetrics Inc.) software.

the affinity of the bis-histidine site for the heme iron [13], as has been observed for other soluble maquettes [14]. As shown by the redox titrations in Figures 5.3 and 5.4, heme *a* and dicyano also raised HP7 midpoint potential substantially. The midpoint potential of bound heme *a* at pH 8 is -72 mV, or 200 mV more positive than the potential measured for heme *b*. The midpoint potential of the dicyano heme in HP7 was 62 mV at pH 8, an astounding 342 mV higher than heme *b* in HP7. This translates to a lower free energy for quinol to heme electron transfer up to 33 kJ when heme *b* is substituted with alternative heme cofactors in HP7.

5.3.2 Comparing AP6 activity to soluble maquette proteins. HP7 quinol-cytochrome *c* oxidoreductase activity was determined using the steady-state turnover assay discussed in chapter four (Figure 5.5) [12]. Shown in purple is the background rate of cytochrome *c* reduction by DBH. The addition of the HP7-heme *b* maquette did not enhance this rate (yellow trace), but HP7 demonstrated increasing levels of catalysis as its midpoint potential was raised. HP7-DADPPIX activity (red) was an order of magnitude faster than the background rate and HP7-heme *a* (green) was twenty times faster. A heme *b* control trace is shown in Figure 4.2; neither DADPPIX nor heme *a* in

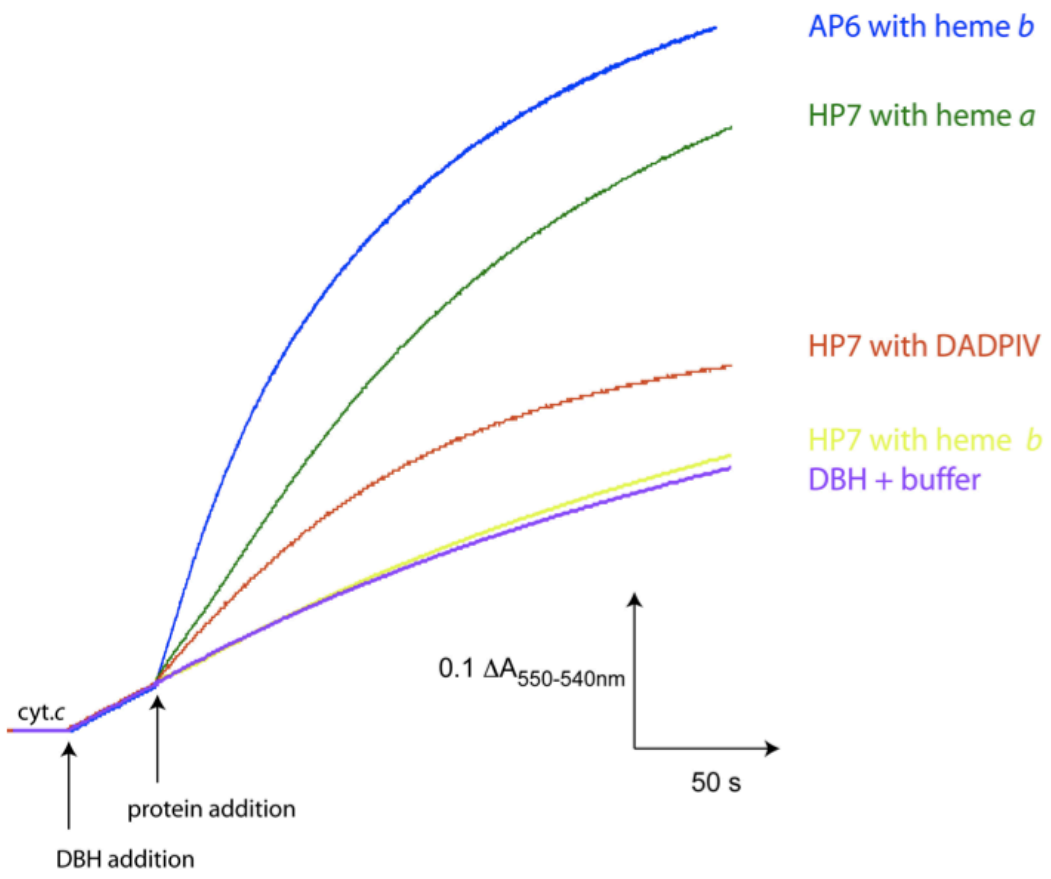

Figure 5.5 Quinol-cytochrome *c* oxidoreductase activity is shown for several different maquette proteins. Activity was quantified as the absorbance difference between reduced (550 nm) and oxidized (540 nm) cytochrome *c* over time. All experiments were completed using buffered solutions containing 100 mM potassium chloride and 50 mM potassium phosphate (pH 8.0). 25 μM cytochrome *c* was incubated in a cuvette to establish a baseline absorbance, and then a concentrated solution of DBH was added to establish a final concentration of 10 μM in the cuvette. After the background rate of direct quinol to cytochrome *c* electron transfer was established (purple), the maquette proteins were added to the cuvette. The soluble maquettes were added at a final concentration of 100 nM. HP7 (yellow) with heme *b* did not have activity that was significant when compared to the background rate. However, when cofactors such as DADPIV (red) and heme *a* (green) were incorporated into HP7, HP7 activity increaed significantly. Experiments with 25 nM AP6 (blue) were conducted slightly differently than those with the soluble maquettes, as AP6 required the assay buffer to also contain 2 mM DPC. AP6 activity was greater than even the most catalytically-active form of HP7, 100 nM HP7 with heme *a* bound.

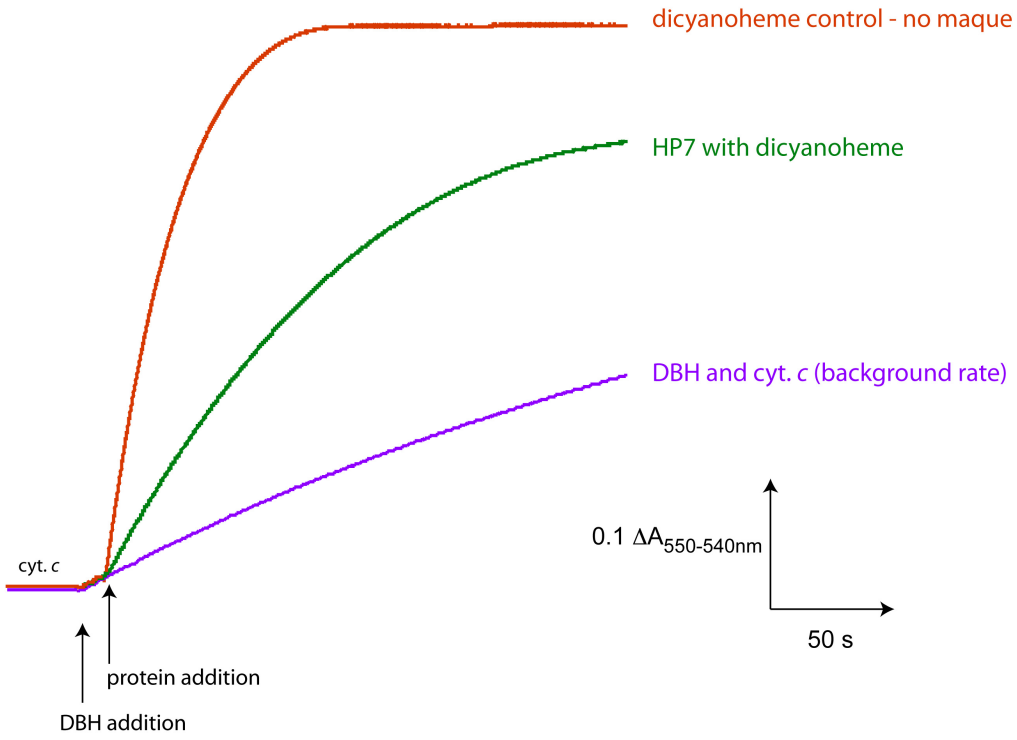

Figure 5.6 Quinol-cytochrome *c* oxidoreductase activity is shown for HP7 and AP6 with iron(III)-dicyanodeuteroporphryin (dicyanoheme) bound. Activity was quantified as the absorbance difference between reduced (550 nm) and oxidized (540 nm) cytochrome *c* over time. All experiments were completed using buffered solutions containing 100 mM potassium chloride and 50 mM potassium phosphate (pH 8.0). 25 μM cytochrome *c* was incubated in a cuvette to establish a baseline absorbance, and then a concentrated solution of DBH was added to establish a final concentration of 10 μM in the cuvette. After the background rate of direct quinol to cytochrome *c* electron transfer was established (purple), the maquette proteins were added to the cuvette. Though 100 nM HP7 (green) had considerable activity with 1 equivalent of the dicyanoheme bound, adding 100 nM dicyanoheme (red) as a control demonstrated more activity than when it is bound to the maquette.

the absence of HP7 generated activity above the DBH background rate (data not shown). Complementary stopped-flow experiments were completed to resolve the k_{cat} values for the various proteins tested in this assay (Table 5.1). When alternative hemes were bound, HP7 had k_{cat} values that were approximately an order of magnitude slower than AP6.

As shown in Figure 5.6, the HP7-dicyano maquette was more reactive than any of the other HP7 complexes; however, the dicyano heme control experiment revealed that the activity of the dicyano heme is greater in solution than bound to the protein, and is almost equivalent to the quinol-cytochrome *c* oxidoreductase activity shown for AP6. This was a surprising result, as none of the other hemes reacted as well in solution as they did when incorporated into a maquette.

5.4 Discussion

5.4.1 Approaching and exceeding the thermodynamic limit for quinol to heme electron transfer. HP7 is able to maintain turnover over a remarkably wide range of for quinol to heme energy differences. As the barrier for quinol to heme electron transfer is raised successively, HP7 activity decreases. However, the quinol/semiquinone to heme electron transfer step reaches an insurmountable thermodynamic barrier when heme *b* is bound to HP7 and HP7 midpoint potential drops to -280 mV. Under these conditions, HP7 no longer contributes to cytochrome *c* reduction, and only the DBH background reduction of cytochrome *c* is observed.

Midpoint potential differences between the different cofactors bound to HP7 can explain most of the results in this chapter. One unexpected finding was free dicyano heme displaying higher catalytic behavior in solution relative to when it was bound to HP7. This can be explained in part due to the impact dicyano heme binding has on HP7

mobility. Bruce Lichtenstein demonstrated that the HP7 histidines are tightly bound to the reduced dicyano heme, eliminating HP7 helical rotations and oxyferrous generation [11]. This indicates that this heme is buried within the core of the HP7 four-helix bundle when it is bound, and much less accessible to diffusible substrates than it is in solution.

5.4.2 Impact of thermodynamic threshold on future AP6 designs. Though this study revealed that lowering the thermodynamic barrier for quinol to heme electron transfer significantly improved HP7 turnover rate, it also validated the design of transmembrane maquette proteins. AP6 was still a better enzyme than HP7 even when its reduction reaction was more unfavorable, suggesting that the midpoint potential of the heme is not the most important factor for reproducing Complex III activity in a synthetic enzyme. Instead, AP6's strong interactions with its quinol and cytochrome *c* redox partners is likely what makes it turnover at a near-natural rate. The hydrophobic environment provided by AP6 and/or its membrane interface helps the quinone substrate bind closer to the AP6 hemes than it can in solution. Additionally, AP6 has the same binding affinity for cytochrome *c* that natural Complex III does for cytochrome c_2, which is not reproduced in HP7.

Still, lowering the thermodynamic barrier for AP6 turnover could increase its enzymatic activity, as was demonstrated for HP7. Subtle residue mutations around the heme binding sites could change the electrostatic environment of the heme and may be enough to shift AP6 midpoint potential. Shifman *et al*. determined that the elimination of glutamate residues around the heme binding site of H10A24 raised the midpoint potential of the hemes bound by 50 mV [4]. There are two glutamate residues, residues 11 and 12, near the "a" binding site in AP6 that could be mutated to a neutral (but polar) residue like

glutamine to raise AP6 midpoint potential. However, charge modifications have a higher propensity for unexpected results and could require several iterative designs to see any changes to the redox environment. Shifman *et al*. also observed that some mutations had no effect because the rotation of the assembled helices was altered depending on the charges on the helix, driving mutated residues away from the hydrophobic core and reducing their effect [4].

In the meantime, AP6 could be redesigned to be more accommodating to alternative heme cofactors that would raise its midpoint potential. AP6 may be limited in the cofactors it can bind tightly because it currently does not have any designed-in control over its structural assembly. Structural constraints could be implemented into the AP6 design to limit conformational flexibility and promote alternative heme binding. A loop sequence (GGSGCGSG) would link two sets of two AP6 helices through a disulfide bond, yielding the single "candelabra" structure adopted by HP7. This new design would require the development of an AP6 expression system, as the length of two AP6 helices linked by the loop sequence would far exceed what is recommended for solid-phase peptide synthesis.

5.5 Conclusion

This work clearly demonstrated that quinol to heme electron transfer is the rate-limiting step for maquette turnover. Raising the midpoint potential of the HP7 model system, and therefore lowering the thermodynamic barrier for quinol to heme electron transfer, increased both HP7 catalytic rate and the total amount of cytochrome *c* substrate reduced.

This work also revealed that transmembrane maquettes are able to perform

electron transfer functions that are inaccessible to soluble protein designs. When HP7 activity was maximized, it still reduced cytochrome *c* an order of magnitude slower than the AP6 design. This suggests that having a favorably redox-active maquette is not the minimum requirement for generating successful model systems to study mitochondrial respiratory chain electron transfer processes. The main functional elements involved in biological energy transduction are invariably contained within membranes and directed vectorially across these membranes. Therefore, creating a library of maquettes capable of reproducing key steps in energy transduction depends upon the redesign and expansion of the AP maquette family.

5.6 References

1. Wiedman, G.R., O'Brien, P.A., Chobot, S.E., Parekh, V.P., Karunakaran, V., Anderson, J.L.R., Dutton, P.L., Discher, B.M., *Building a Function into Simplified Protein Structures: Amphiphilic Maquettes with Multiple Cofactor Binding Sites.* Biochemistry, 2010. **in preparation**.
2. Gibney, B.R., et al., *Self-assembly of heme A and heme B in a designed four-helix bundle: implications for a cytochrome c oxidase maquette.* Biochemistry, 2000. **39**(36): p. 11041-9.
3. Huang, S.S., et al., *The HP-1 maquette: from an apoprotein structure to a structured hemoprotein designed to promote redox-coupled proton exchange.* Proc Natl Acad Sci U S A, 2004. **101**(15): p. 5536-41.
4. Shifman, J.M., et al., *Heme redox potential control in de novo designed four-alpha-helix bundle proteins.* Biochemistry, 2000. **39**(48): p. 14813-21.
5. Robertson, D.E., et al., *Design and synthesis of multi-haem proteins.* Nature, 1994. **368**(6470): p. 425-32.
6. Koder, R.L., et al., *Design and engineering of an O(2) transport protein.* Nature, 2009. **458**(7236): p. 305-9.
7. Ghirlanda, G., et al., *De novo design of a D2-symmetrical protein that reproduces the diheme four-helix bundle in cytochrome bc1.* J Am Chem Soc, 2004. **126**(26): p. 8141-7.
8. Bender, G.M., et al., *De novo design of a single-chain diphenylporphyrin metalloprotein.* J Am Chem Soc, 2007. **129**(35): p. 10732-40.
9. Gibney, B.R. and P.L. Dutton, *Histidine placement in de novo-designed heme proteins.* Protein Sci, 1999. **8**(9): p. 1888-98.

10. Berry, E.A. and B.L. Trumpower, *Simultaneous determination of hemes a, b, and c from pyridine hemochrome spectra.* Anal Biochem, 1987. **161**(1): p. 1-15.
11. Lichtenstein, B.R., *Graduate Thesis.* 2010.
12. Trumpower, B.L. and C.A. Edwards, *Purification of a reconstitutively active iron-sulfur protein (oxidation factor) from succinate . cytochrome c reductase complex of bovine heart mitochondria.* J Biol Chem, 1979. **254**(17): p. 8697-706.
13. Anderson, J.L., *personal communication.* 2010.
14. Zhuang, J., et al., *Evaluation of electron-withdrawing group effects on heme binding in designed proteins: implications for heme a in cytochrome c oxidase.* Inorg Chem, 2006. **45**(12): p. 4685-94.

Chapter 6: Conclusions

Complexity is not an essential requirement for transmembrane proton and electron transfer. The work in this thesis has generated a list of important engineering elements that dictate Complex III activity and supports a simple model for Complex III turnover where electron tunneling reactions are rate-limiting. In this chapter, I will discuss the implications this kind of model will have on the field of Bioenergetics and suggest future directions that could be explored to define a mechanism for Qo oxidation. Portions of this chapter have been included in the following references and are reprinted with permission from SpringerLink and the *Journal of Bioenergetics and Biomembranes* [1, 2].

6.1 Complex III assembly instructions

While there is still progress to be made in the field of *de novo* design, artificial proteins display redox functional characteristics that are within reach of the engineering of natural enzymes [3-5]. The main goal of the maquette approach is to uncover the assembly instructions required to put together biological functions by asking basic questions about how proteins work: How many engineering elements are required? What are the structural and biochemical tolerances of those elements? What portions of structure dictate function and what portions can be ignored? This thesis work aimed to disassemble the complicated history of Complex III and start from scratch, building quinol-cytochrome *c* function one engineering element at a time.

To design AP6 to have quinol-cytochrome *c* oxidoreductase activity, the main elements of these electron transfer reactions in Complex III were extracted and incorporated into AP6: simple α-helical structure to provide a secure, linear scaffold for securing cofactors, both hydrophilic and hydrophobic sections of amino acids to promote interactions with both the membrane and soluble molecules, multiple histidine sites for heme ligation, and a tryptophan molecule for convenience when determining AP6 concentration.

6.2 Developing a simpler model for Complex III electron transfer

Natural electron transfer chains convert the steep exponential fall-off of electron tunneling rate with distance to a near linear dependence [7]. Chains of cofactors become more tolerable to uphill reactions as the chain becomes extended [8]. One of the reasons heme c_1, along with other cofactors in Complex III, is able to accommodate large changes to its active site residues and redox potential is that Complex III is made up of a large

chain of cofactors that can compensate for slight changes in the thermodynamics of a single electron transfer event. Many complicated mechanistic proposals exist that predict specific structural elements of Complex III active sites that dictate their redox behavior [1, 9, 10]. Yet when these residues are eliminated, as they were for heme c_1 in chapter two, the equilibrium midpoint potentials of the cofactor are unaffected and enzyme turnover remains unscathed. Perhaps future experiments and models should begin to question not what singular engineering elements Complex III relies on for catalytic efficiency, but instead what groups of things work together collectively to minimize the costly short-circuits that can be caused by a single electron transfer step.

With no obvious quinone-binding site included in our protein design, AP6 provides clear evidence that a specific quinone-binding site within a membrane protein is not essential for generating significant quinol-cytochrome *c* oxidoreductase enzymatic activity from a heme protein. Proximity of reduced quinol substrates to the hemes in AP6 is accomplished simply by adding an excess of quinone substrate that is free to partition through the hydrophobic membrane interface. This same reserve of excess quinone exists in the mitochondrial respiratory chain as the Q-pool. The absence of Qo from Complex III crystal structures [11-13] suggests that it is mobile [14], diffusing freely between the Q-pool and its active site. In fact, Qo mobility may help Complex III regulate unwanted short-circuit reactions. If Qo is only in its active site during forward turnover, this would be one way of promoting energy transduction over unwanted reverse electron transfer reactions.

Though the contradictions between various experimental results leaves the mechanism of the Qo site undefined, that does not necessarily mean that the mechanistic

suggestions for Complex III turnover need to be overly complex. Qo bifurcation is well understood, but the reversible and robust nature of Complex III electron transfer dictates that the high and low potential chains are inextricably linked. Instead of dividing Complex III into two separate pathways (Figure 1.3), Complex III can instead be thought of as a single chain (shown in Figure 6.1) [6, 8], where shifting the equilibrium of one reaction (*i.e.* midpoint potential or cofactor distance changes) affects the equilibrium of all of the remaining reactions in the cofactor chain. Figure 6.1 is drawn to depict Complex III as a functional monomer, but this simplistic view would still hold true for a functional Complex III dimer; the two single chain monomers would just be electronically connected through their b_L sites. The distribution of electron equivalents within Complex III is solely dependent on the rates of each of the reversible partial reactions, which include all electron tunneling steps, Qo exchange to and from its active sites, and the distal and proximal movement of FeS.

Recently, Cieluch *et al*. proposed a similar model based on the results of their experimental work that modified residues around the *R.capsulatus* heme c_1 binding site to manipulate heme c_1 midpoint potential [6]. In flash experiments without inhibitors added, they observe that the completion of two Qo turnovers and reduction of Qi leaves the FeS cluster and c_1 saturated with electrons. This reaction is driven to completion even in Complex III mutants where the midpoint potential of heme c_1 is 100 mV lower than that of the FeS cluster and the electron transfer reaction is uphill.

When the outflow of electrons from the *b*-chain is blocked by the addition of antimycin in wild-type Complex III, both *b*-hemes remain reduced for a significant amount of time because the low potential chain becomes saturated with electrons. This

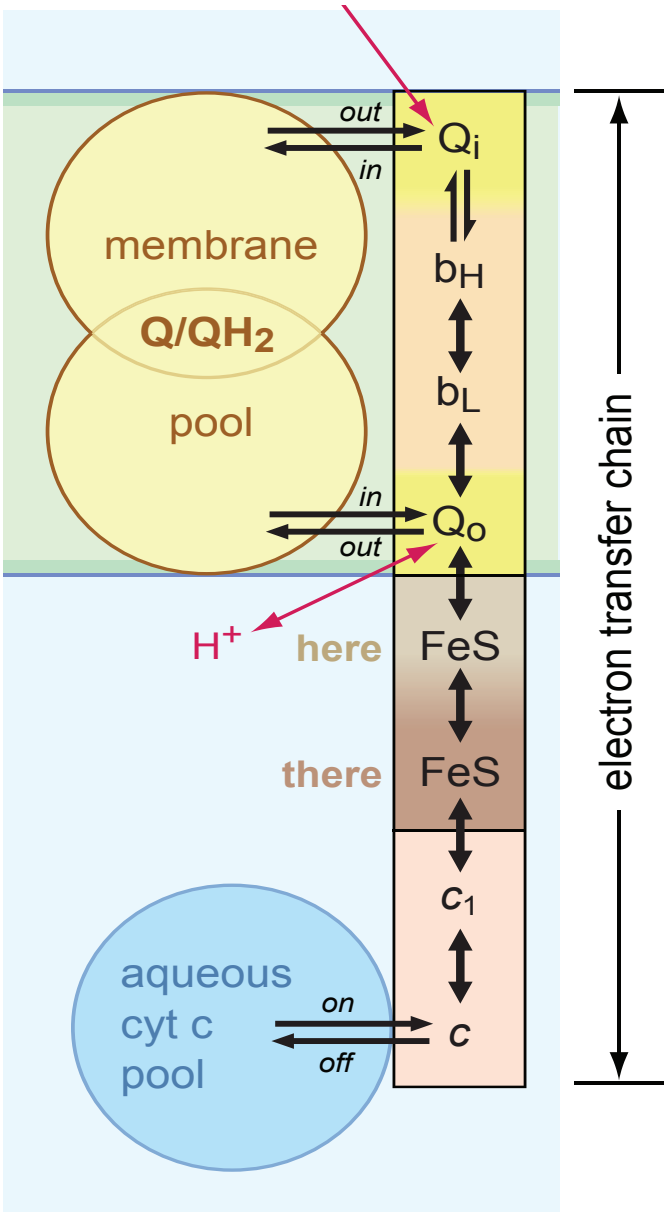

Figure 6.1: A single chain view of Complex III. A similar model was proposed by Cieluch *et al* [6]. In this model, Qo is still delivered to its binding site from a membrane-bound Qpool, but Qo bifurcated oxidation is depicted as two half-reactions along the same chain rather than considering the high and low potential chains of Complex III to be two separate electronic paths. Under these conditions, the equilibrium reactions for each redox step can directly affect any of the other equilibrium reactions occurring in Complex III.

effectively shifts the equilibrium at Qo, as the probability for reverse reactions with reduced b_L is greater with the increase in the effective concentration of reduced heme b_L. Likewise, the equilibrium at Qo can also shift as the concentration of reduced FeS cluster increases, as this substrate can also initiate short-circuit reactions with Qo. The mutants described by Cieluch *et al*. shift the Qo equilibrium in this way by manipulating the FeS-c_1 barrier. The electron distribution in the *b*-chain of these mutants is directly impacted by fluctuations in the electron distribution within the *c*-chain. Therefore, because Qo reactions can occur reversibly, their work confirms that the bifurcation reaction in Complex III does not imply that Complex III transfers electrons to two totally independent redox chains, but that the electrons simply travel in opposite directions from Qo within the same single chain of cofactors.

6.3 Impact of this work on future experiments

6.3.1 Exploiting Complex III thermodynamics to access Qo states. While spectroscopically accessing short-circuit states (Figure 1.6) may stay out of experimental reach for some time to come, stabilizing the green enzyme-substrate and enzyme-product intermediates will be the key to defining the Qo site mechanism. Chapter five revealed that manipulating the thermodynamics of a rate-limiting electron transfer step would modify the reactivity of an enzyme. This concept could conceivably be applied to the Qo oxidation reaction in order to stabilize two key intermediates – Qo fully reduced and Qo fully oxidized (green states in Figure 1.6). The following thermodynamic manipulations could be applied to control Qo site reactivity: 1) replacing ubiquinone with other quinones and analogues that have either a higher redox midpoint potential, such as plastoquinone (PQ) and benzoquinones (BQ), or a lower redox potential, such as

menaquinone (MQ); and 2) using mutants to lower the midpoint potential of FeS or raise the midpoint potential of heme b_L.

For example, by using a FeS mutant with the lowest midpoint potential currently available in combination with substituting PQ for the native ubiquinone (UQ) at Qo, the normally unstable reactant state of reduced quinone and oxidized FeS and heme b_L will become thermodynamically stable and experimentally accessible at the lowest pH values sustainable by Complex III (forest green section of Figure 6.2). Substituting the native UQ in the Qo site with the higher potential BQ creates this same redox state, and it is

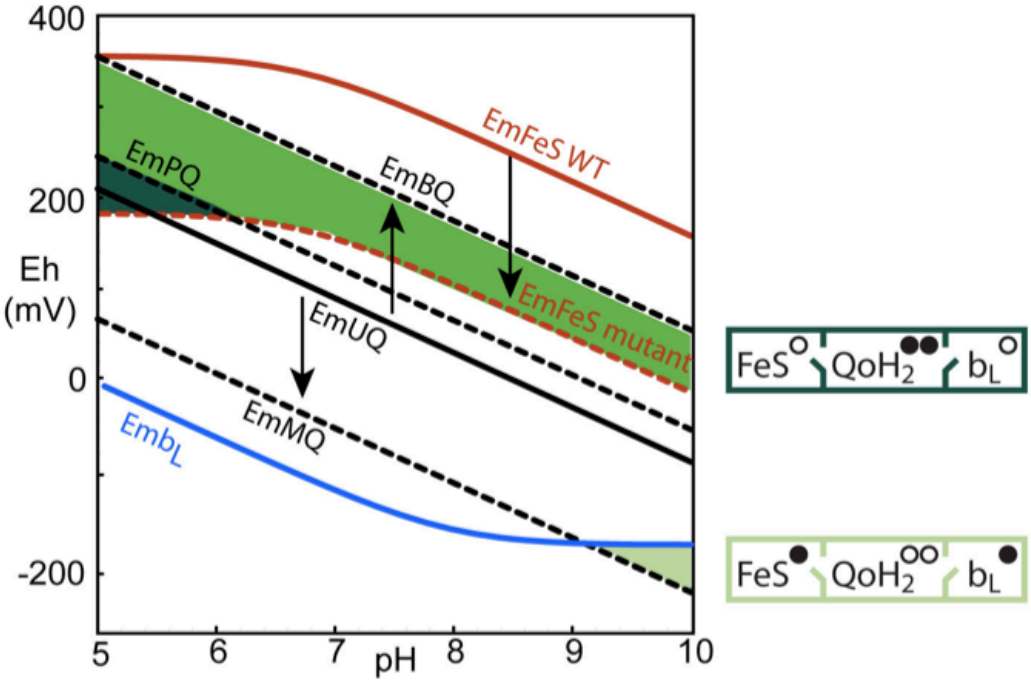

Figure 6.2: Manipulation of the midpoint potentials of cytochrome bc_1 cofactors allows us to create, at equilibrium, two different intermediate states of the Qo site. The darker green regions of the graph represent the midpoint potential and pH combinations that would promote a reduced quinone redox state, where Qo is poised to transfer electrons to FeS and heme b_L. Shown in light green is the fully oxidized Qo redox state, where FeS and heme b_L are both fully reduced. Reprinted with permission from SpringerLink and the *Journal of Bioenergetics and Biomembranes* [2].

more thermodynamically stable over a much wider pH range (lime green area of Figure 6.2). Stabilizing the other catalytically active state, where Qo is oxidized and both FeS and heme b_L are reduced, requires the opposite strategy (light green of Figure 6.2). Attaining thermodynamic stability for this state requires replacing the native UQ with quinones that have intrinsically *lower* midpoint potential values, such as MQ, and *raising* the pH; mutants that *raise* heme b_L midpoint potential can assist the formation of this redox state.

While mutational changes to FeS midpoint potential have created a wide thermodynamic range for exploration [15-18], as shown in Figure 6.3, a similar adjustment of the midpoint of heme b_L has proven more challenging [19-21]. There may

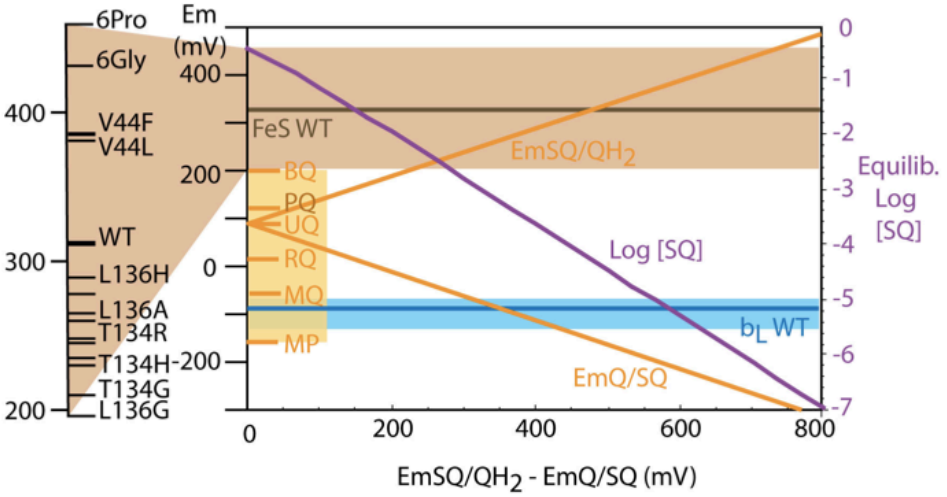

Figure 6.3: The range of midpoint potentials of FeS that are available via characterized mutants are illustrated in brown. So far, heme b_L mutations show a more limited range of midpoint potentials, as shown in blue. Also shown here are the midpoint potentials for several quinone molecules, including ubiquinone (UQ), menaquinone (MQ), plastoquinone (PQ), rhodoquinone (RQ), benzoquinone (BQ), and methanophenazine (MP). As demonstrated in purple, depending on the split of the two electron transfer couples for the quinone, the maximum amount of semiquinone generated on an equilibrium timescale will vary. Reprinted with permission from SpringerLink and the *Journal of Bioenergetics and Biomembranes* [2].

be some hope from preliminary electrostatic calculations that suggest glutamate and arginine residues outside of the PEWY loop could potentally lower heme b_L midpoint potential [22].

Once equilibrium is attained, these two states can be followed by traditional EPR or FTIR approaches, since they would no longer be constrained by a quasi-equilibrium timescale. However, the most important use of this stabilization strategy may be the potential accessibility of these new equilibria to X-ray crystallography techniques. One explanation for the absence of bound quinone in the Qo site is that quinone is only bound in the unstable, catalytically active states [13, 14], a hypothesis that could be confirmed once these states have been stabilized.

While low midpoint potential FeS mutants are potentially useful in stabilizing the physiologically active oxidized and reduced quinone catalytic states for leisurely study at equilibrium, high midpoint potential FeS mutants are potentially useful for facilitating the creation of pseudo-equilibrium Qo semiquinone states using the light activation method of Zhang *et al* [23]. Figure 6.3 shows that as the midpoint potential split between the oxidizing and reducing couple of the two quinone electron transfers gets larger, and the equilibrium concentration of semiquinone at Qo becomes extremely small, the quinone redox couples approach and eventually surpass the midpoint potential values of FeS and heme b_L. By using a mutant of FeS with the highest possible midpoint potential (and therefore, the greatest oxidizing power), it becomes easier to strip one electron off the reduced quinone at Qo and leave the other stranded on the semiquinone when the *b*-chain is fully reduced. Similarly, the use of higher potential quinones instead of native UQ should also facilitate the quasi-equilibrium formation of semiquinone at Qo. Instead of

the pH 9 conditions required for semiquinone formation with native UQ, high midpoint potential FeS mutants and/or quinone substitutes at lower pH values can be used to verify that the semiquinone formed is relevant to the Qo catalytic cycle, and also to detail its engineering in the physiological mechanism.

6.3.2 Maquettes as enzymes – the potential for future designs. Shown in Figure 6.4 are the uncatalyzed and catalyzed rates for Complex III and the synthetic enzymes created by this work. One of the goals of protein design is to be able to understand the engineering of natural proteins enough to design simple model systems that reproduce natural activity levels. The protein design work contained within this thesis is the first example of maquette proteins capable of near-natural turnover rates. The success of the AP6 and HP7 (high potential) designs as Complex III-like enzymes

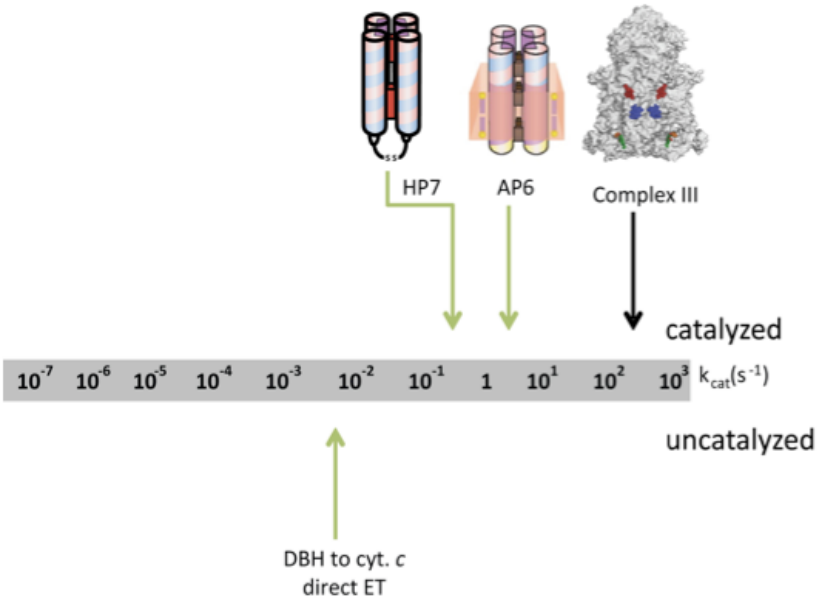

Figure 6.4: Uncatalyzed and catalyzed rates for natural and synthetic quinol-cytochrome *c* oxidoreductase proteins. Black arrows for the catalyzed rates represent natural Complex III and green arrows depict maquettes. The green uncatalyzed arrow represents direct electron transfer between quinol and cytochrome *c*. The maquettes in this work are the first synthetic proteins to demonstrate activity within the range of natural metabolic enzymes.

opens the door for studying other aspects of Complex III turnover, including superoxide production. Complex III and Complex I are both known to be the major sources of superoxide generation, which can generate acute cellular damage when recovering from temporary anoxia [24, 25]. It is also known that superoxide generation by Complex III is closely connected with disruption of mitochondrial membrane permeability, a key step in programmed apoptosis [26]. The superoxide anion midpoint potential has been estimated at –140 mV [27], so either heme b_L or a SQ/Q couple at Qo are capable of supporting single electron reduction of oxygen. Whether heme b_L [14, 28, 29], SQo [25] or both are the immediate donors to oxygen to make superoxide is unknown, and has been difficult to unravel in part because the mechanism at the Qo site remains unknown. Also, another complication is the generation of the heme b_L or SQ reducing states in an oxygen-rich environment is a state far from chemical equilibrium, and controlling the balance between reduced SQo or reduced heme b_L has been an uncertain task. Finally, superoxide generation has almost always been studied with multiple turnover systems of Complex III, where the redox states of all the Complex III components are rapidly changing and interrelated, offering little hope of discriminating between the redox states of heme b_L and SQo in a natural system. Studying superoxide production by maquette proteins yields greater control over the protein system. Instead of trying to unravel results from a complex chain of redox cofactors, specific cofactors can be incorporated into the AP6 maquette to isolate their superoxide production.

Heme b_L is likely to form an oxyferrous state. This would point towards an inner sphere electron transfer mechanism for superoxide production at heme b_L, where an oxy-ferrous transition state exists prior to oxygen reduction and release of superoxide.

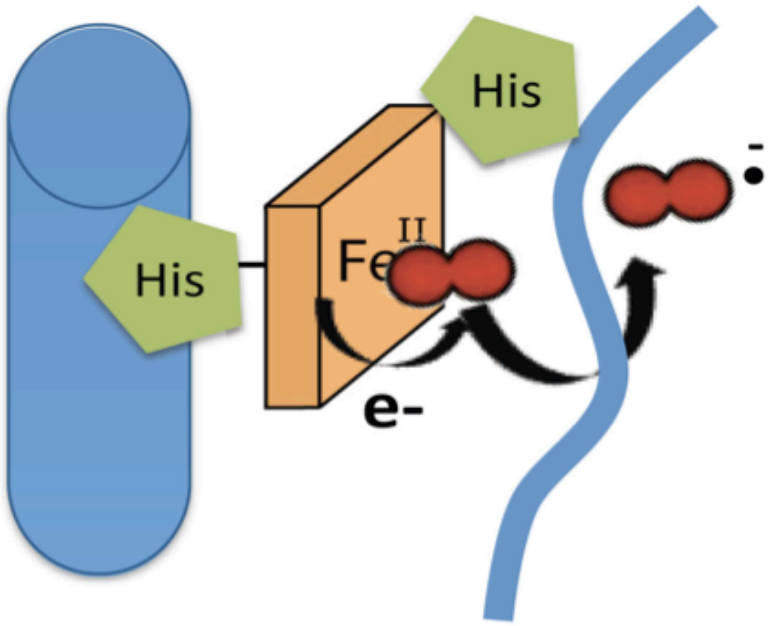

Figure 6.5 Cartoon of inner sphere electron transfer between a reduced heme in AP6 and oxygen to form the superoxide anion. AP6 helices (shown in blue) have a dynamic assembly that permits small ligands, such as oxygen (shown in red), to access the heme binding site (depicted as green histidine imidizole groups in this diagram) and form an oxyferrous intermediate state that then reduces oxygen to superoxide.

Determining the conditions for superoxide production by heme *b* would be feasible using AP6. Figure 6.5 depicts how this reaction could take place in AP6. "Leaky" AP6 assembly does allow oxygen to enter the protein core (Figure 3.9) and associate with a reduced heme cofactor, and should also enable inner sphere electron transfer to form superoxide.

AP6 can also be modified to study superoxide production by a semiquinone state. It has been suggested that Qo mobility would be essential to regulating its role in the

generation of superoxide [30-32]. According to this hypothesis, SQo would reduce oxygen through an outer sphere electron transfer mechanism when the quinone is present in the Qo active site. A quinone cofactor could be fixed in a position along the AP6 helix, in the form of a napthoquinone amino acid, in order to study reactions that produce superoxide in a similar way to reactions that could occur at Qo. However, experiments prolonging the semiquinone redox state in natural Complex III have been successful at determining whether or not SQo is capable of superoxide production [32], and should also be utilized for future studies.

6.4 Conclusion

Assigning a Qo site mechanism remains an elusive goal despite the experimental progress made since Peter Mitchell's Q-cycle proposal in 1976 [33, 34]. In order to differentiate between the mechanisms currently proposed, future studies need to push the boundaries of current Complex III experiments and generate redox states that are, at present, too short-lived to be studied spectroscopically. If these states cannot be distinguished using natural systems, maquette protein designs that target these quinone transition states could be studied in order to accept or reject potential Qo mechanisms.

6.5 References

1. Zhang, H.B., et al., *Quinone and non-quinone redox couples in Complex III.* Journal of Bioenergetics and Biomembranes, 2008. **40**(5): p. 493-499.
2. Chobot, S.E., et al., *Breaking the Q-cycle: finding new ways to study Qo through thermodynamic manipulations.* Journal of Bioenergetics and Biomembranes, 2008. **40**(5): p. 501-507.
3. Chobot, S.E., Wiedman, G.R., Moser, C.C., Discher, B.M., Dutton, P.L., *Demonstrating quinol-cytochrome c oxidoreductase kinetic activity by an amphiphilic maquette protein.* Biochemistry, 2010. **submitted**.
4. Kaplan, J. and W.F. DeGrado, *De novo design of catalytic proteins.* Proc Natl Acad Sci U S A, 2004. **101**(32): p. 11566-70.

5. Jiang, L., et al., *De novo computational design of retro-aldol enzymes.* Science, 2008. **319**(5868): p. 1387-91.
6. Cieluch, E., et al., *Visualizing changes in electron distribution in coupled chains of cytochrome bc(1) by modifying barrier for electron transfer between the FeS cluster and heme c(1).* Biochim Biophys Acta, 2010. **1797**(2): p. 296-303.
7. Moser, C.C., et al., *Distance metrics for heme protein electron tunneling.* Biochimica Et Biophysica Acta-Bioenergetics, 2008. **1777**(7-8): p. 1032-1037.
8. Chobot, S.E., Zhang, H., Marshall, D.A., Osyczka, A., Moser, C.C., Dutton, P.L., *Presenting a simple model for Complex III electron transfer.* in preparation - to be submitted to Biochemistry, 2010.
9. Crofts, A.R., et al., *The Q-cycle reviewed: How well does a monomeric mechanism of the bc(1) complex account for the function of a dimeric complex?* Biochim Biophys Acta, 2008. **1777**(7-8): p. 1001-19.
10. Cape, J.L., M.K. Bowman, and D.M. Kramer, *Understanding the cytochrome bc complexes by what they don't do. The Q-cycle at 30.* Trends Plant Sci, 2006. **11**(1): p. 46-55.
11. Gao, X., et al., *Structural basis for the quinone reduction in the bc1 complex: a comparative analysis of crystal structures of mitochondrial cytochrome bc1 with bound substrate and inhibitors at the Qi site.* Biochemistry, 2003. **42**(30): p. 9067-80.
12. Lange, C. and C. Hunte, *Crystal structure of the yeast cytochrome bc1 complex with its bound substrate cytochrome c.* Proc Natl Acad Sci U S A, 2002. **99**(5): p. 2800-5.
13. Berry, E.A., et al., *X-Ray Structure of Rhodobacter Capsulatus Cytochrome bc (1): Comparison with its Mitochondrial and Chloroplast Counterparts.* Photosynth Res, 2004. **81**(3): p. 251-75.
14. Crofts, A.R., et al., *Proton pumping in the bc1 complex: a new gating mechanism that prevents short circuits.* Biochim Biophys Acta, 2006. **1757**(8): p. 1019-34.
15. Merbitz-Zahradnik, T., et al., *Elimination of the disulfide bridge in the Rieske iron-sulfur protein allows assembly of the [2Fe-2S] cluster into the Rieske protein but damages the ubiquinol oxidation site in the cytochrome bc1 complex.* Biochemistry, 2003. **42**(46): p. 13637-45.
16. Davidson, E., et al., *Potential ligands to the [2Fe-2S] Rieske cluster of the cytochrome bc1 complex of Rhodobacter capsulatus probed by site-directed mutagenesis.* Biochemistry, 1992. **31**(13): p. 3342-51.
17. Darrouzet, E., M. Valkova-Valchanova, and F. Daldal, *The [2Fe-2S] cluster E(m) as an indicator of the iron-sulfur subunit position in the ubihydroquinone oxidation site of the cytochrome bc1 complex.* J Biol Chem, 2002. **277**(5): p. 3464-70.
18. Guergova-Kuras, M., et al., *Specific mutagenesis of the rieske iron-sulfur protein in Rhodobacter sphaeroides shows that both the thermodynamic gradient and the pK of the oxidized form determine the rate of quinol oxidation by the bc(1) complex.* Biochemistry, 2000. **39**(25): p. 7436-44.

19. Liebl, U., et al., *The Rieske FeS center from the gram-positive bacterium PS3 and its interaction with the menaquinone pool studied by EPR.* J Biol Chem, 1992. **267**(20): p. 14068-72.
20. Gong, X., et al., *Evidence for electron equilibrium between the two hemes bL in the dimeric cytochrome bc1 complex.* J Biol Chem, 2005. **280**(10): p. 9251-7.
21. Yang, S., et al., *On the mechanism of quinol oxidation at the QP site in the cytochrome bc1 complex: studied using mutants lacking cytochrome bL or bH.* J Biol Chem, 2008. **283**(42): p. 28767-76.
22. Gunner, M.R., personal communication, 2007.
23. Zhang, H., et al., *Exposing the complex III Qo semiquinone radical.* Biochim Biophys Acta, 2007. **1767**(7): p. 883-7.
24. Chance, B., H. Sies, and A. Boveris, *Hydroperoxide Metabolism In Mammalian Organs.* Physiological Reviews, 1979. **59**(3): p. 527-605.
25. Turrens, J.F., A. Alexandre, and A.L. Lehninger, *Ubisemiquinone Is The Electron-Donor For Superoxide Formation By Complex Iii Of Heart-Mitochondria.* Archives Of Biochemistry And Biophysics, 1985. **237**(2): p. 408-414.
26. Kroemer, G., B. Dallaporta, and M. Resche-Rigon, *The mitochondrial death/life regulator in apoptosis and necrosis.* Annual Review Of Physiology, 1998. **60**: p. 619-642.
27. Petlicki, J. and T.G.M. van de Ven, *The equilibrium between the oxidation of hydrogen peroxide by oxygen and the dismutation of peroxyl or superoxide radicals in aqueous solutions in contact with oxygen.* Journal Of The Chemical Society-Faraday Transactions, 1998. **94**(18): p. 2763-2767.
28. Nohl, H. and W. Jordan, *The Mitochondrial Site Of Superoxide Formation.* Biochemical And Biophysical Research Communications, 1986. **138**(2): p. 533-539.
29. Gong, X., et al., *Evidence for electron equilibrium between the two hemes b(L) in the dimeric cytochrome bc(1) complex.* Journal Of Biological Chemistry, 2005. **280**(10): p. 9251-9257.
30. Cape, J.L., et al., *The respiratory substrate rhodoquinol induces Q-cycle bypass reactions in the yeast cytochrome bc(1) complex: mechanistic and physiological implications.* J Biol Chem, 2005. **280**(41): p. 34654-60.
31. Sun, J. and B.L. Trumpower, *Superoxide anion generation by the cytochrome bc1 complex.* Arch Biochem Biophys, 2003. **419**(2): p. 198-206.
32. Cape, J.L., M.K. Bowman, and D.M. Kramer, *A semiquinone intermediate generated at the Qo site of the cytochrome bc1 complex: importance for the Q-cycle and superoxide production.* Proc Natl Acad Sci U S A, 2007. **104**(19): p. 7887-92.
33. Mitchell, P., *Possible molecular mechanisms of the protonmotive function of cytochrome systems.* J Theor Biol, 1976. **62**(2): p. 327-67.
34. Mitchell, P., *The protonmotive Q cycle: a general formulation.* FEBS Lett, 1975. **59**(2): p. 137-9.

Appendix

A.1 The Moser Dutton equation – a useful predicting tool

The Dutton laboratory has developed an electron transfer rate expression that offers a simple way to examine parameters that directly relate to the oxidoreductase activity of a particular mitochondrial enzyme [1-3]. The Moser-Dutton equation defines the rate of electron transfer as a function of distance (R), midpoint potential (included in ΔG°), reorganization energy (λ), and protein packing density (ρ):

$$\log k_{et}^{exer} = 13 - (1.2 - 0.8\rho)(R - 3.6) - 3.1\frac{(\Delta G^o + \lambda)^2}{\lambda}$$

Equation A.1

This equation is based upon an exponential dependence of electron tunneling with distance through an insulating protein barrier, where the height of the tunneling barrier depends upon how vacuum-like or how bond-like the intervening protein medium is. An elementary structure-based estimate that roughly correlates with effective barrier height is the packing density, which is around 0.76 in a typical protein. Marcus realized that electron tunneling often has a Gaussian dependence of rate vs. distance [4], with a maximal possible rate when the driving force (-ΔG° in eV) matches an energetic term called the reorganization energy for electron tunneling. The reorganization energy can be thought of as the energy required to move the nuclei of the redox cofactors and their surroundings from an equilibrium configuration favored when the electron is on the donor to the equilibrium geometry favored when the electron is on the acceptor, but constraining the electron to remaining on the donor.

Marcus's expression was based on a classical model in which the potential energy surfaces of the reactant (reduced donor and oxidized acceptor) and product (oxidized donor and reduced acceptor) were intersecting, parabolic, simple harmonic oscillator wells, with the reaction coordinate being a generalized one of nuclear vibration/reorganization that carried the reactant equilibrium geometry into the product equilibrium geometry. In the Marcus classical view, the vibrations coupled to electron transfer are all of low enough energy that a non-quantized harmonic oscillator description is sufficient. Previous studies with photosynthetic reaction centers over a wide range of cyrogenic temperatures have demonstrated that the Marcus expression is not as appropriate as an expression that uses vibrations coupled to electron transfer that have an energy higher than Boltzmann κT at room temperature [5]. The weighted characteristic frequency of vibration coupled to electron transfer in reaction centers appears to be close to 0.06 eV, larger than the Boltzmann room temperature energy of about 0.025 eV [6]. Hopfield has previously described an expression that allows this quantized vibrational frequency but maintains a Gaussian free energy dependence on rate [7]. Although this characteristic frequency is rather difficult to access experimentally and may vary from one electron tunneling reaction to another, the generic value appears to give reasonable estimates of electron transfer rates in many cases. The somewhat broader quantized version of the Gaussian dependence of rate on free energy gives rise to the 3.1 coefficient in the room temperature expression of Equation A.1. The corresponding classical Marcus expression would have a coefficient of 4.2.

Equation A.1 relates to exergonic electron transfer reactions; however, many biological electron tunneling reactions are uphill. One way to estimate the rate of an

uphill electron tunneling reaction is to use Equation A.1 to calculate the corresponding downhill electron transfer of the reverse reaction and then, assuming the forward and reverse rates are related by a Boltzmann energy term, slow the forward tunneling rate by an order of magnitude for every 0.06 eV of uphill free energy [3].

Tunneling expressions with fewer parameters are useful in situations where there is a lack of experimental information. Packing density is the easiest parameter to replace with a generic value because it rarely has a dominant effect (see Appendix for an example of this). The 0.76 packing density typical of a protein leads to the 0.6 coefficient leading the distance term. The next parameter to consider replacing with a generic term is reorganization energy, both because it is rarely measured with any precision, and because it does not appear to be engineered in Complex III. 0.7 eV is an adequate generic value, and leads to a two-parameter expression:

$$\log k_{et}^{exer} = 15 - 0.6R - 3.1\frac{(\Delta G^o + 0.7)^2}{0.7}$$

Equation A.2

In order to calculate the electron tunneling rates, user-written programs were constructed in Mathematica 7.0 (Wolfram Research).

A.2 References

1. Page, C.C., et al., *Natural engineering principles of electron tunnelling in biological oxidation-reduction*. Nature, 1999. **402**(6757): p. 47-52.
2. Moser, C.C., et al., *Biological electron transfer*. J Bioenerg Biomembr, 1995. **27**(3): p. 263-74.
3. Moser, C.C., et al., *Electron tunneling chains of mitochondria*. Biochimica Et Biophysica Acta-Bioenergetics, 2006. **1757**(9-10): p. 1096-1109.
4. Marcus, R.A.S., N. , *Electron transfers in chemistry and biology*. Biochim Biophys Acta, 1985.
5. Gunner, M.R., Dutton, P.L., *Temperature and -delta-G-degrees dependence of the electron-transfer from Bph.- to Qa in reaction center protein from Rhodobacter*

sphaeroides with different quinones as Qa. J. Am. Chem. Soc., 1989. **111**: p. 3400-3412.
6. Moser, C.C., et al., *Nature of biological electron transfer*. Nature, 1992. **355**(6363): p. 796-802.
7. Hopfield, J.J., *Electron Transfer Between Biological Molecules by Thermally Activated Tunneling*. Proc Natl Acad Sci U S A, 1974. **71**(9): p. 3640-3644.